AD_____

Award Number: W81XWH-06-1-0414

TITLE: Dietary Influences on Alpha-Methylacyl-CoA Racemase (AMACR) Expression in the Prostate

PRINCIPAL INVESTIGATOR: Vijayalakshmi Ananthanarayanan, M.D.

CONTRACTING ORGANIZATION: University of Illinois at Chicago
Chicago, Illinois, 60612

REPORT DATE: April 2008

TYPE OF REPORT: Annual

PREPARED FOR: U.S. Army Medical Research and Materiel Command
Fort Detrick, Maryland 21702-5012

REPORT DOCUMENTATION PAGE

Form Approved
OMB No. 0704-0188

1. REPORT DATE *(DD-MM-YYYY)*	**2. REPORT TYPE**	**3. DATES COVERED** *(From - To)*
01-04-2008	Annual	1 APR 2007 - 30 MAR 2008

4. TITLE AND SUBTITLE

Dietary Influences on Alpha-Methylacyl-CoA Racemase (AMACR) Expression in the Prostate

5a. CONTRACT NUMBER

5b. GRANT NUMBER
W81XWH-06-1-0414

5c. PROGRAM ELEMENT NUMBER

6. AUTHOR(S)
Vijayalakshmi Ananthanarayanan, M.D.

5d. PROJECT NUMBER

5e. TASK NUMBER

5f. WORK UNIT NUMBER

7. PERFORMING ORGANIZATION NAME(S) AND ADDRESS(ES)

University of Illinois at Chicago
Chicago, Illinois 60612

8. PERFORMING ORGANIZATION REPORT NUMBER

9. SPONSORING / MONITORING AGENCY NAME(S) AND ADDRESS(ES)
U.S. Army Medical Research and Materiel Command
Fort Detrick, Maryland 21702-5012

10. SPONSOR/MONITOR'S ACRONYM(S)

11. SPONSOR/MONITOR'S REPORT NUMBER(S)

12. DISTRIBUTION / AVAILABILITY STATEMENT
Approved for Public Release; Distribution Unlimited

13. SUPPLEMENTARY NOTES

14. ABSTRACT
Alpha Methyl Acyl CoA Racemase (AMACR), a peroxisomal and mitochondrial enzyme, is up regulated in majority of prostate cancers (PCa). This enzyme is involved in the breakdown of phytanic & pristanic acids, which are derived primarily through the ingestion of dairy and red meat products. There are no studies done so far that have examined the relationship of this enzyme with red meat and dairy intake and therefore PCa risk. The current research focuses on examining the relationships between AMACR expression in the prostate and phytanic/pristanic acid levels in the blood and prostate. So far, 19 patients with Pca have been recruited in the study. Research staff has been trained to obtain dietary information as well as process tissue and blood samples from participants. Protocols for processing biological samples have been established. Preliminary optimization of laboratory assays including assays for quantifying AMACR using automated image analysis tools have been developed.

15. SUBJECT TERMS
AMACR, Prostate Cancer, Dairy, Red meat, Phytanic acid, Pristanic acid

16. SECURITY CLASSIFICATION OF:			**17. LIMITATION OF ABSTRACT**	**18. NUMBER OF PAGES**	**19a. NAME OF RESPONSIBLE PERSON**
a. REPORT	**b. ABSTRACT**	**c. THIS PAGE**			USAMRMC
U	U	U	UU	57	**19b. TELEPHONE NUMBER** *(include area code)*

Table of Contents

Introduction

Alpha Methyl Acyl coA Racemase (AMACR), a peroxisomal and mitochondrial enzyme, is known to be up regulated in majority of prostate cancers at the protein and mRNA transcript level. This enzyme is involved in the breakdown of phytanic and pristanic acids, which are branched chain fatty acids. These fatty acids cannot be produced de-novo by humans and are derived primarily through the ingestion of dairy and red meat products. Although, epidemiologic studies in the past have shown association between dairy/red meat ingestion and prostate cancer risk, there are no studies done so far that examined the relationship of this enzyme with red meat and dairy intake and therefore prostate cancer risk. The current research focuses on examining the relationships between AMACR expression in the prostate and phytanic/pristanic acid levels in the blood and prostate. We postulate that men with higher intake of red meat and dairy will have higher levels phytanic/pristanic acid in their blood and prostates and consequently have and elevated risk of prostate cancer. Sixty men with prostate cancer will be recruited in this study. Dietary measures for red meat and dairy intake will be evaluated using food frequency questionnaires (FFQ). Phytanic/pristanic acids will be measured in their blood and prostates. In addition, tissue expression for AMACR will be studied at both the protein and RNA level. This study will help us better understand the relationships of dairy/red meat ingestion and prostate cancer risk. It would also help us better understand the exact role of AMACR in prostate carcinogenesis.

Body

The study is currently enrolling participants with prostate cancer from two institutions; the University of Illinois at Chicago (UIC) hospital and the Jesse Brown Veterans Administration Medical Center (JBVAMC). All men with prostate cancer undergoing radical prostatectomy as a treatment are eligible to participate provided they have not received hormonal ablation or neo-adjuvant chemotherapy. Participating subjects have to complete two research visits as a part of this study. A basic schema about patient enrollment is provided in **Figure 1.**

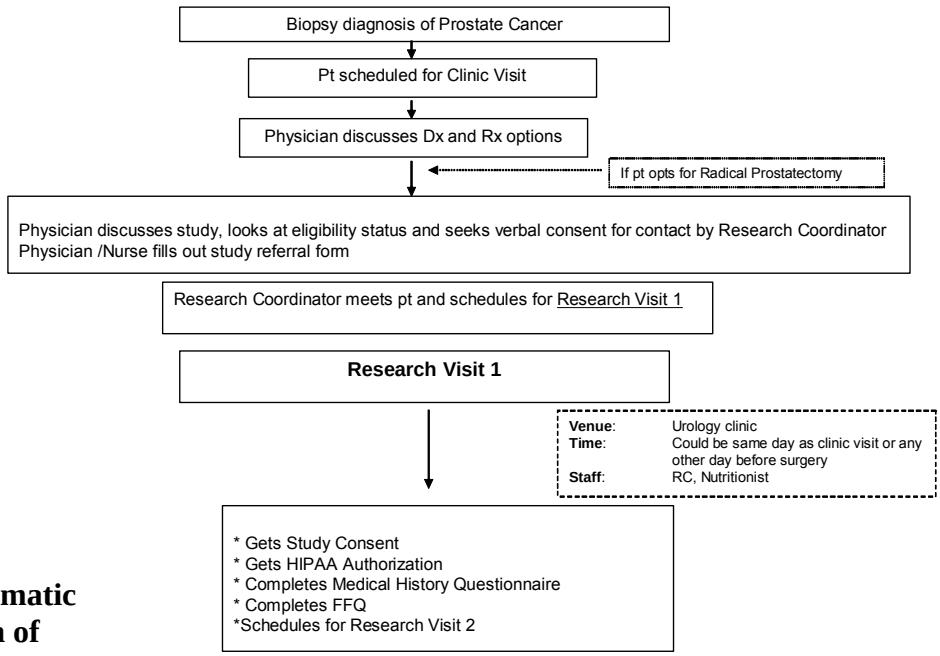

Figure 1. Schematic Representation of Subject Recruitment

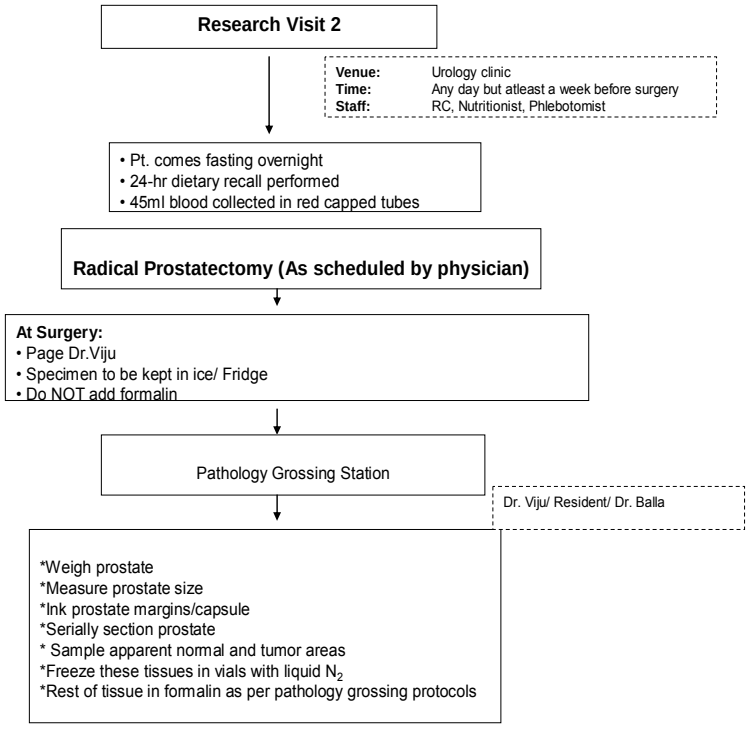

Research Activities

We have accomplished the following goals as specified in the statement of work included with the original grant proposal.

Institutional Review Board
Institutional Review Board (IRB) approvals from UIC and JBVAMC have been obtained in addition to the HSRRB approval.

Staff Training
Staff involved in the project has met training requirements in human subject's protections before their involvement in the research in addition to HIPAA research training. We have a dedicated research coordinator who is fully trained to recruit participants for the study. Staff has also been trained to process samples and data from these subjects. The data includes dietary data in addition to medical data.

Data Management
A Microsoft Access® database has been developed to record participant information. This database is located on a secure server and access to this database is password protected. The database keeps track of patient information, their surgery dates, the research visit dates as well as tracks their tissue and blood samples. In addition, once a potential participant declines to participate his identifying information is automatically deleted from the database through the use of a macro coded within the database.

Participant Enrollment

Table 1: AMACR Study Recruitment Status (UIC+JBVAMC)

	Number
Potential Participants	55
Number of subjects who consented	22
Number of participants who withdrew from the study	3
Number of participants on study	19

Fifteen of the consented participants are African-American while the other four are white.

Laboratory Assays

Blood Processing
A protocol for processing blood samples has been developed and is described in detail in the Appendix (Section A). The protocol enables us to separate blood components and store them for future use. In addition, it will enable us to cryopreserve WBCs. Staff members have been trained in blood processing and handling of biohazardous material. We have approximately 162 aliquots of serum, 76 aliquots of plasma and 114 aliquots of

RBCs from these consented participants. This makes it valuable sample resource for this study as well as subsequent studies in the future.

Measurement of Phytanic/Pristanic Acid

Phytanic and pristanic acid are branched chain fatty acids and known substrates for AMACR. These fatty acids will be measured in the serum and prostate using LCMS-MS. Dr. Richard VanBreemen's laboratory at UIC has developed assays for simultaneous measurement of phytanic and pristanic acid using LCMS-MS. The have estimated that approximately 10 mg of prostatic tissue and 100ul of serum will be required to do the phytanic/pristanic acid estimation. We have procured paired normal and cancer frozen prostatic tissue from UIC's tissue bank resource to perform this initial standardization run.

AMACR Protein Expression

As mentioned in the aims, we intend to study AMACR expression at a protein level using immunohistochemistry and immunofluorescence. Quantification of AMACR can be done manually or using state of the art image analysis systems. As manual scores are semi-quantitative in nature, use of image analysis systems for quantification provides continuous and reproducible measurements especially at lower expression levels. We are developing two novel approaches: one using standard brightfield digital microscopy (ScanScope®, Aperio Corp.) and one using laser scanning cytometry (LSC) with fluorescence (iCys®, CompuCyte) for automated scoring of tissue images.

Scanscope® is a digital bright field microscope with automatic slide scanning properties. The Scanscope® scans glass slides into digital slide images. These images can then be viewed, browsed and scored over the web. There are inbuilt scoring algorithms that can be used to quantify expression of nuclear, cytoplasmic markers. In addition, we have recently added Spectrum™ Plus to the ScanScope hardware. Spectrum Plus is comprehensive, web-based digital pathology information management software developed for digital slide viewing and conferencing, workflow management, data archival, and image analysis. This system greatly facilitates digital microscopic image review and analysis by providing whole slide digital images and enabling the user to view multiple images simultaneously. In addition, image analysis throughput is greatly increased owing to batch image analysis capabilities.

A representative screen shot of Aperio viewing software and Spectrum™ Plus is shown below (**Figure 2**). We are procuring the clinical Hematoxylin and Eosin (H&E) slides for the prostatectomy specimens from our study participants and adding these slides to the Spectrum database. These H&E slides will be mapped in detail for cancer and normal areas and will be used subsequently to create a tissue microarray (**Figure 2**).

Figure 2: Annotation of Histologic Compartments on a web slide within Spectrum™ Plus and ImageScope®

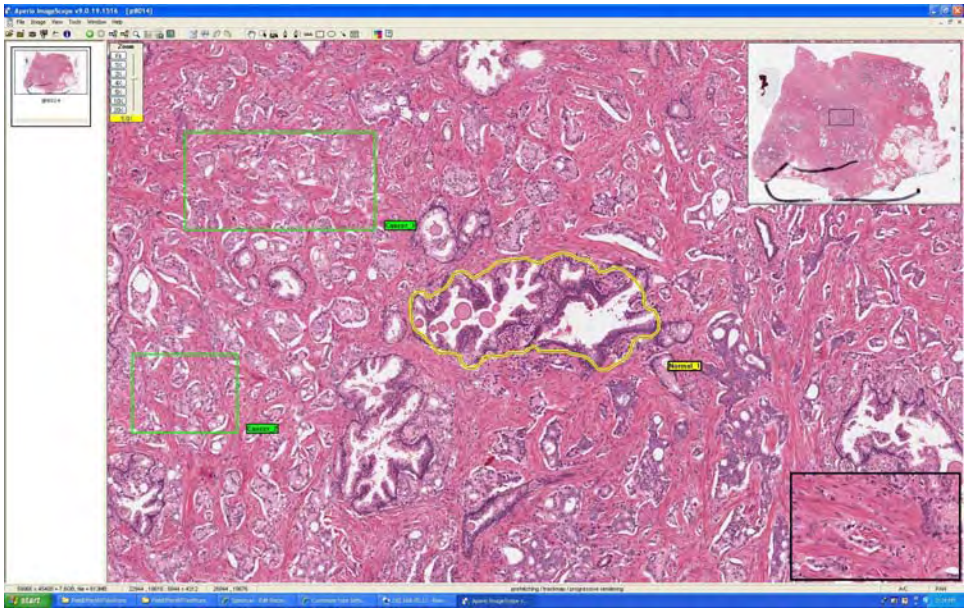

Previously we have shown that AMACR expression in normal glands from patients subsequently diagnosed with prostate cancer was higher than those who did not. No difference was observed for AMACR expression in HGPIN glands [1]. To validate scoring algorithms, we scanned the same biopsy set using the ScanScope CS and digital web slides were created. Regions of interests (ROI) were drawn within benign and HGPIN compartments and scored using 'Positive Pixel Count™' and 'Co-Localization' algorithms of the Aperio software. Separate scores for benign and HGPIN glands were computed as the product of percent area positive and mean intensity of staining. We found that with automated image analysis, normal as well as HGPIN glands showed higher AMACR expression in biopsies with a subsequent diagnosis of cancer (**Figure 3**).

This work was presented at the 2007 Frontiers in Cancer Prevention Research Meeting. For more details, see Appendix –Section B

Laser Scanning Cytometer (LSC) is a laser based system that is capable of simultaneous acquisition of multiple-fluorescence and brightfield laser-scatter images, from as many as 3 lasers and 5 multiplexed light sensors. The LSC obtains quantitative data using 'Phantom contouring'. Phantoms are round pseudo-objects that are randomly placed on an image and co-localization of various colors within each phantom is recorded and quantified. By staining prostate tissues for both AMACR and Cytokeratin, we can accurately gate out the non-epithelial elements from the image and quantify AMACR expression in the epithelium. More details about quantifying using LSC data can be found in the poster (Appendix –Section C)

Figure 3: AMACR quantification in Prostatic Biopsies with HGPIN using Automated Image Analysis (AIA)

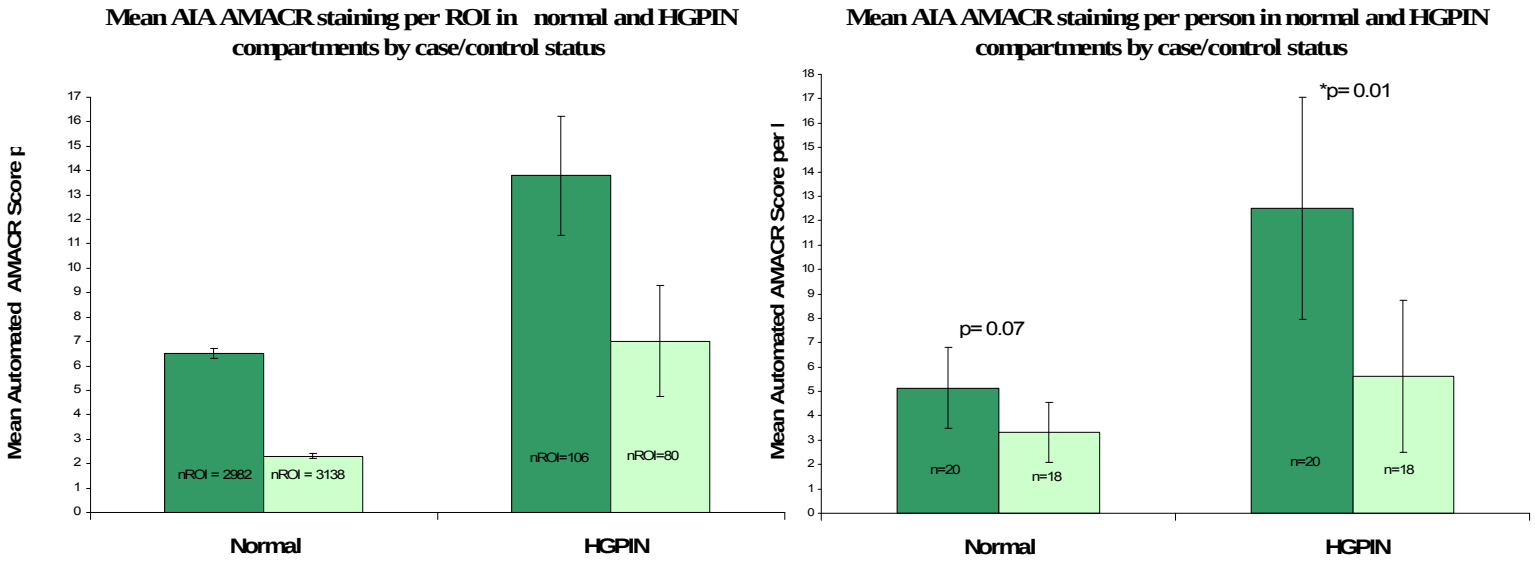

AMACR mRNA Expression

As specified in our aims, we will also evaluate AMACR mRNA expression from fresh prostate tissue sampled at the time of grossing. AMACR mRNA will be quantified in both normal and tumor areas sampled. Tumors in the prostate are difficult to identify grossly and it is possible that the sampled areas may not represent tumor at all. Hence, it is imperative that alternate methods for extracting RNA from formalin fixed paraffin embedded sections are devised. Dr. Larissa Nonn has developed protocols for RNA extraction on formalin fixed paraffin embedded prostatic biopsies. RNA is first extracted with the RecoverAll™ Total Nucleic Acid Isolation Kit (Ambion Inc., Austin, TX, USA) according to the manufacturer's

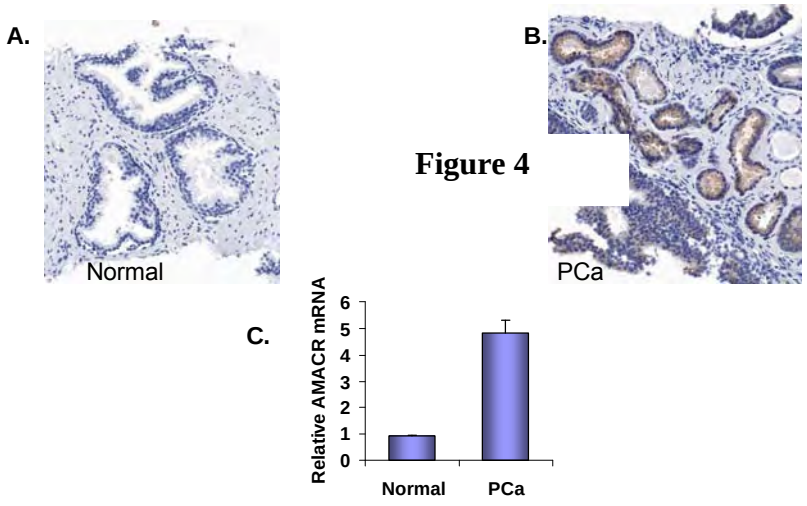

Figure 4

Figure. AMACR mRNA and protein expression in prostate biopsy specimen. Immunohistochemical staining with anti-AMACR in**, A**, normal and, **B**, adenocarcinoma in FFPE-prostate biopsy. **C**, Real-time qRT-PCR analysis of AMACR mRNA expression in macro-dissected normal and PCa epithelium. mRNA levels are shown relative to normal prostate epithelium and normalize to the expression of TBP, B2M and cytokeratin-8. Error represent SEM from two separate experiments (triplicate samples for each).

protocol with the following modifications; protease digestion at 50º C for 4 hours and DNase digestion at 37º C for 1 hour. RNA quality and quantity is measured on the NanoDrop® ND-1000 (NanoDrop Technologies, Wilmington, DE, USA) and RNA is stored in RNA Storage Solution at -80º C. 10 ng of total RNA is the input for the RT reaction. RNA is isolated and mRNA expression analyzed by quantitative reverse-transcription polymerase chain reaction (qRT-PCR)[2] as using RETROscript RT® (Ambion, Austin, TX, USA) and SYBR® Green PCR Master Mix (Applied Biosystems, Foster City, CA, USA). Oligo forward and reverse primers have been designed and optimized for AMACR (5'- agctggccacgatatcaact -3', 5'-ggcatacggattctcaccac-3'). Expression will be normalized to four housekeeping genes; TATA-box binding protein (TBP), hypoxanthine phosphoribosyl transferase 1 (HPRT1), beta-actin, and beta-2 microglobulin (B2M). qPCR will be run and analyzed on the Applied Biosystems 7900HT Real-Time PCR System.We have successfully extracted RNA from macro dissected prostatic biopsies and have demonstrated a significant up regulation of AMACR mRNA in prostate cancer as against normal epithelium (**Figure 4**) consistent with previous reports [3, 4]

Primary Cell Cultures

We have developed protocols for generating primary cell cultures from normal and tumor areas from prostatectomy samples of our study subjects. We propose to use a small portion of apparently normal and tumor regions sampled at the time of grossing to develop these cell cultures. These cell cultures are different from cell lines by virtue of their limited doublings. Details about the protocol for developing primary cultures are available in Appendix C. Primary cell cultures are valuable *in vitro* model systems to study cancer prevention and treatment strategies. We have IRB approval to develop these cell culture systems and currently have primary cell cultures growing for 5 subjects.

Key Research Accomplishments

A summary list of key research accomplishments is listed below:

Establishment of a secure database for subject and sample tracking

Organization of research data

Recruitment of subjects

Digitized web slide database

Image analysis development for quantifying AMACR protein expression in tissue

Protocols for procuring AMACR mRNA expression in formalin fixed paraffin embedded samples.

Primary cell culture systems

Reportable Outcomes

Poster Presentations

Ananthanarayanan V, Deaton RJ, Poon R, Gann PH. Validation of Automated Image Analysis Methods for Evaluation of AMACR Expression in Prostate Biopsies with High Grade Prostatic Intraepithelial Neoplasia. AACR International Conference on Frontiers in Cancer Prevention Research, ,2007

Oral Presentations

January 2008	Quantitative Imaging Cytometry Symposium, Cold Spring Harbor Laboratory, NY.
February 2008	Prostate Cancer Research Working Group Seminar, University of Illinois at Chicago.

Conclusions

There is a crucial need to identify the biological pathways through which diet affects prostate carcinogenesis. Results of this study could help define important causal links between suspected dietary risk factors for prostate cancer and clinically relevant biomarkers like AMACR. Earlier studies have shown that increased AMACR expression in the normal prostate could be a characteristic of high-risk tissue. If our results confirm a link between diet and AMACR expression, the following inferences will be strengthened: 1) the associations between red meat and dairy intake and prostate cancer risk will be more biologically plausible, leading to the possibility of dietary risk reduction and better identification of high-risk men, and 2) the phytanic/pristanic acid/AMACR pathway will be a more enticing target for discovery of chemopreventive and possibly therapeutic agents. This project could make a number of methodological contributions as well, including the determination as to whether simple food frequency questionnaires or serum samples are capable of predicting tissue levels and whether advanced image analysis techniques provide an important advantage in evaluating pre-malignant changes in tissue. So far, we have recruited 19 participants on the study. In order to facilitate recruitment, we are planning on opening the study at Loyola University Medical Center (LUMC). Dr. Flanigan is the chair of Urology at LUMC and performs approximately 80-90 radical prostatectomy surgeries annually. If we add LUMC as another site for recruitment then we can substantially improve the recruitment process. All laboratory assays for blood and tissue processing have been standardized. Assays for measurement of phytanic acid have been developed and need to be validated on actual patient samples. Sophisticated state of the art image analysis tools are available for quantifying AMACR expression at the protein level using immunofluorescence and immunohistochemistry.

References

1. Ananthanarayanan V, Deaton RJ, Yang XJ, Pins MR, Gann PH: Alpha-methylacyl-CoA racemase (AMACR) expression in normal prostatic glands and high-grade prostatic intraepithelial neoplasia (HGPIN): association with diagnosis of prostate cancer. *Prostate* 2005, 63:341-346.

2. Nonn L, Peng L, Feldman D, Peehl DM: Inhibition of p38 by vitamin D reduces interleukin-6 production in normal prostate cells via mitogen-activated protein kinase phosphatase 5: implications for prostate cancer prevention by vitamin D. *Cancer Res* 2006, 66:4516-4524.

3. Zhou M, Chinnaiyan AM, Kleer CG, Lucas PC, Rubin MA: Alpha-Methylacyl-CoA racemase: a novel tumor marker over-expressed in several human cancers and their precursor lesions. *Am J Surg Pathol* 2002, 26:926-931.

4. Jiang Z, Wu CL, Woda BA, Iczkowski KA, Chu PG, Tretiakova MS, Young RH, Weiss LM, Blute RD, Jr., Brendler CB, et al: Alpha-methylacyl-CoA racemase: a multi-institutional study of a new prostate cancer marker. *Histopathology* 2004, 45:218-225.

Appendix

- **Section A – Blood Processing Protocol**
- **Section B- Tissue Processing Protocol**
- **Section C- ImPACT Poster**
- **Section D- Prevention AACR Poster**
- **Section E – Bibliographic Material**

AMACR Blood Processing Protocol

Collect blood in one 15ml red capped tube and multiple 6ml purple top tubes. Total amount of blood collected will be approximately 45ml.

15ml Red Top – Serum Separation

- First of all, transfer blood from Vacutainer tube to a 15ml corning tube, before the sample clots. (The centrifuge will not close if a 15ml Vacutainer is used)
- Centrifuge at 3000 rpm for 15 min to separate the serum.
- Aliquot the serum into 0.2 ml aliquots
- Label tubes
- Freeze at -80c

20ml Purple Top (or multiple 6ml purple top tubes) – Plasma, WBC and RBC Separation

- 6ml gets separated for WBC harvesting (described below).
- Transfer the rest into a 15ml corning tube. Centrifuge at 3000 rpm for 15 min to obtain plasma. Separate plasma into four 2ml cryovials.
- Separate the RBCs into another corning tube. Wash multiple times in PBS. Centrifuge at 1200 rpm for 10min. Discard the supernatant and freeze the RBCs into multiple aliquots.

WBC Harvesting

- Sigma Procedure # 1119
  - Using a 15ml tube, add 4ml of Histopaque-1119(in the 4° fridge)
  - Carefully, layer 4ml of Histopaque-1077 onto Histopaque-1119.
  - Carefully layer 6ml of whole blood on top of Histopaque-1077.
  - Centrifuge at room temperature at ~2000rpm for 50 minutes.
  - Collect the mononuclear cell layer (above Histopaque-1077) and the granulocyte layer (between the 2 Histopaque layers). {First separate them into 2 tubes and mix if there is no RBC contamination. There are chances of RBC contamination when one is trying to get to the PMN layer).

- Transfer them into one 15ml tube.
- Wash the cells in PBS (bring it to 12-13ml mark) and centrifuge for 10 minutes at 1200rpm.
- Discard the supernatant.
- Resuspend the cells with 9ml of (PBS 0.1mM DFO & 0.1mM DTPA) solution. [To prepare this solution - add 2ul of DFO (500mM) and 2ul (500mM) of DTPA to10ml of PBS. See pg 3 for DFO and DTPA preparation].
- Centrifuge for 10 minutes at ~1900rpm.
- Discard the supernatant.
- The pellet from the previous step is re suspended in 3ml of freezing mix. Freezing mix is a mixture of 90% Fetal Bovine Serum and 10% DMSO. (i.e 2.7ml of FBS and 0.3ml of DMSO).
- Aliquot into six 0.5ml cryovials.
- Place into RT 'Mr.Freeze' and transfer to -80c. Samples stay at-80c O/N and are subsequently transferred to liquid N2 next day.

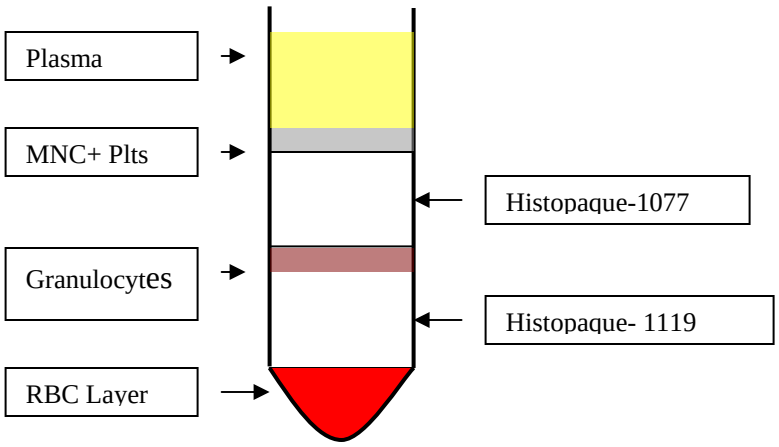

Reagents for WBC separation

1. Deferoxamine Mesylate, desferal (DFO) 500mM Stock (500mM DFO)

- Use 1 vial (1gm) of DFO salt (Sigma-D9533)
- Add 3.0 ml of Nuclease free water (Fisher-BP 561-1)
- Filter into sterile tube and store at 4c upto 1-2 months.

2. Diethylenetriaminepentaacetic acid (DTPA) 500mM stock (500 mM DTPA):D6518-10G, DTPA FW =393.35, prepare 10ml of 500mM stock:

Weight [g] =393.35gx0.5Mx0.01L=1.96675g

- DTPA 1.96675g
- Nuclease free water ~ 7 ml
- Stir at RT for 1 hr. Check pH. Titrate with 10 N NaOH (dissolve 10.25gm of Sodium hydroxide pellets in 25ml of distilled water). Observe changes of pH. Initial pH=2.27, addition of ~ 2000ul of 10 N NaOH changes ph to7.6. DTPA was completely dissolved. In my case, DTPA was completely dissolved at a much higher pH (8.1).
- Add additional water to make solution to 10ml.
- Filter into sterile tube and store at 4c upto 1-2 months.

3. PBS+ 0.1mM DFO +0.1mM DTPA (PBS-DFO/DTPA)

Prepare fresh 10ml, for complete wash of each sample.

To prepare this solution add 2ul of DFO (500mM) and 2ul (500mM) of DTPA to10ml of PBS.

SUMMARY

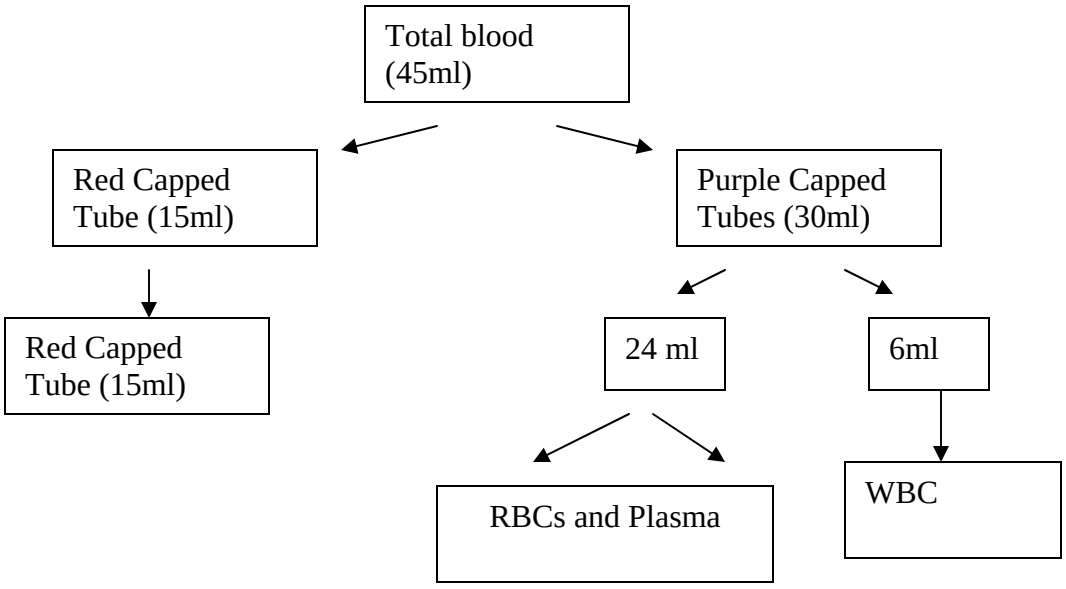

Section B - Prostate Grossing Protocol

- Radical prostatectomy specimen is received fresh and unfixed from the OR.
- Weigh and measure the prostate in three dimensions. Measure the seminal vesicles and vas deferens (length x diameter). Orient the specimen so that right and left, anterior and posterior, superior and inferior may be identified.
- Examine the outer surface for smoothness, irregularity and disruption of the capsule. Record the exact location of the abnormal areas.
- Remove any staples or sutures.
- Ink the outer surfaces with orienting colors (black indicating the right side and blue the left side).
- Amputate the seminal vesicles, and submit the basal section of each one, at its junction with the prostate for paraffin embedding. The apex and base are amputated at a thickness of 4-5 mm. These are then cut into sagittal sections and submitted in its entirety for paraffin embedding (See Diagrammatic representation below).
- The remaining prostate is sectioned at 3mm intervals starting at the distal urethra, 2-3 mm thick, using a blade to create parallel transverse sections perpendicular to the long axis. The first level (subsequent to apex) will be Level 1 and subsequent levels 2, 3, etc.
- Line prostate slices up in an anatomic sequence, onto a labeled and oriented sheet. Identify and describe any lesion of the parenchyma.

- Make sure there is enough tissue for histological diagnosis before taking any slice for research. Thereafter, select slices 1, 3, 5, etc. for permanent histology and slices 2, 4, 6, etc. for the study. In the event of the odd numbered slices showing gross tumor and the even numbered slices not showing tumor, sample a small piece of tumor (5mmx 5mm) for studying AMACR RNA expression in tumor.
- Mark each slice selected for research at 12 o'clock with a drop of hematoxylin for future orientation. Proceed to strip off the capsule from each slice, leaving at least 2mm of underlying parenchyma attached. Make 2 nicks at 12'o and 6'o clock positions to obtain separate fragment representing the right and left portions of the capsule. These capsular fragments are to be submitted entirely for paraffin sectioning to rule out presence of capsular invasion.
- Odd numbered slices (i.e. Levels 1, 3, 5 etc) are further sectioned into four quadrants each- Right anterior, right posterior, left anterior, left posterior. These quadrant sections are submitted for paraffin embedding and sectioning.
- To obtain tissue for generating primary cell cultures obtain two $3mm^2$ punches/ sections from apparently normal looking peripheral zones and tumor areas. The research slices from where these tissue pieces are sampled are marked with ink to facilitate subsequent histologic identification of the tissue surrounding the punch. These tissues will be dissociated into cell suspension. Cells may be cultured to select for either epithelial or stromal fibroblasts or both. To select for epithelial cells, the cells are plated onto collagen-coated dishes in specialized serum-free medium. To select for stromal fibroblasts, the cells are plated onto normal culture dishes in a specialized serum-containing medium. The success rate for viable cell

cultures from this protocol is 80 % for normal cultures and 50 % for cancer cultures. The cell types are verified by expression analysis of cytokeratin and epithelial cell markers. The fresh cells are frozen in liquid nitrogen in 50 or more aliquots for future research use. Once thawed, the cells have ~15-40 population doublings.

- Place remaining sections meant for the AMACR study, in appropriately labeled Ziploc (specimen) bags. Transfer it to dry ice and 100% ethanol slurry as soon as possible. Do not section into quadrants.
- The hematoxylin dot will be used for future orientation. These levels will be further sectioned based on the histology of the adjoining paraffin sections. For example, if quadrant A3 (see diagram below) shows only normal tissue then FSA7 quadrant (cut from FS–level 2) will be used for estimation of tissue phytanic and pristanic acid.
- For AMACR RNA, LCM will be performed on sections showing both normal and tumor areas. Sections on which LCM are to be performed, will be brought out of -80c and kept on dry ice. These will then be placed in the cryostat, and allowed to equilibrate to -20c and sections will then be cut onto slides. Unused slides and remaining tissue sample will be transferred back to -80c freezer.

APPENDIX C

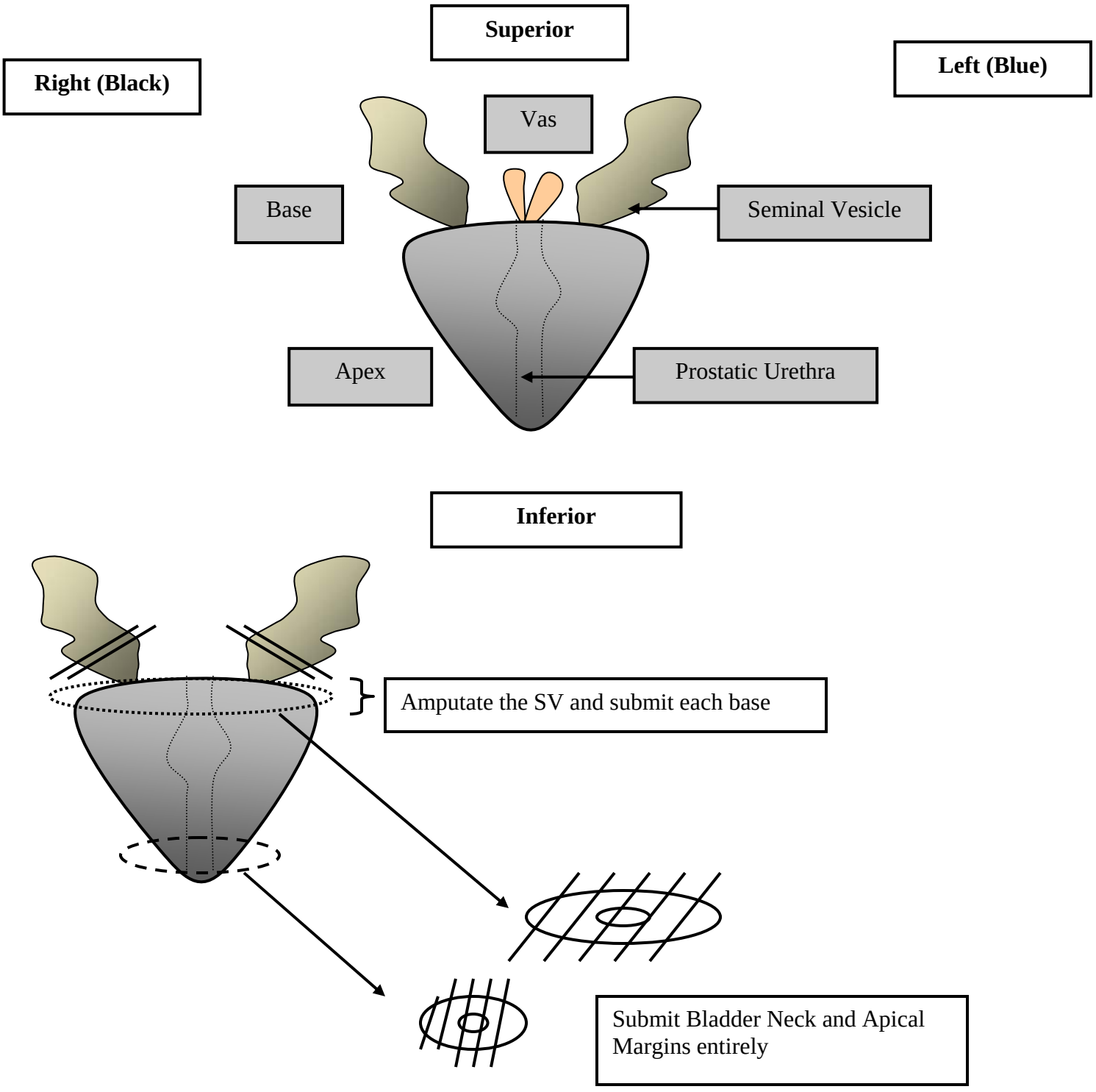
Superior
Right (Black)
Left (Blue)
Vas
Base
Seminal Vesicle
Apex
Prostatic Urethra
Inferior
Amputate the SV and submit each base
Submit Bladder Neck and Apical Margins entirely

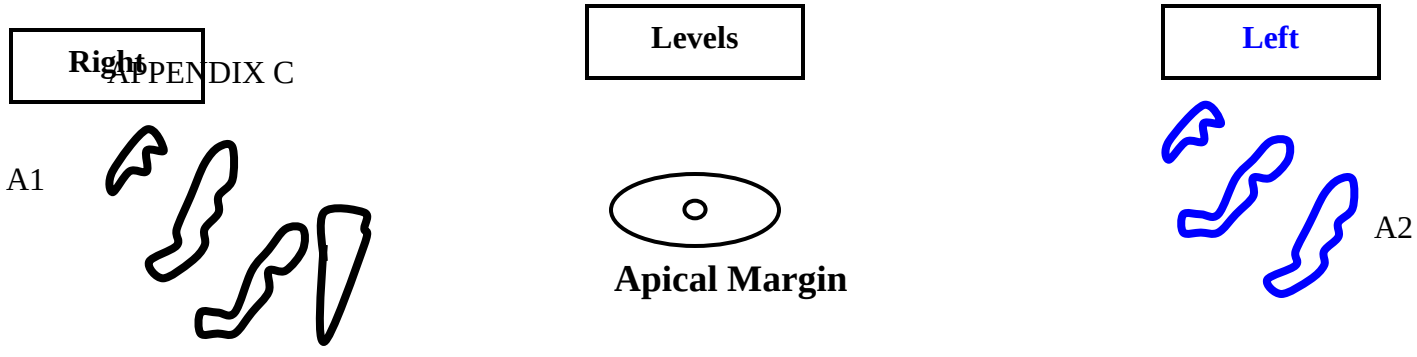
Right
Levels
Left
A1
A2
Apical Margin

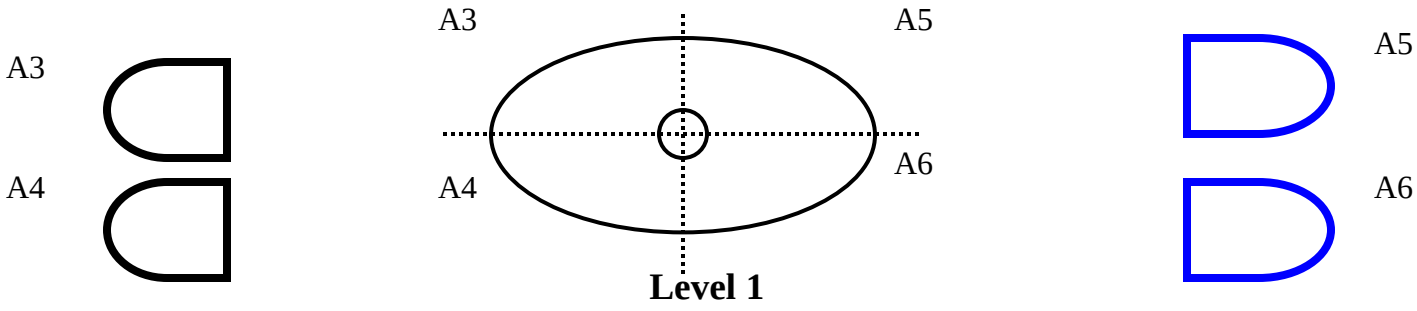
A3
A5
A3
A5
A4
A6
A4
A6
Level 1

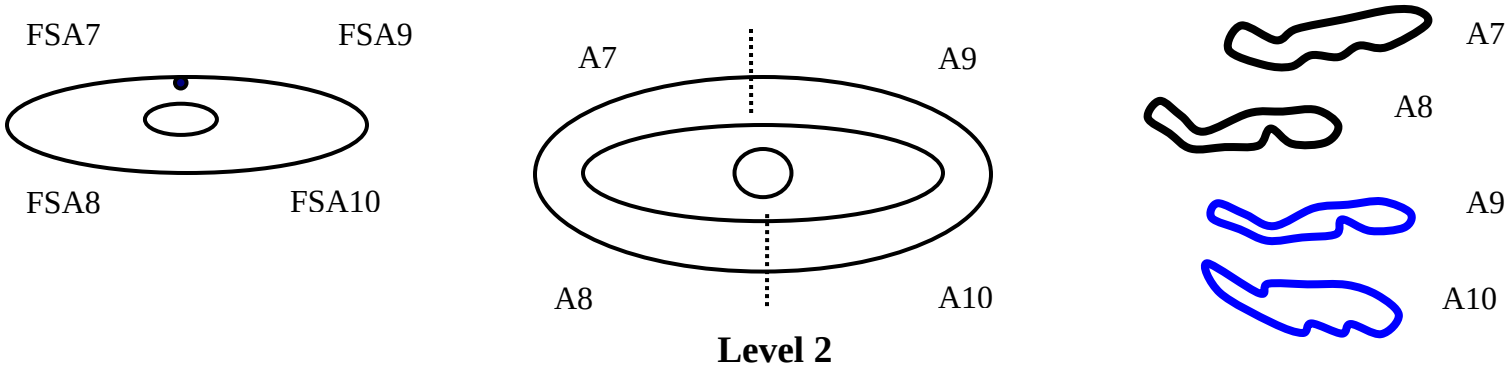
FSA7
FSA9
FSA8
FSA10
A7
A9
A8
A10
A7
A8
A9
A10
Level 2

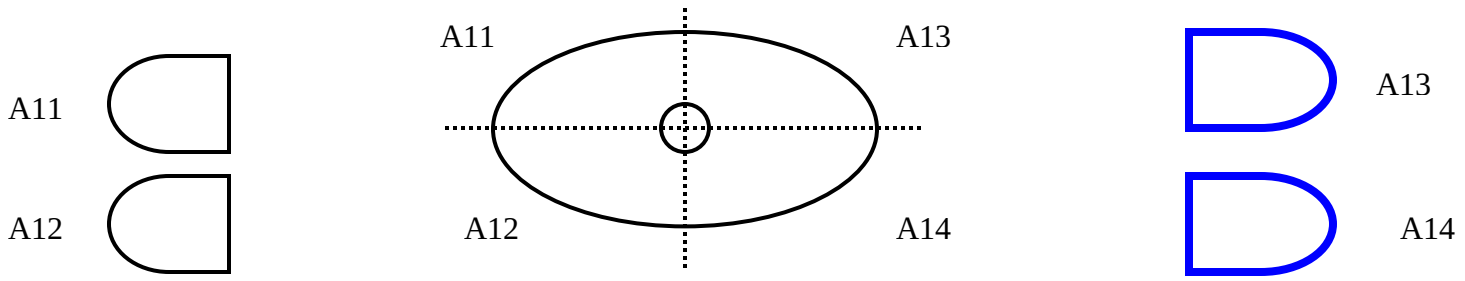
A11
A13
A11
A13
A12
A14
A12
A14
Level 3

APPENDIX C

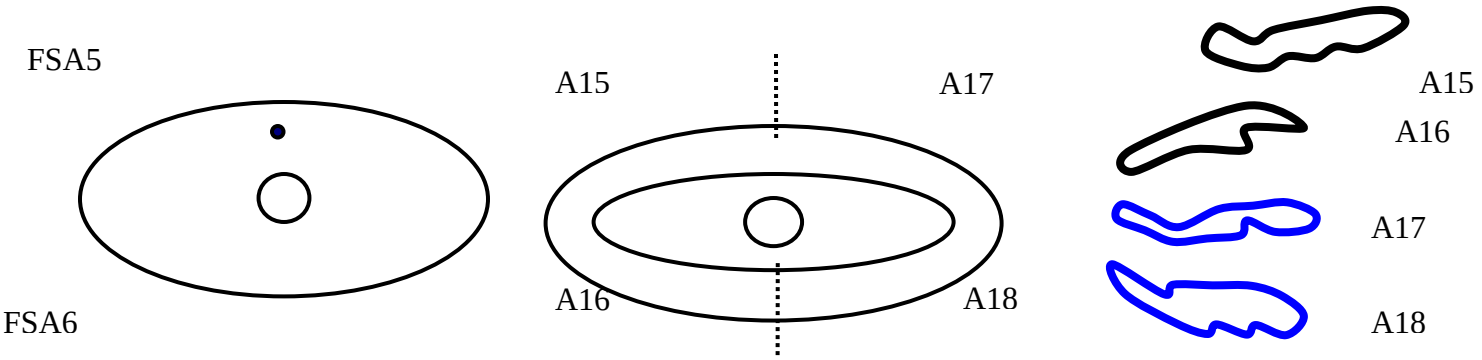

Level 4

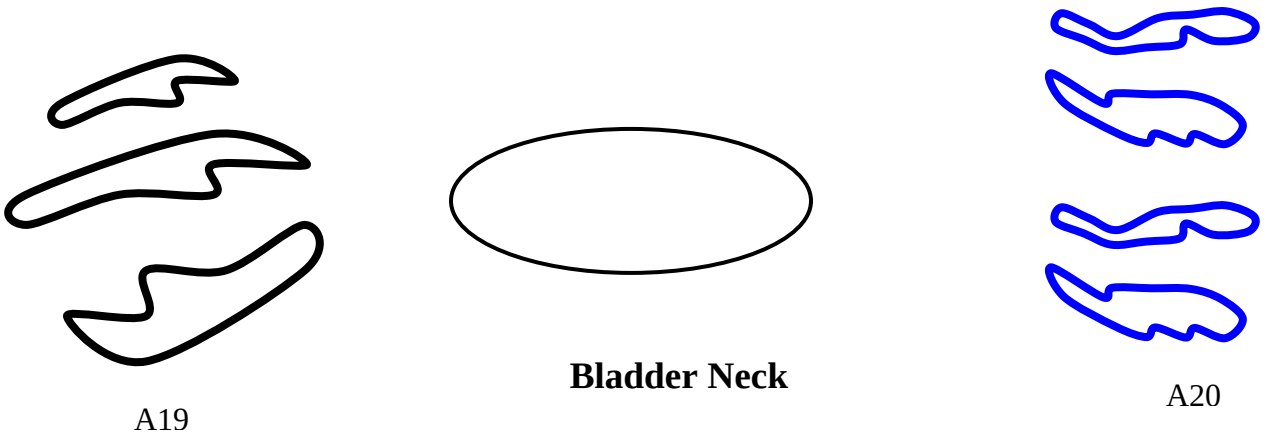

Right SV Base

Left SV Base

APPENDIX C

Template for Reporting
Gross Description

Radical prostatectomy specimen is received fresh and unfixed, consisting of prostate and attached seminal vesicles. The prostate weighs _____ gm and measures _____ x _____ x _____ cm. The left seminal vesicle measures _____x _____ cm and the right _____ x _____ cm, both with no grossly identifiable lesion. Vasa deferentia are unremarkable and measure _____ x _____ cm. The external surface _____.
After removal of sutures and staples, the outer surface is inked with orienting colors: blue on the left and black on the right side. Seminal vesicles, apex and base are amputated and the prostate is then serially sectioned at 2-3 mm intervals, into _____ levels, starting at the distal urethra and excluding apical and basal margins. The parenchyma _____
_____
_____.
Levels _____ are submitted for histological diagnosis and levels _____ are reserved for the AMACR study. The specimen is submitted according to the accompanying diagram.

Cassette designation (For paraffin embedding):

A1-A2	Apical margin
A3	Level 1 Right Anterior Quadrant
A4	Level 1 Right Posterior Quadrant
A5	Level 1 Left Anterior Quadrant
A6	Level 1 Left Posterior Quadrant
A7	Level 2 Right Anterior Capsule
A8	Level 2 Right Posterior Capsule
A9	Level 2 Left Anterior Capsule
A10	Level 2 Left Posterior Capsule
A11	Level 3 Right Anterior Quadrant
A12	Level 3 Right Posterior Quadrant
A13	Level 3 Left Anterior Quadrant
A14	Level 3 Left Posterior Quadrant
A15	Level 4 Right Anterior Capsule
A16	Level 4 Right Posterior Capsule
A17	Level 4 Left Anterior Capsule
A18	Level 4 Left Posterior Capsule
A19-A20	Bladder Neck Margin
A21	Right Seminal Vesicle Base and Vas Deferens
A22	Left Seminal Vesicle Base and Vas Deferens

APPENDIX C

Automated Digital Analysis of Tissue Microarrays with Brightfield and Laser-Based Systems: Application to Subcellular Localization of P27 and Prostate Cancer Recurrence

Vijayalakshmi Ananthanarayanan[1], Ryan J. Deaton[1], Ed Luther[2], Lindsay Gallagher[1], Vicki Macias[1], Andre Balla[1], Peter H. Gann[1]. [1]Department of Pathology, University of Illinois at Chicago, [2]Compucyte Corporation, Cambridge, MA

Abstract No.158

Abstract

Automated analysis of immunostained tissue microarrays (TMAs) can provide more rapid, sensitive and reproducible results than manual scoring. We are developing two novel approaches: one using standard brightfield microscopy (ScanScope®, Aperio Corp.) and one using laser scanning cytometry (LSC) with fluorescence (iCyt®, CompuCyte). Several groups have reported that decreased nuclear expression of the cell cycle inhibitor p27 is an independent predictor of prostate cancer (PCa) recurrence; recent data also suggest that cytoplasmic (cyto) translocation indicates lost function. We are analyzing TMAs, provided by the Cooperative Prostate Cancer Tissue Resource, containing quadruplicate tumor samples from 202 patients with PSA recurrence, matched 1:1 (for year of surgery, race, age, Gleason score and stage) with samples from patients without recurrence. For brightfield analysis, TMA sections are immunostained with DAB chromagen and counterstained with hematoxylin. Epithelial nuclei are identified by segmentation and size/shape filtering algorithms, and nuclear p27 score is calculated as the sum optical density (OD) that is DAB-positive (brown) over total nuclear area. A cyto p27 score is derived by subtracting nuclear brown from total brown OD and dividing by epithelial area determined by pancytokeratin staining of an adjacent section. For LSC analysis, sections are triple-stained with fluorophores for nuclei (DAPI), pancytokeratin (Cy5) and p27 (Alexa488), and scanned by 3 separate lasers. Thousands of phantom dots (pseudo-objects slightly bigger than nuclei) are randomly placed on the images and co-localization of cyto within each phantom is recorded. Phantoms are then displayed on scatterplots similar to those used in flow cytometry, to identify phantoms containing epithelial tissue, and within that subset, phantoms with either nuclear or cyto predominance. The distributions of fluorescence intensity for p27 within these "nuclear" and cyto" phantoms are the primary data output. For each histospot we obtain both a nuclear and cyto index (% of phantoms times mean fluorescence), and a Kolmogorov-Smirnov statistic. Preliminary results from 84 case-control sets using the brightfield system showed higher nuclear p27 and higher cyto:nuclear ratio among cases (borderline significance) and no difference in cyto p27. In early LSC results from 42 patient pairs, cases had higher cyto, lower nuclear, and higher cyto:nuclear ratio compared to controls; however, differences did not reach statistical significance. The K-S statistics for nuclear, cyto and cyto:nuclear ratio were also in the hypothesized direction but not significant. Completion of this project will allow comparison of both methods to manual scoring, and differences between methods will be resolved in an effort to standardize automated scoring of TMAs.

Background

•Potentially, automated analysis of immunostained tissue microarrays (TMAs) can provide more rapid, sensitive and reproducible results than manual scoring.

•We are developing two novel approaches: one using standard brightfield digital microscopy (ScanScope®, Aperio Corp.) and one using laser scanning cytometry (LSC) with fluorescence (iCyt®, CompuCyte) for automated scoring of tissue images.

•Several groups have reported that decreased nuclear expression of the cell cycle inhibitor p27 is an independent predictor of prostate cancer (PCa) recurrence [1-3]. A recent study also suggested that cytoplasmic translocation indicates lost p27 function and higher risk of recurrence[4].

•In this study, we compare these two automated methods vs. manual scoring on a set of TMAs containing matched pairs of patients (n=202 pairs total) with and without PCa recurrence. We also evaluated a computer-assisted method with the digital microscope, in which a pathologist used a draw tool to exclude non-cancer areas on each histospot.

Research Questions

1. How reproducible is each method for measuring nuclear p27, cytoplasmic p27 and the cytoplasmic:nuclear ratio?

2. What is the relationship of p27 expression to PCa grade, stage and pre-surgical PSA for each method?

3. What is the relationship between p27 expression and PCa recurrence for each method?

Methods

Tissue Microarrays. We obtained 5 TMA blocks from the Cooperative Prostate Cancer Tissue Resource, with quadruplicate 0.6 mm diam. tumor samples from a total of 202 patients with PSA recurrence, matched 1:1 (for year of surgery, race, age, Gleason score and stage) with samples from patients without recurrence. Case-control pairs were placed within the same TMA block, scattered within a block to reduce the effect of any regional staining variation.

Tissue staining. For brightfield analysis, TMA sections (4μ thickness) were immunostained with DAB chromagen and counterstained with hematoxylin. For fluorescent LSC analysis, adjacent sections were triple-stained with fluorophores for nuclei (DAPI), pancytokeratin (Cy5) and p27 (Alexa488), and scanned by 3 separate lasers. Laser and photomultiplier detector settings were optimized to reduce interference by autofluorescence.

Manual scoring. A single pathologist, blinded to case-control status, scored each histospot for both nuclear and cytoplasmic p27. Nuclei were marked as positive or negative. The % of cytoplasm area at each of 3 stain intensity levels (0-3) was recorded. Scoring measures were: % strong positive nuclei, % total positive nuclei, cytoplasmic staining index (% multiplied times staining level, summed), and the nuclear:cytoplasmic staining ratio.

Brightfield digital microscopy (BDM) analysis. TMA slides immunostained for p27 were scanned at 400x on a Scanscope CS® digital microscope. We used a color co-localization algorithm (Aperio) to classify each pixel as containing dark blue (negative nuclear), dark blue and brown (positive nuclear), and brown only (positive cytoplasmic). This approach does not require the software to recognize and segment objects such as nuclei.

$$\text{Nuclear p27 score} = \frac{\#\ pixels[(Blue / Brown)}{\#\ pixels[(Blue + Blue / Brown)}$$

Mean p27 intensity = average optical density of all Brown pixels

$$\text{Nuclear/cytoplasmic ratio} = \frac{\#\ pixels[(Blue / Brown)}{\#\ pixels[(Brown)}$$

In a fully automated analysis (BDM-Auto), these scoring algorithms were run on all tissue areas on all spots from all 5 TMAs. In a computer-assisted analysis (BDM-Assist), a pathologist used a draw tool to exclude areas of non-cancer epithelium and stroma from each spot on a single TMA (TMA1) before scoring.

Figure 1. Aperio IHC and Markup images of a representative P27 stained spot

Laser scan cytometry scoring. All TMAs were scanned at 400x on the iCyts® LSC. This system can obtain quantitative data by "phantom contouring", in which thousands of phantom circles (pseudo-objects slightly bigger than nuclei) are randomly placed on the images in a dense array and co-localization of color within each phantom is recorded. Phantoms, treated as individual objects, are then displayed on scatterplots similar to those used in flow cytometry, and gating is used to isolate epithelial phantoms (containing cytokeratin, RED) (**Figure 2a**).

Image algebra is then performed after splitting the composite image into 3 grayscale images that show optical density in each color channel (RED = cytokeratin, BLUE = DAPI, GREEN = p27) (**Figure 2b**).

To obtain a pure nuclear p27 image, the cytokeratin image is subtracted from the p27 image; to obtain a pure cytoplasmic p27 image, the DAPI image is subtracted from the p27 image. The same phantoms are then "dropped" on these pure nuclear or cytoplasmic p27 images, and the integrated fluorescence intensity of p27 (GREEN) within each phantom is recorded. The frequency distribution of p27 intensity in all the epithelial phantoms per histospot provides the basic raw data for analysis (**Figure 2c**).

Figure 2.

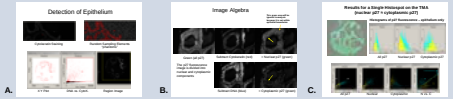

Data Analysis

Data analysis. For LSC and BDM-Auto, results were available from all 5 TMAs; for BDM-Assist and Manual, results only for TMA1. Reproducibility was assessed by computing the CV (coefficient of variation, sd/mean) for each subject across all of their cores, and then obtaining the mean/median CV per subject. The Intraclass Correlation Coefficient (ICC), which is the proportion of total variance attributable to between- as opposed to within-subject variation, was computed by variance components analysis with a hierarchical linear model with random effects (PROC MIXED in SAS®). Methods were compared for TMA1 by scatterplots and calculation of Spearman correlation coefficients at the subject level. The association of p27 scores with Gleason grade, PSA and stage was evaluated by means and 95% CIs across grade/stage/PSA categories and independent t-tests. The association of p27 scores with PCa recurrence was evaluated by paired t-tests comparing matched cases and controls, and for LSC by conditional logistic regression models to obtain Odds Ratios and 95% CIs, after placing each subject within a quartile based on the scores for all subjects.

Results

Table 1 shows the characteristics of the PCa patients contributing samples to the TMAs. For details regarding this CPCTR TMA, see www.cpctr.cancer.gov.

Table 2 shows the mean and median CVs and ICCs per subject for each method. CVs were relatively high for all methods and measures, with the exception of Mean p27 Intensity for BDM-Auto and BDM-Assist. Nuclear and cytoplasmic scores were moderately-strongly correlated *within* automated method. When metrics were comparable across methods, positive correlations from weak-strong were observed (e.g., LSC-cyt vs. Man-cyt, r = 0.16, LSC-nuc vs. BDM-Assist mean p27, r = 0.29, Man-nuc% vs. BDM-Assist nuc%, r = 0.86). The ICCs for LSC were large for all metrics but ratio.

Table 1. Selected Characteristics of Patients

	Controls (n=202)	Case (n=202)
Age (Median)	64	64
Race		
Caucasian	181	181
African-American	20	20
Asian	1	1
Tumor Stage		
pT_{2a}	1	1
pT_{2c}	17	16
pT_{3b}	117	118
pT_{3c}	61	61
pT_{3b}	6	6
Gleason Categories		
Gleason Score <7	49	49
Gleason Score = 7 (3+4)	103	103
Gleason Score = 7 (4+3)	31	31
Gleason Score ≥ 8	19	19

Table 2. Mean CV and ICC for p27 Measurements by All Methods

Method	Measure	CV Mean (95%CI)	ICC
BDM-Auto			
	Nuclear	23.18 (20.77, 25.58)	0.75
	MeanP27Intensity	3.31 (3.03, 3.59)	0.80
	Ratio	30.10 (20.77, 25.59)	0.46
BDM-Assist			
	Nuclear	39.47 (33.74, 45.21)	0.57
	MeanP27Intensity	2.46 (2.08, 2.83)	0.55
	Ratio	34.67 (30.60, 38.73)	0.60
Manual			
	Nuclear	27.61 (21.80, 33.41)	0.51
	Cytoplasmic	52.92 (42.63, 63.21)	0.52
	Ratio	52.54 (42.67, 62.40)	0.48
LSC			
	Nuclear p27	31.55 (29.27, 33.83)	0.58
	Cytoplasmic p27	29.42 (27.15, 31.68)	0.66
	Ratio	65.92 (61.70, 70.13)	0.07

Figure 3. Mean and 95% CI for Nuclear p27 Scores by A.) BDM-Auto, B.) BDM Assist, C.) Manual, D.) LSC Methods

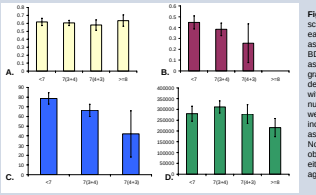

Figure 3 shows the mean nuclear p27 scores across Gleason grade levels for each method. BDM-Auto was not associated with grade by any measure. BDM-Assist showed a weak inverse association between nuclear p27 and grade. Manual scoring showed a definite downward trend in nuclear p27 with increasing grade. For LSC, total, nuclear and cytoplasmic p27 scores were significantly lower as grade increased. No ratio measures were associated with grade by any method. No associations by any method were observed between p27 scores and either PSA or tumor stage, in agreement with an earlier study[1].

Table 3 presents the Odds Ratios for PCa recurrence associated with successive quartiles for LSC metrics. There was a significant downward trend for risk of recurrence with increasing nuclear or cytoplasmic p27

Table 3. Odds Ratios and 95% CIs for Prostate Cancer Recurrence by Quartile of p27 Expression, Measured by Laser Scanning Cytometry*

	Quartile 1 OR (95%CI)	2 OR (95%CI)	3 OR (95%CI)	4 OR (95%CI)	P Trend
Nuclear p27	**1.00**	**0.61** (0.24, 1.55)	**0.68** (0.26, 1.80)	**0.42** (0.18, 0.98)	0.04
Cytoplasmic p27	**1.00**	**0.85** (0.35, 2.06)	**0.58** (0.27, 1.24)	**0.39** (0.18, 0.84)	0.01
Nuclear: Cytoplasmic Ratio	**1.00**	**0.90** (0.43, 1.86)	**1.80** (0.89, 3.64)	**1.91** (0.99, 3.66)	0.02
Total p27	**1.00**	**0.83** (0.39, 1.77)	**0.46** (0.21, 1.01)	**0.50** (0.22, 1.14)	0.05

*Adjusted for age, grade and stage by matching, and for PSA by conditional logistic regression

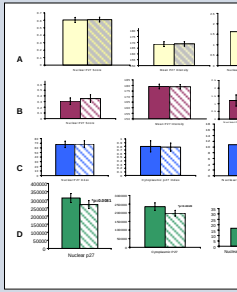

Figure 4 shows the means and 95% CIs for cases vs. controls for each method (**A**) BDM-Auto, **B**) BDM-Assisted, **C**) Manual, **D**) LSC] The only significant differences observed were for the LSC method: both nuclear and cytoplasmic p27 was greater in controls than cases; the nuclear:cytoplasmic ratio was not different. For Manual, controls had slightly higher strong nuclear scores, but the differences could easily be explained by chance. The BDM-Auto method found no differences between cases and controls, whereas the BDM-Assist method found that cases has a non-significant increase in nuclear score and a non-significant decrease in Nuc:Cyt ratio.

Conclusions

•The LSC was the only approach that demonstrated loss of nuclear p27 in patients with PCa recurrence, a finding that has been reported by several groups. Importantly, this association is independent of tumor grade and stage.

•None of the methods, including LSC, found evidence to support the importance of the nuclear:cytoplasmic ratio (or of cytoplasmic translocation) in PCa progression or recurrence

•Inverse associations between nuclear p27 scores and Gleason grade were detectable by LSC, manual scoring and Brightfield Digital Microscopy (only when non-cancer areas were deleted)

•The variation between histospots from each individual tumor is substantial regardless of method; this argues for the importance of multiple samples (4 histospots per tumor here).

•Tissue heterogeneity in TMAs is a major concern for automated analysis, especially when tumors are small and infiltrated with stroma (as most PCa are). Methods that can isolate epithelium are required.

Ongoing work includes:

Refined analysis of LSC results using Kolmogorov-Smironov statistics to quantify differences in distributions

LSC analysis of TMAs using the peripheral contour technique

LSC analysis of chromagen-stained slides based on light scatter and absorption

Refinement of Aperio scoring by using cytokeratin stain and a modified co-localization algorithm

References

1. Cote RJ, Shi Y, Groshen S, Feng AC, Cordon-Cardo C, Skinner D, Lieskovsky G. **Association of p27Kip1 levels with recurrence and survival in patients with stage C prostate carcinoma.** *J Natl Cancer Inst* 1998, **90**:916-920.

2.Freedland SJ, de Gregorio F, Sacoolidge JC, Ehrhmatt YI, Csathy GS, Elashoff DA, Reiter RE, Aronson WJ. **Predicting biochemical recurrence after radical prostatectomy for patients with organ-confined disease using p27 expression.** *Urology* 2003, **61**:1187-1192.

3.Yang RM, Naitoh J, Murphy M, Wang HJ, Phillipson J, deKernion JB, Loda M, Reiter RE. **Low p27 expression predicts poor disease-free survival in patients with prostate cancer.** *J Urol* 1998, **159**:941-945.

4.Li R, Wheeler TM, Dai H, Sayeeduddin M, Scardino PT, Frolov A, Ayala GE. **Biological correlates of p27 compartmental expression in prostate cancer.** *J Urol* 2006, **175**:528-532.

Dietary Influences on Alpha-MethylAcyl-CoA Racemase (AMACR) Expression in the Prostate

Vijayalakshmi Ananthanarayanan, Rachel Poon, Ryan J. Deaton, Erika Enk, Gayatri Borthakur, Rooholah Sharifi, Peter H. Gann.
[1]Department of Pathology, University of Illinois at Chicago, Chicago, IL.

UIC Department of Pathology, University of Illinois at Chicago, College of Medicine

Poster no. P18-10

Background

Alpha-MethylAcyl-CoA Racemase (AMACR), a peroxisomal and mitochondrial enzyme, involved in the racemization of phytanic and pristanic acids, is up regulated in most prostate cancers at the protein and mRNA level. This overexpression occurs so commonly in prostate cancer that immunostaining for AMACR is used clinically to resolve ambiguous biopsies. These fatty acid substrates of AMACR cannot be synthesized by humans and are derived through the ingestion of dairy and red meat products. Although some epidemiologic studies have shown associations between dairy/red meat ingestion and prostate cancer risk, no studies have examined the relationship between red meat and dairy intake, phytanic/pristanic acid levels in the blood and prostate tissue and AMACR expression. We postulate that men with higher intake of red meat and dairy food will have higher levels phytanic/pristanic acid in their blood and prostates and higher AMACR expression in their normal prostatic tissue. This study will help us understand whether the increased AMACR expression that occurs in prostate cancer is merely an epiphenomenon or whether it provides evidence for a causal link between dietary factors and prostate cancer risk.

The aims for this presentation are as follows:

1: To describe the overall design and protocol for this clinical study

2: To present preliminary data on the use of automated image analysis methods for evaluating AMACR expression in normal and high grade prostatic intraepithelial neoplasia (HGPIN) lesions in prostatic biopsies.

Study Aims

1: To study the association between dietary intake of red meat/dairy foods and AMACR expression (RNA and protein) in normal prostatic tisssue. Dietary measures of phytanic acid intake will be through the use of FFQ and 24 hr dietary recalls.

2: To estimate the association between dietary intake of red meat/dairy foods and phytanic/pristanic acid expression in the serum and normal prostatic tissue.

3: To measure the degree of association between serum/prostatic tissue phytanic acid levels and AMACR.

Enrollment

The study will recruit 60 patients with prostate cancer from the University of Illinois at Chicago (UIC) Hospital and the Jesse Brown Veterans Administration Medical Center (JBVAMC). All men with prostate cancer undergoing radical prostatectomy as a treatment are eligible to participate, provided they have not received neo-adjuvant or hormonal ablation therapy. Participants complete two research visits as shown in **Figure 1.**

Data and Biological Sample Collection

Participants complete a Block 98.2 Food Frequency Questionnaire (FFQ) in addition to a medical history questionnaire. The FFQ provides estimates of overall calorie intake and macronutrient composition of the diet and the data will allow us to accurately identify subjects with very high or very low intake of red meat and dairy foods.

Figure 1. Schematic Representation of Study Procedures

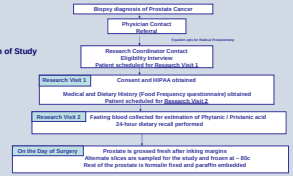

In addition to the FFQ, 24-hour dietary recall information will be collected using the NDS-R version 5.0_35 (Nutrition Coordinating Center, University of Minnesota). As the literature on pharmacokinetics of phytanic acid/pristanic acid metabolism is sparse, short-term and long-term dietary assessments might better reflect phytanic acid/ pristanic acid levels in blood and normal prostatic tissue. After surgery, the prostate is grossed fresh under sterile and nuclease free conditions. The prostate is then serially sectioned at 2-3 mm intervals starting from apex to base. Alternate slices are submitted for purposes of the study after stripping off the capsule and are stored at -80c. The rest of the prostate is submitted for routine pathology evaluation.

Figure 2 shows how the biologic samples are processed for the proposed assays

Figure 2. Proposed assays for Blood and Prostate

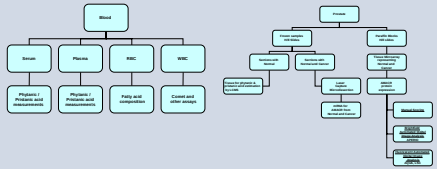

Participant Enrollment

To date, 12 subjects have consented to participate in the study; of which 9 are African-American, two are Caucasian and one is Hispanic. **Table 1** provides information about the recruitment status of these subjects.

Table 1: AMACR Study Recruitment Status

	Number of subjects
Evaluated for eligibility	**27**
Consented, on-study	**12**
Drop out, no tissue available at the end of study	**3**
Completed Study	**7**

Preliminary Data

One of our main aims is to quantify AMACR protein expression in both normal and cancer compartments. AMACR protein will be stained using standard immunohistochemical and immunofluorescent methods and quantified manually as well as using state of the art image analysis systems. Image analysis systems for quantification provide continuous and reproducible measurements especially at lower expression levels. We are developing two novel approaches: one using standard brightfield digital microscopy (ScanScope®, Aperio Corp.) and one using laser scanning cytometry (LSC) with fluorescence (iCys®, CompuCyte) for automated scoring of tissue images. Previously, we have shown that patients with higher expression of AMACR in their normal glands have a higher risk of subsequent biopsy being diagnosed with cancer.[1] Here, we present data on AMACR expression quantified using automated image analysis method, on this set of previously scored HGPIN biopsies

Materials and Methods

Samples

AMACR expression was studied in a biopsy set of 44 patients with HGPIN. 23 of these patients (Cases) had a subsequent biopsy diagnosis positive for cancer. The remaining 21 patients (Controls) were free of cancer on their subsequent biopsy.

Immunohistochemistry and Image Analysis

Sections were immunostained with a primary rabbit monoclonal antibody for AMACR using protocols described previously.[1] Immunostained biopsy slides were digitally scanned at 20x magnification using the ScanScope® (Aperio Corporation). Regions of interest (ROIs) were drawn around all normal and HGPIN glands, such that, areas of non-specific staining and stroma were excluded.

Scoring algorithms

The scanned slides were then scored using two algorithms, Co-Localization (CoLoc) and the Positive Pixel Count (PPC). The threshold limits for brown staining was kept between 0-200 units for both scoring methods.

AMACR expression by both methods was calculated as follows

CoLoc AMACR Score = Brown area x Average brown intensity / Total Stained area

PPC AMACR Score = [(Number of weak positive pixels x Average intensity of weak positive pixels) + (Number of moderate positive pixels x Average intensity of moderate positive pixels) + (Number of strong positive pixels x Average intensity of strong positive pixels)] / Total Stained area

Mean AMACR scores were computed at a 'person' or 'ROI' level.

Figure 3 shows images of normal (A) and HGPIN (B) glands with AMACR staining and the corresponding markup images for the CoLoc (C and D) and PPC (E and F) algorithms.

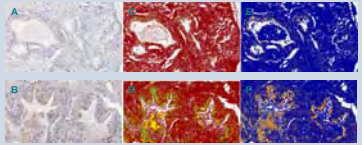

Results

Figure 4a shows results of AMACR expression by various methods at a person level. HGPIN glands in the cases had a higher AMACR expression than controls by the PPC and CoLoc methods. The results also approached significance for a case-control difference in the normal compartment by the PPC method. Manual scores at a person level did not show significant difference between cases and controls for either compartment.

Figure 4a. Mean AMACR staining per person with 95% CIs in normal and HGPIN glands by A) Manual B) CoLoc and C) PPC methods

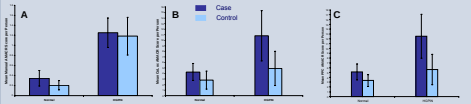

Figure 4b shows a significant difference in AMACR expression between cases and controls in the normal compartment by all three methods when the unit of analysis was a gland or a ROI. The difference in the HGPIN compartment was observed only for the automated methods

Figure 4b. Mean AMACR staining per gland/ ROI with 95% CIs in normal and HGPIN glands by A) Manual B) CoLoc and C) PPC methods

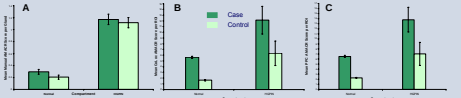

Conclusions

1: Mean AMACR score by the automated scoring algorithms was significantly higher in HGPIN glands than normal glands, consistent with previously reported literature.

2: Case-control difference in AMACR expression for the normal glands was observed at the ROI/gland level by all three methods.

3: Case-control difference in AMACR expression for the HGPIN glands at either level of measurement was observed only with the automated scoring methods.

4: Automated scoring methods provide continuous and reproducible measurements especially at low expression levels.

Other Ongoing work

- Development of assays for extraction of RNA from formalin fixed paraffin embedded blocks.
- Optimization of assays for measurement of phytanic/pristanic acid in the tissues and serum.
- Addition of Loyola University Medical Center as another study recruitment site.

References and Acknowledgements

1. Ananthanarayanan V, Deaton RJ, Yang XJ, Pins MR, Gann PH: Alpha-methylacyl-CoA racemase (AMACR) expression in normal prostatic glands and high-grade prostatic intraepithelial neoplasia (HGPIN): association with diagnosis of prostate cancer. Prostate 2005, 63:341-346.

We wish to acknowledge the important contributions of several individuals including Dr. Larisa Nonn, Lindsay Gallagher, Dr. David Hepps. Effort on this project was supported by the W81XWH-06-1-0414 grant from the Department of Defense.

Validation of Automated Image Analysis Methods for Evaluation of AMACR Expression in Prostate Biopsies with High Grade Prostatic Intraepithelial Neoplasia

UIC Department of Pathology, University of Illinois at Chicago, College of Medicine

Vijayalakshmi Ananthanarayanan, Ryan J. Deaton, Rachel Poon, Peter H. Gann Department of Pathology, University of Illinois at Chicago

Abstract

Automated image analysis (AIA) systems for quantification of immunostained tissue could provide more accurate and sensitive results than manual scoring by a pathologist. Previously we have shown that AMACR expression in normal glands from patients subsequently diagnosed with prostate cancer was higher than those who did not. No difference was observed for AMACR expression in HGPIN glands. In this study, we hypothesize that the difference in AMACR expression between the two subsets of patients might be better quantified using AIA.

Prostatic needle biopsies from 44 patients with HGPIN were immunostained for AMACR. 21 patients (cases) showed cancer on a later biopsy and 22 (controls) had no cancer and at least 3 negative biopsies. Immunostained slides were digitally scanned using the ScanScope CS ® (Aperio Technologies, CA). Regions of interests were drawn within benign and HGPIN compartments and scored using 'Positive Pixel Count™' algorithm. Separate scores for benign and HGPIN glands were computed as the product of percent area positive and mean intensity of staining. Manual scoring was performed on an ordinal scale of 0-3 intensity by a single pathologist.

For the normal compartment, the mean manual score per gland for the cases (0.29) was higher than that of the controls (0.21) [p=0.05]. AIA score for the normal compartment was higher in the cases than controls, but not significant (p=0.07). For the HGPIN compartment, mean manual score was 1.25 and 1.18 for the cases and controls respectively [p= 0.77]. However, AIA score within the HGPIN compartment of cases (12.52) was significantly higher than controls (5.62) [p=0.01].

The ability to discriminate HGPIN according to risk of subsequent cancer supports the hypothesis that AIA has enhanced sensitivity and biological validity. This method might provide improved measurements for research and clinical prediction.

Introduction

High grade prostatic intraepithelial neoplasia (HGPIN) is a putative pre-malignant lesion in the prostate. Molecular markers that predict progression to cancer in these lesions could therefore serve as attractive endpoints for Phase 2 chemoprevention trials and as clinically useful tests for risk stratification of patients with negative biopsies. Currently, expression of proteins and other *in situ* biomarkers is typically evaluated using immunohistochemistry coupled with manual scoring methods. Automated or computer-assisted image analysis (AIA) systems for quantification of such immunostained tissues could provide more accurate and cost-effective results, and in particular, may provide the sensitivity needed to evaluate subtle effects in non-malignant tissue in prevention studies.

In previously published data, we demonstrated that Alpha-Methylacyl-CoA Racemase (AMACR) expression in normal epithelium from negative biopsies, scored manually, was significantly higher in men who later developed prostate cancer compared to men who remained cancer-free. (Ananthanarayanan, 2005) However, no difference in AMACR expression was noted for the HGPIN glands. In the present work we determined whether these results could be re-capitulated when AMACR was scored by automated or computer-assisted methods.

Objectives

- How do AIA methods compare to the manual method for evaluation of AMACR expression in prostatic biopsies?
- Does AMACR expression using AIA in normal and HGPIN compartments differ between men who later develop prostate cancer and those who do not?
- What is the correlation between manual and AIA scores for normal and HGPIN glands?

Methods

Subjects

Forty-five patients with biopsies revealing isolated HGPIN (i.e., no cancer) were identified from medical records. *"Cases"* (n=23) were defined as patients who later had a biopsy positive for cancer. *"Controls"* (n=22) had no subsequent diagnosis of prostate cancer and at least 3 negative biopsies in total. The earliest biopsy with diagnosis of HGPIN was used for the study. Several important subject characteristics are shown in Table 1; subjects in both groups were comparable in terms of age.

Immunohistochemistry for AMACR

Two adjacent sections were cut from each paraffin block, the first was stained by Hematoxylin and Eosin and the second was immunostained for AMACR using a rabbit monoclonal antibody (Zeta Corp, P504S) at 1:100 dilution for ½ hr at room temperature. The reaction was developed using EnVision+ system (Dako) with DAB as the chromogen.

Scoring

Manual scoring

Immunostained slides were mounted with photo-etched cover slips containing 520 numbered grids each measuring 0.6 x 0.6 mm. All HGPIN glands and benign glands from ten grids selected by a random number generator were scored for AMACR intensity on an ordinal scale of 0-3.

Automated and computer-assisted image analysis scoring

Immunostained slides were digitally scanned at 20x magnification with a ScanScope CS® (Aperio Technologies, CA). The ScanScope generates high quality digital images of whole glass slides stitched together in a seamless fashion. The images can be viewed through the ImageScope™ application which is available for free download through http://aperio.com/. Scanning slides with gridded cover slips can cause problems with focusing. In the process of re-cover slipping these slides with regular cover slips we lost some sections. Some of the images produced were not optimal for further evaluation. Therefore, AIA data could be obtained only from 18 cases and 20 controls (Table 1). Regions of interest (ROIs) were drawn meticulously around normal and HGPIN glands with a digital pen tool. Areas of non-specific staining were excluded using the 'negative-pen' tool. ROIs were scored using the Positive Pixel Algorithm (PPC) ™. This algorithm classifies pixels as being negative, weakly, moderately or strongly positive depending on the intensity of staining. Thresholds were adjusted such that background staining was excluded. Examples of markup images generated after scoring with the PPC algorithm are depicted in Figure 1.

Figure 1 shows images of normal (A) and HGPIN (B) glands with AMACR staining and the corresponding markup images using PPC (C and D) algorithm.

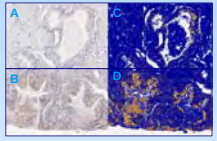

Automated score for AMACR was calculated as the summed product of staining intensity level (as a continuous variable from 0-255) times the percentage of tissue area (pixels) in each intensity level. Drawing ROIs is a labor intensive process; therefore, scoring was also performed without drawing ROIs (i.e. fully automated).

Statistical Analysis

Two types of AMACR scores were obtained. One was a mean AMACR staining per subject per compartment (i.e normal or HGPIN) and the other was a mean AMACR staining per gland or ROI per compartment. In addition, for the AIA, separate scores per person were also obtained when data were analyzed without ROIs. Ignoring the ROIs essentially adds stromal pixels to the denominator of the AIA score. Arithmetic mean scores and 95% confidence intervals were calculated and compared using t-tests

Results

Several important characteristics of the patients are shown in Table 1.

Table 1: Selected characteristics of the study group (mean ± standard deviation)

	Control		Case	
	Manual	Automated	Manual	Automated
n	22	20	23	18
Average age	65.2 ± 6.9	65.4 ± 7.0	64.5 ± 6.8	65.2 ± 6.2
Days between HGPIN and last biopsy	504.6 ± 495.3	534.5 ± 506.4	291.7 ± 384.5	268.8 ± 386.5
Number of biopsies	3.7 ± 0.8	3.8 ± 0.8	2.7 ± 0.8	2.7 ± 0.8

Figure 2A shows the mean manual AMACR staining per gland in the normal and HGPIN compartments by their case/control status. The mean AMACR staining per gland in the normal compartment was significantly higher in the cases when compared to controls. There was no difference between the two groups for the HGPIN compartment.

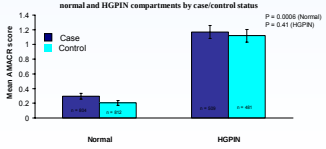

Figure 2B shows the mean manual AMACR staining per person in the normal and HGPIN compartments by their case/control status. The mean AMACR staining per person in the normal compartment of cases was higher than controls, although not statistically significant. At the person level analysis, there was no difference between cases and controls for the HGPIN compartment.

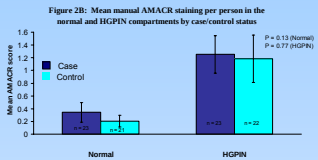

Figure 3A shows the mean automated AMACR staining per ROI in the normal and HGPIN compartments by their case/control status. The mean AMACR staining per ROI was significantly higher in the cases than controls regardless of the compartment of analysis. This case-control difference was apparent even at the person level of analysis for the HGPIN compartment **(Figure 3B).** On the other hand, the difference between cases and controls for the normal compartment at the person level was of borderline significance (p=0.07).

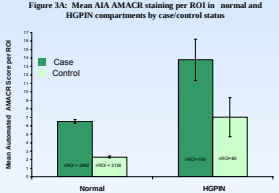

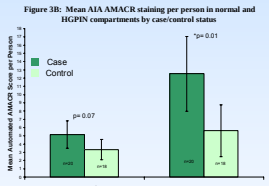

When AIA data were analyzed without ROIs **(Figure 3C)**, HGPIN lesions were likewise found to be significantly different between cases and controls. Similarly, normal glands of cases had higher values when compared to controls, although again the difference was below conventional statistical significance.

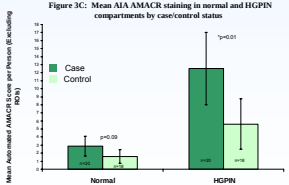

Box-plots for AIA scores by IHC results are shown in **Figure 4A**. Correlation coefficients between manual and automated scores for the normal and HGPIN glands per person are depicted in Figures **4B and 4C** respectively. Lower correlation coefficients observed for the normal compartment could be explained by a 'Floor Effect' phenomenon, which occurs primarily with low expression.

4A

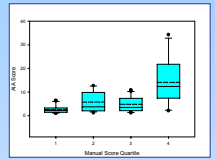

4B

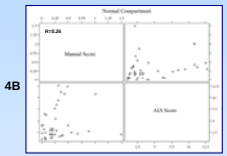

4C

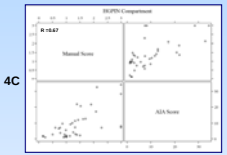

Conclusions

- Mean AMACR scores in HGPIN glands were significantly higher than in normal glands by both scoring methods, whether the patient was later diagnosed with prostate cancer or not.
- As previously reported using manual scoring, computer-assisted scoring gave significantly higher mean AMACR scores per gland or ROI in the normal compartment among cases later diagnosed with prostate cancer than among the controls.
- AMACR score in the HGPIN glands of cases was significantly higher than controls when evaluated using AIA. This difference was not observed using manual scoring method.
- A trend for higher AMACR expression in cases was observed even when ROIs were not drawn, suggesting that drawing epithelial regions of interest might not be essential for automated analysis, especially for clean and specific immunomarkers like AMACR.
- The ability to discriminate both HGPIN and normal glands in negative biopsies according to risk of subsequent cancer supports the hypothesis that AIA has enhanced sensitivity and biological validity. This method might provide improved measurements for research and clinical prediction.

References

Ananthanarayanan, V., R. J. Deaton, et al. (2005). "Alpha-methylacyl-CoA racemase (AMACR) expression in normal prostatic glands and high-grade prostatic intraepithelial neoplasia (HGPIN): association with diagnosis of prostate cancer." Prostate **63**(4): 341-6.

Santinelli, A., R. Mazzucchelli, et al. (2007). "alpha-Methylacyl coenzyme A racemase, Ki-67, and topoisomerase IIalpha in cystoprostatectomies with incidental prostate cancer." Am J Clin Pathol **128**(4): 657-66.

Histopathology 2004, **45**, 218–225

Alpha-methylacyl-CoA racemase: a multi-institutional study of a new prostate cancer marker

Z Jiang, C L Wu,[1] B A Woda, K A Iczkowski,[2] P G Chu,[3] M S Tretiakova,[4] R H Young,[1] L M Weiss,[3] R D Blute Jr, C B Brendler,[4] T Krausz,[4] J C Xu,[5] K L Rock, M B Amin[6] & X J Yang[4,7]

University of Massachusetts Medical School, Worcester, MA, [1]Massachusetts General Hospital, Harvard Medical School, Boston, MA, [2]University of Florida and Veterans Affairs Medical Center, Gainesville, FL, [3]City of Hope National Medical Center, Duarte, CA, [4]The University of Chicago, Chicago, IL, [5]Corixa Corporation, Seattle, WA, [6]Emory University School of Medicine, Atlanta, GA and [7]Northwestern University, Feinberg School of Medicine, Chicago, IL, USA

Date of submission 17 December 2003
Accepted for publication 12 March 2004

Jiang Z, Wu C L, Woda B A, Iczkowski K A, Chu P G, Tretiakova M S, Young R H, Weiss L M, Blute R D Jr, Brendler C B, Krausz T, Xu J C, Rock K L, Amin M B & Yang X J
(2004) *Histopathology* **45**, 218–225

Alpha-methylacyl-CoA racemase: a multi-institutional study of a new prostate cancer marker

Aim: To test whether α-methylacyl-CoA racemase (AMACR) is a sensitive and specific marker of prostate cancer.
Methods and results: The expression levels of AMACR mRNA were measured by real-time polymerase chain reaction. A total of 807 prostatic specimens were further examined by immunohistochemistry specific for AMACR. Quantitative immunostaining analyses were carried out by using the ChromaVision Automated Cellular Imaging System and the Ariol SL-50 Imaging System, respectively. AMACR mRNA levels measured in prostatic adenocarcinoma were 55 times higher than those in benign prostate tissue. Of 454 cases of prostatic adenocarcinoma, 441 were positive for AMACR, while 254 of 277 cases of benign prostate were negative for AMACR. The sensitivity and specificity of AMACR immunodetection of prostatic adenocarcinomas were 97% and 92%, respectively. Both positive and negative predictive values were 95%. By automatic imaging analyses, the AMACR immunostaining intensity and percentage in prostatic adenocarcinomas were also significantly higher than those in benign prostatic tissue (105.9 versus 16.1 for intensity, 45.7% versus 0.02% and 35.03% versus 4.64% for percentage, respectively).
Conclusions: We have demonstrated the promising features of AMACR as a biomarker for prostate cancer in this large series and the potential to develop automated quantitative diagnostic tests.

Keywords: α-methylacyl-CoA racemase, AMACR, biomarker, P504S, prostate cancer

Abbreviations: ACIS, automatic cellular imaging system; AMACR, α-methylacyl-CoA racemase; PIN, prostatic intraepithelial neoplasia; PSA, prostate specific antigen

Introduction

Considerable effort has been made to identify prostate cancer markers, which may be valuable in the early diagnosis, staging, therapeutic monitoring, post-therapeutic follow-up and targeted treatment of prostate cancer. Currently, prostate specific antigen (PSA) is the most commonly used biomarker for the diagnosis and the prediction of prognosis of prostate cancer.[1–3] However, PSA is not a cancer-specific marker, as it is present in both benign and malignant prostatic epithelial cells.[4] Serum PSA levels are frequently elevated in benign conditions such as benign prostate hyperplasia and prostatitis in addition to prostate cancer.[5,6] Consequently, patients with elevated serum PSA must

Address for correspondence: Ximing J Yang MD, PhD, Feinberg 7–334, Northwestern Memorial Hospital, 251 East Huron Street, Chicago, IL 60611, USA. e-mail: xyang@northwestern.edu

undergo a biopsy to confirm or exclude the presence of prostate cancer.

The definitive diagnosis of prostate cancer is established by the morphological identification of malignant epithelium in tissue sections. The diagnosis of small foci of prostate cancer on needle biopsy is a major challenge for pathologists because the establishment of a pathological diagnosis requires the presence of a combination of multiple histological features of tumour cells such as an infiltrating pattern, nuclear atypia, and the presence of characteristic extracellular material in malignant epithelium.[7–9] No single diagnostic feature of prostatic adenocarcinoma can be used alone reliably. In addition, many benign conditions can mimic the morphology of prostate cancer, despite their benign biological behaviour. Unfortunately, misdiagnosis of prostate cancer may be associated with severe adverse consequences for the patient. Therefore, a biochemical marker specific for prostate cancer would be very useful in clinical practice.

Recent advances in molecular biology have already had a great impact on the clinical practice of medicine. In particular, newly developed techniques such as RNA subtraction hybridization and cDNA microarrays allow the identification and comparison of genes differentially expressed between malignant and benign cells. The application of these new techniques has led to the discovery of α-methylacyl CoA racemase (AMACR), also termed P504S, in prostate cancer.[10] AMACR is an enzyme with 382 amino acid residues encoded by a 1621-bp cDNA. Overexpression of AMACR in prostatic adenocarcinoma has recently been reported.[11–13] Two previous studies[12,13] mostly utilized the small cores of tissue present in tissue microarrays and polycolonal antibodies with weak to moderate protein staining intensity in benign atrophic prostatic glands.[12] Using a monoclonal antibody[10] specific for AMACR, we have shown that AMACR is a good marker for prostate cancer, but the limited number of clinical samples did not allow us to demonstrate its significant clinical utility.[11]

To investigate more conclusively the clinical importance of this molecular marker, we included a number of expert urological pathologists and analysed the sensitivity and specificity of an immunohistochemical test using a highly specific monoclonal antibody for AMACR in a large number of patients from a variety of geographical locations in the USA. An antibody specific for high-molecular-weight keratins (34BE12), which detects basal cells in benign prostatic glands but is usually non-reactive in prostatic adenocarcinoma,[14,15] was used for comparison. We also used quantitative real-time polymerase chain reaction (PCR) and two newly developed automated imaging analysis systems: the ChromaVision Automated Cellular Imaging System (ACIS) and the Ariol SL-50 Imaging System (ArioISL-50), respectively, to compare the mRNA and protein levels of AMACR between benign and neoplastic prostate tissues.

Materials and methods

CASES

Twenty-eight prostate specimens, including 17 with adenocarcinoma and 11 benign prostates, were used for quantitative RNA analysis. Additionally, a total of 807cases of formalin-fixed paraffin-embedded tissues (Table 1) including prostatic adenocarcinoma ($n = 454$), benign prostatic tissue ($n = 277$) and high-grade prostatic intraepithelial neoplasia (PIN; $n = 76$) were retrieved for conventional haematoxylin and eosin (H–E) staining and immunostaining. All cases were collected between January 2000 and May 2002 and the diagnoses were confirmed by at least two pathologists. The specimens were obtained from five academic medical centres located, respectively, in the East (University of Massachusetts Medical School and Massachusetts General Hospital), Midwest (University of Chicago), South (Veterans Affairs Medical Center, Gainesville, FL) and West (City of Hope National Medical Center, CA) of the USA. The patient ages ranged from 43 to 82 years. The serum PSA levels ranged from 2.1 to 72. The Gleason score ranged from 5 to 10.

QUANTITATIVE REAL-TIME PCR

Fresh tissue was frozen in liquid nitrogen and homogenized with a polytron (Kinematica, Littau-Lucerne, Switzerland). Messenger RNA was extracted using a RNA extraction kit with Trizol reagent (Invitrogen Corp., Carlsbad, CA, USA). Quantitative real-time PCR assay was performed as described previously[16] using

Table 1. Selection of cases

Specimens	No. of cases	Carcinoma	HGPIN	Benign
Prostatectomy	195	178	9	8
Needle biopsy	550	270	62	218
TURP	62	6	5	51
Total	807	454	76	277

HGPIN, High-grade prostatic intraepithelial neoplasia; TURP, transurethral resection of prostate.

300 nM of AMACR forward (5′-GATTTGGCCAGTCA GGAAGC-3′) and reverse (5′-GAACACCTGACAAAGCC AAATAGTT-3′) primers. PCR was performed on a PE Biosystems GeneAmp 5700 instrument using cDNA reversed-transcribed from RNA of benign and malignant prostate tissues. β-actin was used as an internal reference.

IMMUNOHISTOCHEMISTRY AND IMMUNOFLUORESCENCE

Immunohistochemical studies were performed on 5-μm sections of formalin-fixed paraffin-embedded tissue by using an avidin-biotinylated peroxidase complex system as previously described.[11] The sections were incubated with either a rabbit monoclonal antibody specific for AMACR (P504S; Corixa, Seattle, WA, USA) at a 0.5 μg/ml dilution or a mouse monoclonal antibody specific for high-molecular-weight cytokeratin (34βE12, 1 : 50 dilution; Dako, Carpinteria, CA, USA). Diaminobenzidine was used as a chromogen. Double immunostaining was performed with the AMACR and 34βE12 antibodies, as well as biotinylated secondary IgG sequentially. Diaminobenzidine was used for detection of the AMACR reaction and a different peroxidase substrate, VIP (Vector, Burlingame, CA, USA), which yielded a purple product, was applied for visualizing the reaction of the 34βE12 antibody. The sections were finally counterstained with methyl green.

Immunofluorescent staining was performed with the AMACR antibody (5 μg/ml) and the 34βE12 antibody. Visualization of each localized antibody was achieved by first incubating the sections with 10 μg/ml anti-rabbit secondary antibody (Vector) conjugated with Texas red followed by an incubation with 10 μg/ml antimouse secondary antibody (Vector) conjugated with fluorescein (green).

EVALUATION OF THE IMMUNOSTAINING

Six surgical pathologists with extensive experience in prostate pathology from five medical centres in the USA participated in the study. The original morphological diagnosis was generated by each participating pathologist. For each case, both AMACR and 34βE12 stains were examined. Positive AMACR staining was defined as continuous dark cytoplasmic staining or apical granular staining patterns in cells, which could be easily observed at low-power magnification (≤ × 100). Scant fine granular background staining of epithelial and stromal cells, which could not be seen at low-power magnification (≤ × 100), was considered negative staining.

QUANTITATIVE ANALYSIS OF THE IMMUNOSTAINING

The Automated Cellular Imaging System (ACIS; ChromaVision Medical System Inc., San Juan Capistrano, CA, USA) and Ariol Imaging System (Applied Imaging Corp., Santa Clara, CA, USA) were used to evaluate the immunostaining in prostatic adenocarcinoma compared with adjacent benign prostatic tissue in the same section. Positive staining is calculated by applying two thresholds with one recognizing blue background (haematoxylin stained) cells and another recognizing brown positive cells. The percentage of positivity is the area detected by the brown threshold divided by the sum of the area detected by the brown and blue thresholds. The intensity is calculated by masking out all areas not selected by the brown threshold and calculating the integrated optical density of brown within the remaining area. This value is divided by the area in pixels of the brown mask to calculate an average intensity of a selected area. The values from 60 areas of benign prostatic epithelium and 60 areas of malignant prostatic epithelium were obtained and analysed by using the ChromaVision ACIS. The values from 60 areas including benign prostatic tissue ($n = 24$), prostatic adenocarcinoma ($n = 20$) and high-grade PIN ($n = 16$) were analysed by using the Ariol Imaging System.

STATISTICAL ANALYSIS

The Wilcoxon rank sum test was used to compare scale difference of quantitative real-time PCR and immunostaining results between benign and neoplastic prostate samples.

Results

AMACR mRNA LEVELS MEASURED BY QUANTITATIVE REAL-TIME PCR ANALYSIS

The results of real-time PCR performed to quantitatively assess the expression levels of AMACR mRNA in benign and prostate cancer tissues are shown in Figure 1. The copy number of AMACR was standardized with units of β-actin mRNA measured in the same specimen and expressed as copies/ng β-actin. AMACR mRNA in benign prostate ranged from 191 to 7467 copies/ng β-actin ($n = 11$, mean = 3588), while AMACR mRNA in prostatic adenocarcinoma ranged from 40 799 to 494 465 copies/ng β-actin ($n = 17$, mean = 198 051). The average level of AMACR expression in prostate cancer was 55.2 times ($P < 0.001$) that of benign prostatic tissue.

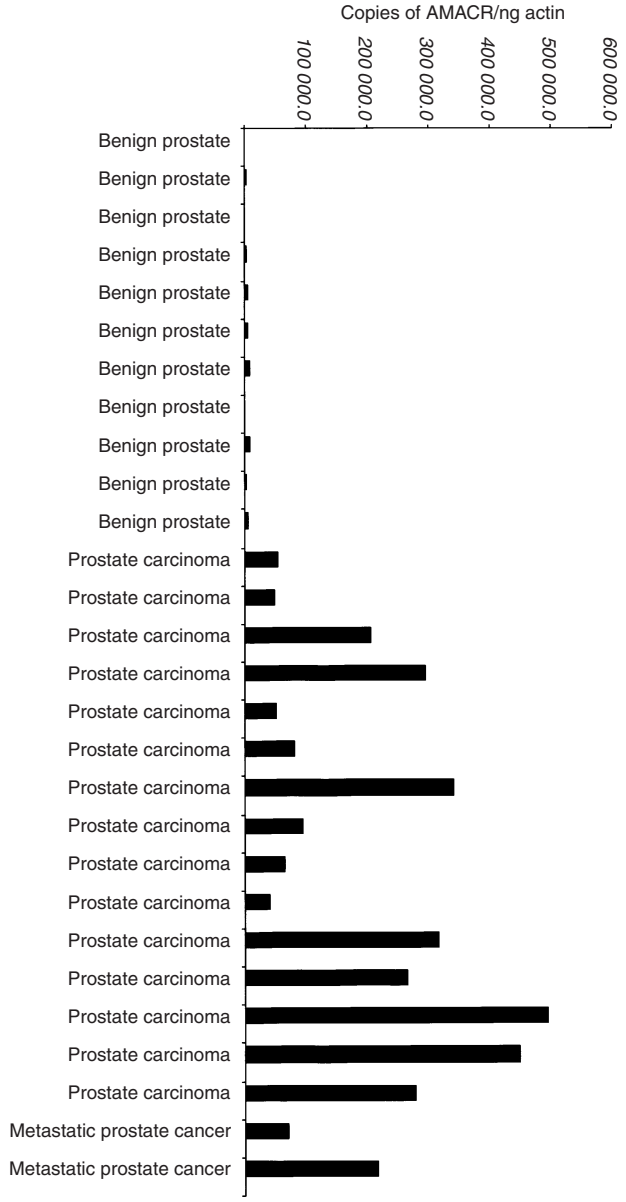

Figure 1. Quantitative real-time polymerase chain reaction analysis of α-methylacyl-CoA racemase (AMACR) mRNA levels in benign ($n = 11$) and malignant ($n = 17$) prostatic tissues. β-actin mRNA levels were used as an internal control.

AMACR IN BENIGN PROSTATIC TISSUES, HIGH-GRADE PIN AND PROSTATIC ADENOCARCINOMAS

Of 454 prostatic adenocarcinomas, 441 (97%) were positive for AMACR (Figure 2A,B) including those with Gleason score 5 (23/24, 96%), Gleason score 6 (244/250, 98%), Gleason score 7 (105/107, 98%), and Gleason score ≥8 (69/73, 95%). The AMACR-positive rates in different Gleason scores (Table 2) were not significantly different. In addition, AMACR was also positive in 67 of 76 cases (88%) of high-grade PIN (Figure 2C). High-grade PIN displayed patchy basal cells (Figure 2C), while all 454 prostate cancer cases showed non-reactivity for the basal cell marker 34βE12 (Figure 2B,D).

To determine the specificity of the AMACR test, we analysed its expression in benign prostates. Only 23 out of 277 cases of benign prostate showed detectable levels of AMACR expression by immunohistochemistry. The AMACR immunoreactivity in benign prostatic epithelium was typically weaker and focal. All 277 cases of benign prostatic tissues contained basal cells demonstrated by immunoreactivity for 34βE12. Particularly important, the benign glands adjacent to the malignant glands were also negative for AMACR and positive for 34βE12 (Figure 2B–D). Double-labelling methods with either immunoperoxidase staining (Figure 2B,D) or immunofluorescence (Figure 2C) could easily differentiate malignant from benign glands. The expression of AMACR and 34βE12 appeared mutually exclusive in malignant (positive for AMACR, negative for 34βE12) or benign prostatic tissues (negative for AMACR, positive for 34βE12). Most high-grade PIN glands (88% of cases) were reactive for both AMACR and 34βE12 (Figure 2C).

The AMACR immunohistochemical assay had an overall sensitivity of 97%, a specificity of 92%, a positive predictive value of 95% and a negative predictive value of 95%. The sensitivities varied from 96% to 100% (Centre A, 97%; Centre B, 97%; Centre C, 96%; Centre D, 100%; Centre E, 98%).

QUANTIFICATION OF AMACR IMMUNOREACTIVITY IN BENIGN AND NEOPLASTIC PROSTATIC TISSUES BY AUTOMATIC IMAGING SYSTEMS

As measured by the ACIS, the average percentage of AMACR-positive staining was 45.7% in prostatic carcinomas and 0.02% in benign prostatic tissues ($P < 0.001$). The average intensity of AMACR-positive cells was 105.9 in prostatic carcinoma and 16.1 in benign prostatic tissues ($P < 0.02$, Figure 3). While using another automatic system, the Ariol SL-50, the mean percentages of AMACR immunostaining were 4.64 (ranging from 0 to 24.51) in benign prostatic tissue, 21.84 (ranging from 2.69 to 57.66) in high-grade PIN, and 35.03 (ranging from 6.22 to 78.64) in prostatic adenocarcinomas. The differences are statistically significant ($P < 0.001$).

Discussion

Recent advances in molecular biology have been translated into significant progress in clinical medicine.

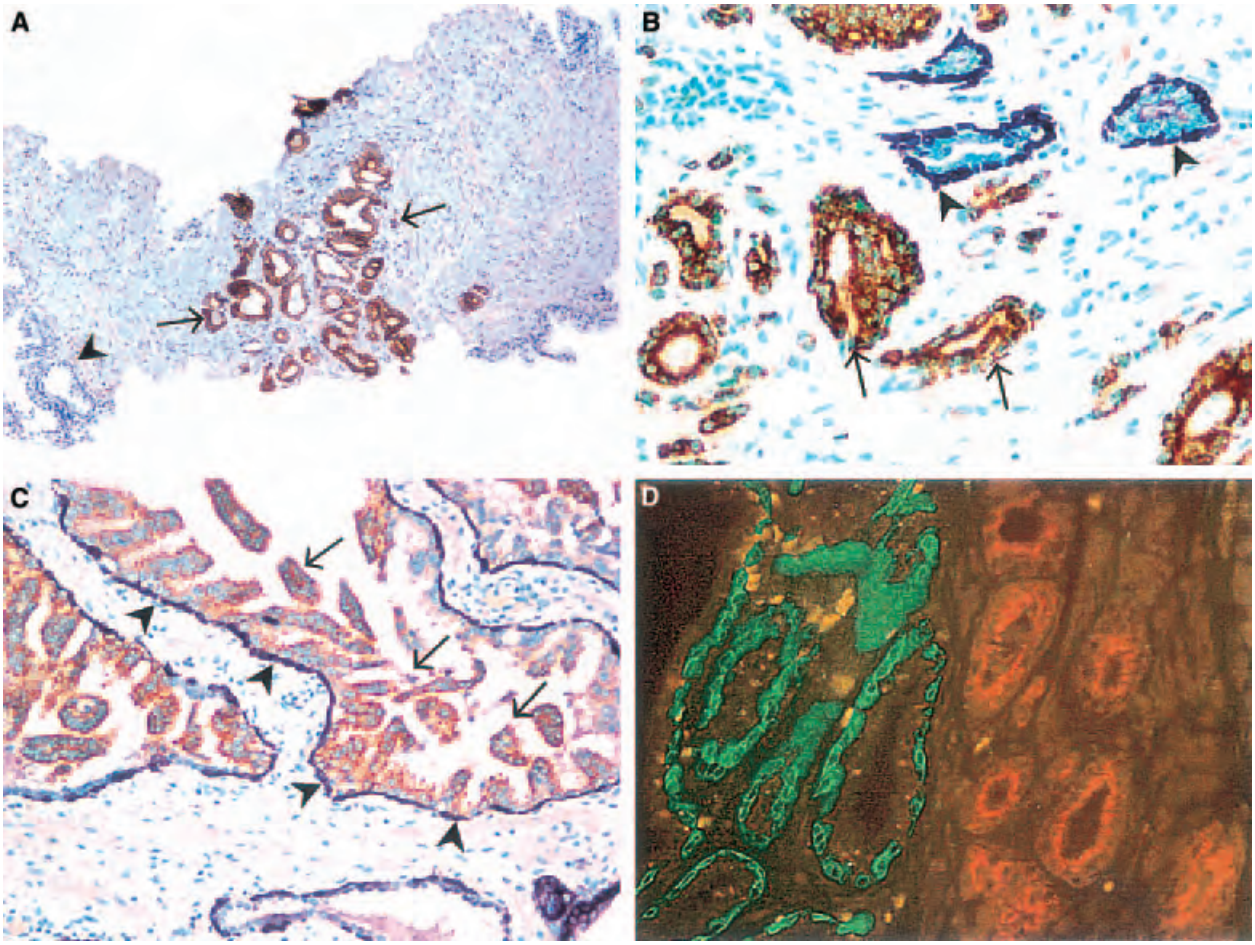

Figure 2. **A,** α-methylacyl-CoA racemase (AMACR) immunostaining on a needle biopsy core showing small focus of prostatic adenocarcinoma (arrows) with intense, continuous, granular cytoplasmic (brown) staining and no AMACR staining in adjacent benign glands (arrowheads). **B,** Double immunostaining on prostatic tissue showing prostatic adenocarcinoma with brown AMACR staining (arrows) and benign glands with blue-purple basal cell (34βE12) staining (arrowheads). **C,** Double immunostaining on prostatic tissue showing high-grade prostatic intraepithelial neoplasia with both brown AMACR staining in neoplastic cells (arrows) and discontinuous blue-purple staining in basal cells (arrowheads). **D,** Immunofluorescence of prostatic tissue showing benign glands (left) stained with the 34βE12 antibody labelled with fluorescence (green) and prostatic adenocarcinoma (right) stained with the AMACR antibody labelled with Texas red (orange).

Table 2. Expression of α-methylacyl-CoA racemase in prostatic adenocarcinoma

Gleason score	No. of cases	Positive	Negative	Positive rate, %
5	24	23	1	96
6	250	244	6	98
7	107	105	2	98
≥8	73	69	4	95
Total	454	441	13	97

One of the most powerful new techniques is genetic profiling using microarray (gene chip) technology.[17–19] However, despite the detection of many prostate cancer markers discovered by microarrays, very few if any have been used in clinical practice. In this study, we tested the hypothesis that AMACR is a biomarker for prostate cancer. Our study of AMACR in 807 cases of benign and malignant prostatic diseases from five different medical institutions has demonstrated the promising potential of AMACR as a marker for prostate cancer. The quantitative analyses of AMACR mRNA and protein expression levels further strengthen the findings. AMACR may be the first gene identified from prostate cancer by cDNA microarrays to be suitable for

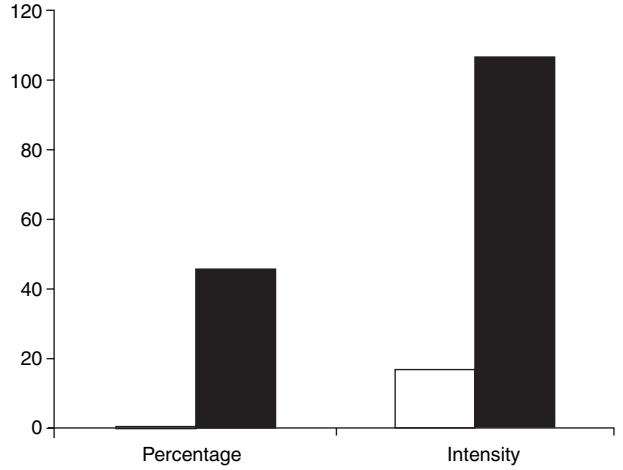

Figure 3. Comparison of the percentage and intensity of α-methylacyl-CoA racemase immunostaining between benign (□) and malignant (■) prostatic tissues analysed by ChromaVision Automated Cellular Imaging System.

clinical practice and potentially improve the diagnosis and treatment of prostate cancer.

The wide use of serum PSA screening has resulted in an increased detection of patients with prostate cancer. A tissue diagnosis (prostate needle biopsy or transurethral resection of prostate) is mandatory for a patient with prostate cancer to receive appropriate therapy to minimize morbidity and mortality. However, tissue diagnosis can be difficult and inaccurate if the cancer is very limited. Over-diagnosis (false positivity) may cause unnecessary treatment of men without prostate cancer and lead to incontinence or impotence. Under-diagnosis (false negativity) may delay effective treatment to patients with prostate cancer and may lead to recognition of disease at a more advanced stage. Unfortunately, there is a significant error rate in pathological diagnosis of prostate cancer in general practice because discrimination between benign and malignant glands can be difficult in a small biopsy specimen and this can be even more difficult for pathologists who are not specialized in urological pathology. A recent study comparing the diagnoses of general pathologists and an expert urological pathologist in 224 prostate needle biopsies has shown a misdiagnosis rate of prostate needle biopsy of 12.3%.[20] If the significant error rate of prostate biopsies is even only 1% of the approximately one million prostate needle biopsies performed each year in the USA, 10 000 cases could be misdiagnosed. Considering the large number of prostate needle biopsies performed in the USa and around the world each year, this error rate is alarming and could have a significant health and economic impact. The accuracy of pathological diagnosis of prostate cancer could be improved by the application of a more objective and reliable specific marker for prostatic cancer cells.

AMACR displays several attractive features for a prostate cancer marker, first, with significant levels of overexpression, including 55-fold of mRNA levels by real-time PCR and 34-fold of protein levels by Western blotting,[11] 6.6-fold (ACIS intensity), 7.5-fold (Ariol SL-50%) and 2285-fold (ACIS percentage). AMACR is one of the few genes consistently detected in prostate cancer cells by conventional methods such as immunohistochemistry or immunoflorescence in paraffin-embedded tissue specimens. Our study showed that 441 of 454 cases (97%) of routine prostatic adenocarcinoma specimens were positive in an AMACR assay. The positive predictive value is 95%. In this study, we deployed two newly developed automatic imaging systems. Automatic imaging analysis, still in its early phase of development, allows more accurate and objective measurement of immunoreactivity instead of relatively primitive 1+, 2+ and 3+ quantification. These analyses all demonstrated a significant difference between benign prostates and prostate cancer, although the conditions of these systems remain to be perfected.

Second, AMACR is a marker with high specificity for prostate adenocarcinoma. In contrast to carcinoma, most benign cases and the benign prostate tissue adjacent to carcinoma were negative for AMACR. The negative predictive value is 95%. Some benign prostatic conditions mimicking cancer including atrophy, basal cell hyperplasia and inflammatory glands can be easily distinguished from prostate cancer by their non-detectable AMACR. Other previously identified markers such as P503S and P510S may have only limited clinical utility because they are present in both benign and malignant prostatic epithelia.[10]

Finally, AMACR is present in different grades of prostate cancer. Another prostate cancer marker, hepsin, also recently identified by microarrays,[21,22] may have promising clinical utility. However, the hepsin expression level is significantly decreased in high-grade prostate cancer.[23]

Recently, elevated AMACR expression has been reported in a smaller percentage of precursor lesions of prostate cancer, including atypical adenomatous hyperplasia[24] as well as high-grade PIN,[11–13] suggesting a role for AMACR at an earlier phase of prostatic carcinogenesis. Further functional and biochemical analysis of AMACR may provide insights into the basis of the development of prostate cancer and potentially lead to preventive measures. Additionally, both high-

grade PIN and atypical adenomatous hyperplasia retain basal cells that can be demonstrated by 34βE12 immunostaining. Therefore, it is easy to distinguish high-grade PIN and atypical adenomatous hyperplasia from malignant glands with the combination of staining for AMACR and basal cell markers.

The differences between cancer and benign glands can be accentuated by double immunostaining methods. With available specific antibodies and current techniques, we were able to show for the first time two distinct colours between malignant (brown or red) and benign (blue or green) epithelia of the prostate (Figure 2B,D) in conventional paraffin-embedded tissue specimens. Although these methods are unlikely to replace the conventional H–E stain for pathological evaluation of slides, our results using double immunostaining and the ChromaVision ACIS may provide the basis for an automated screening test for prostate cancer. There may be broader applications for AMACR in the diagnosis and treatment of prostate cancer. In contrast to PSA, AMACR is relatively specific for prostate cancer. An antibody-based or PCR-based serum or seminal fluid test for AMACR is unlikely to be affected by benign prostatic diseases. In addition, if an AMACR antibody is conjugated with a fluorescent or radioactive indicator, the uptake and binding of AMACR antibody by prostate cancer cells may delineate the entire tumour and provide preoperative information about tumour volume for primary or metastatic prostate cancer. Finally, an AMACR antibody may be used to target prostate cancer or deliver therapeutic agents locally for treatment of prostate cancer.

Epidemiological and animal studies have shown an association between dietary factors and increased risk for prostate cancer.[25,26] Although increased fat content has been observed in prostate cancer cells, the molecular mechanism of this association is unclear. AMACR, an essential enzyme for the degradation of branched-chain fatty acids by β-oxidation, catalyses the conversion of several (2*R*)-methyl-branched-chain fatty acyl-CoAs to their (*S*)-stereoisomers.[27] High levels of branched chain fatty acids have been found in some dietary sources such as beef, milk and dairy products. Accumulation of branched chain fatty acids in prostatic epithelium may lead to increased levels of AMACR. The discovery of AMACR overexpression in prostate cancer suggests a link between AMACR and dietary fat in the development of prostate cancer. The mechanism of AMACR in prostatic carcinogenesis should be further investigated.

In summary, this is the first multi-institutional study to evaluate the potential clinical application of α-methylacyl-CoA racemase in the diagnosis of prostate cancer. By using conventional immunohistochemical analysis and a number of quantitative analyses, we have demonstrated that α-methylacyl-CoA racemase is an excellent biochemical maker of prostate cancer with high sensitivity and specificity. The potential to develop enhanced and novel diagnostic and treatment methods of prostate cancer using this maker is promising.

Acknowledgements

The authors thank Karen Dresser at University of Massachusetts Medical School for her excellent technical support. The authors also thank Marty Bartholdi and Tara Ruddy from Applied Imaging Corporation for providing analysis of AMACR immunostaining on the Ariol SL-50 Imaging System.

References

1. Wang MC, Papsidero LD, Kuriyama M, Valenzuela LA, Murphy GP, Chu TM. Prostate antigen: a new potential marker for prostatic cancer. *Prostate* 1981; **2;** 89–96.
2. Catalona WJ, Richie JP, Ahmann FR *et al.* Comparison of digital rectal examination and serum prostate specific antigen in the early detection of prostate cancer: results of a multicenter clinical trial of 6,630 men. *J. Urol.* 1994; **151;** 1283–1290.
3. Epstein JI. PSAP and PSA as immunohistochemical markers. *Urologic Clin. N. Am.* 1993; **20;** 757–770.
4. Polascik TJ, Oesterling JE, Partin AW. Prostate specific antigen: a decade of discovery—what have we learned and where are we going. *J. Urol.* 1999; **162;** 293–306.
5. Hasui Y, Marutsuka K, Asada Y *et al.* Relationship between serum prostate specific antigen and histological prostatitis in patients with benign prostatic hyperplasia. *Prostate* 1994; **25;** 91–96.
6. Nadler RB, Humphrey PA, Smith DS *et al.* Effect of inflammation and benign prostatic hyperplasia on elevated serum prostate specific antigen levels. *J. Urol.* 1995; **154;** 407–413.
7. Epstein JI. Diagnostic criteria of limited adenocarcinoma of the prostate on needle biopsy. *Hum. Pathol.* 1995; **26;** 233–239.
8. Young RH, Sringley JR, Amin MB *et al. Tumors of the prostate glands, seminal vesicles, male urethra, and penis.* Third series. Washington, DC: Armed Forces Institute of Pathology, 2000; 154–175; 289–344.
9. Epstein JI, Yang XJ. *Prostate biopsy interpretation,* 3rd edn. Philadelphia: Lippincott Williams & Wilkins, 2002; 64–91.
10. Xu J, Stolk JA, Zhang X *et al.* Identification of differentially expressed genes in human prostate cancer using subtraction and microarray. *Cancer Res.* 2000; **60;** 1677–1682.
11. Jiang Z, Woda BA, Rock KL *et al.* P504S: a new molecular marker for the detection of prostate carcinoma. *Am. J. Surg. Pathol.* 2001; **25;** 1397–1404.
12. Rubin MA, Zhou M, Dhanasekaran SM *et al.* α-methylacyl coenzyme a racemase as a tissue biomarker for prostate cancer. *JAMA* 2002; **287;** 1662–1670.
13. Lou J, Zha S, Gage WR *et al.* α-methylacyl-CoA racemase: a new molecular marker for prostate cancer. *Cancer Res.* 2002; **62;** 2220–2226.

14. Gown AM, Vogel AM. Monoclonal antibodies to human intermediate filament proteins: distribution of filament proteins in normal human tissues. *Am. J. Pathol.* 1984; **114;** 309–321.
15. Wojno KJ, Epstein JI. The utility of basal cell-specific anticytokeratin antibody (34βE12) in the diagnosis of prostate cancer. *Am. J. Surg. Pathol.* 1995; **19;** 251–260.
16. Jiang Y, Harlocker S, Molesh DA *et al.* Discovery of breast cancer antigens using subtraction cDNA libraries and cDNA microarray. *Oncogene* 2002; **21;** 2270–2282.
17. Schena M, Shalon D, Davis RW *et al.* Quantitative monitoring of gene expression patterns with a complementary DNA microarray. *Science* 1995; **20;** 467–470.
18. Lockhart DJ, Winzeler EA. Genomics, gene expression and DNA arrays. *Nature* 2001; **405;** 827–836.
19. Welsh JB, Sapinoso LM, Su AI *et al.* Analysis of gene expression identifies candidate markers and pharmacological targets in prostate cancer. *Cancer Res.* 2001; **61;** 5974–5993.
20. Griffith RC, Epstein JI. Review of prostate needle biopsies by an expert. *Mod. Pathol.* 2001; **14;** 110A.
21. Magee JA, Araki T, Patil S *et al.* Expression profiling reveals hepsin overexpression in prostate cancer. *Cancer Res.* 2001; **61;** 5692–5696.
22. Stamey TA, Warrington JA, Caldwell MC *et al.* Molecular genetic profiling of Gleason grade 4/5 prostate cancers compared to benign prostatic hyperplasia. *J. Urol.* 2001; **166;** 2171–2177.
23. Dhanasekaran SM, Barrette TR, Ghosh D *et al.* Delineation of prognostic biomarkers in prostate cancer. *Nature* 2001; **412;** 822–826.
24. Yang XJ, Wu CL, Woda BA *et al.* Expression of α-methylacyl Co A racemase (P504S) in atypical adenomatous hyperplasia of the prostate. *Am. J. Surg. Pathol.* 2002; **26;** 921–925.
25. Giovannucci E, Rimm EB, Colditz GA *et al.* A prospective study of dietary fat and risk of prostate cancer. *J. Natl Cancer Inst.* 1993; **85;** 1571–1579.
26. Le Marchand L, Kolonel LN, Wilkens LR *et al.* Animal fat consumption and prostate cancer: a prospective study in Hawaii. *Epidemiology* 1994; **5;** 276–282.
27. Ferdinandusse S, Denis SIJ, Ist L *et al.* Subcellular localization and physiological role of a α-methylacyl-CoA racemase. *J. Lipid Res.* 2000; **41;** 1890–1896.

Inhibition of p38 by Vitamin D Reduces Interleukin-6 Production in Normal Prostate Cells via Mitogen-Activated Protein Kinase Phosphatase 5: Implications for Prostate Cancer Prevention by Vitamin D

Larisa Nonn,[1] Lihong Peng,[2] David Feldman,[2] and Donna M. Peehl[1]

Departments of [1]Urology and [2]Medicine, Stanford University School of Medicine, Stanford, California

Abstract

Although numerous studies have implicated vitamin D in preventing prostate cancer, the underlying mechanism(s) remains unclear. Using normal human prostatic epithelial cells, we examined the role of mitogen-activated protein kinase phosphatase 5 (MKP5) in mediating cancer preventive activities of vitamin D. Up-regulation of MKP5 mRNA by 1,25-dihydroxyvitamin-D_3 (1,25D) was dependent on the vitamin D receptor. We also identified a putative positive vitamin D response element within the MKP5 promoter that associated with the vitamin D receptor following 1,25D treatment. MKP5 dephosphorylates/inactivates the stress-activated protein kinase p38. Treatment of prostate cells with 1,25D inhibited p38 phosphorylation, and MKP5 small interfering RNA blocked this effect. Activation of p38 and downstream production of interleukin 6 (IL-6) are proinflammatory. Inflammation and IL-6 overexpression have been implicated in the initiation and progression of prostate cancer. 1,25D pretreatment inhibited both UV- and tumor necrosis factor α–stimulated IL-6 production in normal cells via p38 inhibition. Consistent with inhibition of p38, 1,25D decreased UV-stimulated IL-6 mRNA stabilization. The ability of 1,25D to up-regulate MKP5 was maintained in primary prostatic adenocarcinoma cells but was absent in metastases-derived prostate cancer cell lines. The inability of 1,25D to regulate MKP5 in the metastasis-derived cancer cells suggests there may be selective pressure to eliminate key tumor suppressor functions of vitamin D during cancer progression. These studies reveal MKP5 as a mediator of p38 inactivation and decreased IL-6 expression by 1,25D in primary prostatic cultures of normal and adenocarcinoma cells, implicating decreased prostatic inflammation as a potential mechanism for prostate cancer prevention by 1,25D. (Cancer Res 2006; 66(8): 4516-24)

Introduction

Prostate cancer (PCa) is unique among malignancies in that it generally grows very slowly, likely for decades, before symptoms arise and a diagnosis is finally made. Seemingly, the latency observed in PCa should provide a long window of opportunity for intervention by chemopreventive agents. Laboratory and epidemiologic studies have shown a potential role for vitamin D in the prevention of PCa. Evidence supporting a role for vitamin D in PCa prevention began with studies that linked reduced serum levels of vitamin D metabolites to PCa incidence. Low serum levels of 1,25-dihydroxyvitamin D_3 (1,25D), the active vitamin D metabolite, are associated with increased risk of PCa in older men (1). Decreased serum levels of 25-hydroxyvitamin D_3 (25D), the circulating precursor to 1,25D, also correlate with an increased risk of PCa (1). The latter finding has become more compelling since the discovery that prostate cells are not only sensitive to circulating 1,25D but can also synthesize 1,25D from circulating 25D. Conversion of 25D to active 1,25D by vitamin D 1α-hydroxylase (1) occurs within the normal prostate and suggests that local production of 1,25D may play a critical role in maintaining normal growth and differentiation.

Studies showing that 1,25D inhibits the growth of primary cultures of prostate cells, established PCa cell lines, and prostate xenograft tumors provide direct evidence for anticancer activity of vitamin D (1). However, mechanisms other than growth inhibition may be responsible for the prevention of PCa by vitamin D.

Using cDNA microarrays, we recently identified a new vitamin D–responsive gene, mitogen-activated protein kinase phosphatase 5 (*MKP5*; ref. 2). The up-regulation of MKP5, also known as dual-specificity phosphatase 10, was consistently increased by 1,25D treatment of primary cultures of prostatic epithelial cells (2). As a member of the dual-specificity MKP family of proteins that dephosphorylate mitogen-activated protein kinases, MKP5 dephosphorylates p38 and c-jun NH_2-terminal kinase, but not extracellular signal–regulated kinase (3, 4).

The potential ability of vitamin D to inhibit p38 through MKP5 is of interest to PCa prevention because p38 is activated by oxidative stress, hypoxia, and inflammation (5), all of which contribute to PCa development (6, 7). In particular, inflammation plays a causal role in the progression of many cancers including liver, bladder, and gastric cancers (8) and a similar role for inflammation in the development of PCa is now emerging (7). The strongest evidence linking inflammation to PCa is from recent findings that show (*a*) regular administration of nonsteroidal anti-inflammatory drugs significantly decreases PCa risk in older men by 60 to 80% (9, 10) and (*b*) men with chronic and/or acute inflammation of the prostate have an increased risk of developing PCa (7, 11).

Inhibitors of p38 are classically anti-inflammatory, suggesting that some of the activities attributed to vitamin D, including PCa prevention, may be a result of p38 inhibition and decreased inflammation. One of the downstream consequences of p38 protein kinase pathway activation is an increase in proinflammatory cytokine production to amplify the inflammatory response (12, 13). Interleukin 6 (IL-6) is a p38-regulated pleiotropic cytokine that has

Note: Supplementary data for this article are available at Cancer Research Online (http://cancerres.aacrjournals.org/).

Requests for reprints: Donna M. Peehl, Department of Urology, Stanford Medical Center, 300 Pasteur Drive, Stanford, CA 94305-5118. Phone: 650-725-5531; Fax: 650-723-4200; E-mail: dpeehl@stanford.edu.

doi:10.1158/0008-5472.CAN-05-3796

been historically associated with PCa (14, 15). Elevated levels of IL-6 are found in the serum of PCa patients and primary PCa tumors overexpress IL-6 (14, 16). IL-6 is also involved in the progression of PCa to androgen-independent PCa because it can facilitate androgen receptor signaling in the absence of androgens (15, 17).

Because there is increasing evidence linking inflammation to PCa development, our studies focused on characterizing regulation of IL-6 production via p38 inhibition by 1,25D as a potentially significant cancer prevention activity. Using primary epithelial cell cultures derived from the normal peripheral zone (E-PZ; the major site of origin of prostatic adenocarcinomas; ref. 18) and from primary adenocarcinomas of the prostate (E-CA) as our model system, we characterized MKP5 induction by 1,25D and revealed MKP5 as the mediator of p38 kinase inhibition and decreased IL-6 production by 1,25D. Prostate cancer cell lines derived from metastases, however, have lost the ability to up-regulate MKP5 in response to 1,25D, suggesting selection against this anticancer activity of vitamin D.

Materials and Methods

Cell culture and reagents. Human primary prostatic epithelial and stromal cells were derived from radical prostatectomy specimens. The patients did not have prior chemical, hormonal, or radiation therapy. Histologic characterization and cell culture of the prostate cells was as previously described (19). Epithelial cells (E-PZ and E-CA) were cultured in supplemented MCDB 105 (Sigma-Aldrich, St. Louis, MO) or PFMR-4A as previously described (19). Stromal cells (F-PZ) were cultured in MCDB 105/10% fetal bovine serum (FBS). pRNS1-1 cells are immortalized E-PZ cells (20) and are cultured in keratinocyte serum-free medium (Invitrogen, Carlsbad, CA). Human PCa cell lines LNCaP, PC-3, and DU 145 were acquired from American Type Culture Collection (Manassas, VA). LNCaP cells were cultured in MCDB 105/10% FBS and PC-3 and DU 145 in DMEM (Invitrogen)/10% FBS. Normal human keratinocytes were obtained from Cambrex (East Rutherford, NJ) and cultured according to the instructions of the supplier. Squamous cell carcinoma cell lines SCC-25 and A431 were obtained from Dr. Paul Khavari (Stanford University, Stanford, CA) and cultured in DMEM/10% FBS. All chemicals were obtained from Sigma-Aldrich unless otherwise noted. 1,25-dihydroxyvitamin D_3 (Biomol International, Plymouth Meeting, PA) was reconstituted in 100% ethanol at 10 mmol/L and stored at −20°C.

RNA isolation and quantitative real-time reverse transcription-PCR. RNA was isolated from cells by Trizol (Invitrogen) followed by chloroform extraction. The aqueous phase was then precipitated in 100% isopropanol and the pellet washed in 75% ethanol before resuspension in water. RNA concentration and quality were determined by absorbance ratio at 260/280 nm using a UV spectrophotometer. Total RNA (2 μg) was reverse transcribed using Thermoscript RT (Invitrogen). Resulting cDNA was used for quantitative PCR amplification with gene-specific primers and the DyNAMO SYBR Green kit (Finnzymes, Espoo, Finland) in the Opticon 2 thermocycler (MJ Research, South San Francisco, CA). PCR conditions for all primer sets were optimized and have similar amplification efficiency under the following thermocycler conditions: 95°C 5 minutes, 34 × (95°C 30 seconds, 58°C 30 seconds, 72°C 60 seconds), 72°C 5 minutes. Relative mRNA levels were calculated from the point where each curve crossed the threshold line (Ct) using the following equation: Rel. value = $2^{-[Ct(control) - Ct(test)]test\ gene} / 2^{-[Ct(control) - Ct(test)]housekeeping\ gene}$ (21). Reactions were done in triplicate and the values normalized to the expression of the housekeeping gene TATA-box binding protein (*TBP*; ref. 22). Primer sets were TBP, 5′-tgctgagaagagtgtgctggag-3′ and 5′-tctgaataggctgtggggtc-3′; total MKP5, 5′-atcttgcccttcctgttcct-3′ and 5′-attggtcgtttgcctttgac-3′; MKP5 isoform 1 specific, 5′-tgaatgtgcgagtccatagc-3′ and 5′-gttagcagggcaggtggtag-3′; MKP5 isoform 2 specific, 5′-tggatgcagctgagattctg-3′ and 5′-ggttctgcttgttgctgtca-3′; MKP5 isoform 3 specific, 5′-atttatgaagtggacttagt-3′ and 5′-ggttctgcttgttgctgtca-3′; and CYP24, 5′-ggcaacagttctgggtgaat-3′ and 5′-tatttgcggacaatccaaca-3′.

Cell lysate preparation and immunoblot. Cells were lysed in ice-cold 1× Cell Lysis Buffer (Cell Signaling, Beverly, MA) containing 1 μmol/L phenylmethylsulfonyl fluoride and 100 nmol/L okadaic acid. Cells were disrupted by sonication and insoluble cell debris removed by centrifugation at 15,000 × *g*, 4° C. Protein concentrations of the cell lysates were quantified using the Bio-Rad Protein Dye (Bio-Rad, Hercules, CA). Cell lysates were used fresh or stored at −70°C. Cell lysates (10-30 μg) were mixed with LDS NuPAGE Sample Buffer and separated by electrophoresis through 10% NuPAGE Bis-Tris Gels (Invitrogen) and transferred onto polyvinylidene difluoride membrane. Fresh cell lysates were used for analysis of phosphorylated proteins. Membranes were probed with the following primary antibodies: anti–phospho-p38 rabbit polyclonal and anti-p38 rabbit polyclonal from Cell Signaling, anti–vitamin D receptor (VDR) monoclonal (Santa Cruz Biotechnology, Santa Cruz, CA), and monoclonal anti-actin (Santa Cruz Biotechnology). Following primary antibody incubation overnight at 4°C, the blots were incubated with appropriate secondary horseradish peroxidase–conjugated antibodies (Cell Signaling) and developed with HyGlo enhanced chemiluminescence reagent (Denville Scientific, Metuchen, NJ).

Small interfering RNA transfection. Cells at 75% confluency were transfected with 10 nmol/L of negative control (Ambion, Austin, TX), VDR-specific small interfering RNA (siRNA; Santa Cruz Biotechnology), or MKP5-specific siRNA (Ambion) using siPORT NeoFX (Ambion). Cells were used for experiments after transfection as indicated in results and figure legends.

Chromatin immunoprecipitation. Chromatin immunoprecipitation assays were carried out using Upstate Biologics (Waltham, MA) protocol and reagents. Briefly, cells (1-100-mm dish per treatment) were cross-linked with 1% formaldehyde, harvested, and sonicated before immunoprecipitation. One microgram each of anti-VDR (H-81) and anti-VDR (N-20) rabbit polyclonal antibodies (Santa Cruz Biotechnology) was used for overnight 4°C immunoprecipitation. Protein A-agarose beads were then used to pull down immune complexes. Beads were washed, then reverse cross-linked with NaCl at 65°C. The DNA was extracted with spin columns. PCR (30 cycles) was done on 10% of the recovered DNA using primers flanking the vitamin D response element (VDRE) in the MKP5 promoter; VDRE-MKP5: 5′-ccagagccgagtgcaaatag-3′ and 5′-gcaactttcctgcagttcc-3′. Primers for the glyceraldehyde-3-phosphate dehydrogenase (GAPDH) promoter (5′-cggctactagcggttttacg-3′ and 5′-aagaagatgcggctgactgt-3′) were used as a negative control. PCR products were electrophoresed through 1.5% agarose gels containing 1 μg/mL of ethidium bromide and visualized by UV.

UV irradiation. Prostate cell cultures were exposed to 1,000 J/m^2 (~45 seconds) of UVB irradiation using calibrated UVB bulbs with a Kodaceal filter. The lid of the cell culture dish and phenol red–containing media were removed during UV irradiation.

***In vitro* p38 kinase assay.** All reagents, antibodies, and protocol for this assay were supplied by Cell Signaling Technologies. Fresh cell lysate was prepared as described above under *Cell lysate preparation and immunoblot.* Cell lysates containing 250 μg of protein were incubated overnight with immobilized phospho-p38 monoclonal antibody to immunoprecipitate activated p38. Bead-immune complexes were washed and resuspended in 1× kinase buffer containing 200 μmol/L ATP and recombinant activating transcription factor-2 (ATF-2) fusion protein as the substrate and incubated at 30°C for 30 minutes to allow phosphorylation of ATF-2. Reactions were terminated by addition of LDS sample buffer. Samples were then heated at 95°C for 5 minutes and kinase activity was determined by immunoblot analysis with phospho-ATF-2 antibody. Input protein (20 μg) was also immunoblotted and probed with anti-p38.

IL-6 ELISA. Prostate cells (10^5) were plated in 24-well culture plates. After 24 hours, fresh media containing various agents were added (as described in Results and figure legends). Conditioned media were collected following treatment and used at a 2:1 dilution to determine amount of secreted IL-6 with the Human IL-6 ELISA Kit II (BD Biosciences, San Diego, CA). Results were calculated from a standard curve and are expressed as pg/mL IL-6/10^6 cells or pg/10^5 cells.

IL-6 promoter activity. A pGL3 luciferase construct containing a 651-bp fragment of the IL-6 promoter and pRL-null-renilla (Promega, Madison, WI) were transiently transfected into E-PZ cells using NeoFX reagent. pGL3-IL-6 was a generous gift from Dr. Oliver Eikelberg at the University of Giessen (Giessen, Germany). Eight hours after transfection, cells were treated with vehicle or 50 nmol/L 1,25D. Cells were UV irradiated 14 hours after vehicle or 1,25D treatment. Luciferase activity was measured 24 hours after UV using the Dual-Luciferase Assay Kit (Promega). The ratio of luciferase to renilla-luciferase was determined to correct for transfection efficiency.

Results

1,25D increases MKP5 mRNA expression in primary cultures of normal prostatic epithelial cells. We previously showed that MKP5 mRNA was increased 3- to 10-fold after 6 hours of treatment with 50 nmol/L of 1,25D in three independent primary cultures of normal human prostatic epithelial cells (E-PZ; ref. 2). The optimal concentration of 1,25D required to up-regulate MKP5 mRNA was determined by quantitative reverse transcription-PCR (RT-PCR). A dose-response curve showed that 1 nmol/L of 1,25D was sufficient to increase MKP5 mRNA in E-PZ cells by 6 hours, but 50 nmol/L of 1,25D was required to maintain MKP5 mRNA up-regulation at 24 hours (Fig. 1*A*). Higher concentrations of 1,25D are needed at the time points >12 hours because high density E-PZ cells rapidly metabolize and inactivate 1,25D (23). In all subsequent experiments, 50 nmol/L of 1,25D was used to treat subconfluent cultures of E-PZ cells. Upon treatment with 50 nmol/L of 1,25D, increased MKP5 expression was observed as early as 3 hours and maintained for 24 hours in E-PZ cells (Fig. 1*B*).

The *MKP5* gene is located on chromosome 1 and is transcribed into three distinct mRNA splice variants that putatively encode two different proteins (24). MKP5 splice variant 1 encodes the full-length 52-kDa protein whereas variants 2 and 3 both encode a truncated 16-kDa protein that only contains the dual-specificity phosphatase domain (Fig. 1*D*). Because the biological significance of the MKP5 splice variants has not yet been characterized, we examined the ability of 1,25D to regulate the mRNA expression of the three MKP5 splice variants by quantitative RT-PCR. All of the MKP5 mRNA splice variants were induced following 6 hours of treatment with 50 nmol/L of 1,25D, but splice variant 1 seemed to be most abundant and achieved the highest level of mRNA induction in the E-PZ cells (Fig. 1*C*). Primers within exons 3 to 5 of MKP5, the conserved region present in all MKP5 mRNAs, were used for all subsequent experiments.

Up-regulation of MKP5 mRNA by 1,25D is VDR dependent and MKP5 promoter contains a putative VDRE that associates with VDR on 1,25D treatment. The rapid induction of MKP5 mRNA by 1,25D suggested that MKP5 is a direct target of 1,25D. Direct targets of 1,25D contain one or more VDREs in the promoter region, which mediate transcriptional regulation by VDR binding. Knockdown of VDR levels by VDR siRNA in E-PZ cells abolished the induction of MKP5 by 1,25D (Fig. 2*A*), showing that induction of MKP5 by 1,25D is VDR dependent. The mRNA expression of vitamin D 24-hydroxylase (CYP24), a well-characterized target of 1,25D, was similarly suppressed in cells transfected with VDR siRNA (Fig. 2*A*) whereas the expression of *TBP*, a housekeeping gene, was not affected by VDR siRNA transfection. On sequence analysis, a putative VDRE was identified −1,320 bp upstream of the 5′ untranslated region in the MKP5 promoter (Fig. 2*B*). The putative MKP5-VDRE was highly similar to the characterized VDREs present in the promoters of CYP24 and parathyroid hormone–related protein. Chromatin immunoprecipitation assay showed an increased interaction between VDR and the putative MKP5-VDRE that exhibited time-dependent changes on stimulation with 50 nmol/L of 1,25D in E-PZ cells (Fig. 2*C*). The cyclic nature of VDR interaction with the MKP5 promoter observed in the chromatin immunoprecipitation experiments is consistent with previously described interactions of nuclear hormone receptors with DNA (25). The siRNA and chromatin immunoprecipitation data together provide strong support that MKP5 is directly regulated by 1,25D at the transcription level.

MKP5-mediated p38 inactivation by 1,25D occurs in E-PZ cells and not in PCa cell lines. Phosphorylation of p38 is required for activation of p38 kinase activity. MKP5 dephosphorylates p38, thus reducing p38 kinase activity. Vitamin D has been shown to

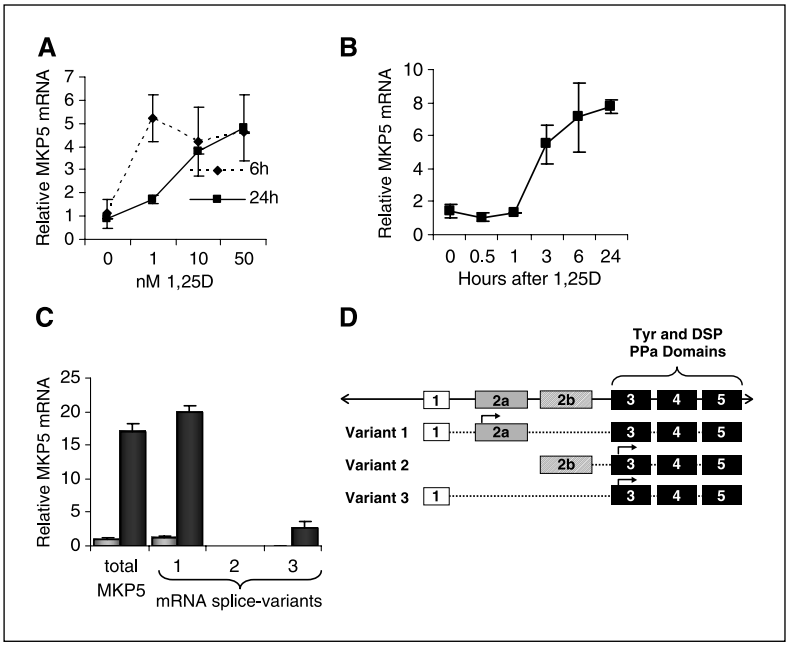

Figure 1. 1,25D increases MKP5 mRNA expression in primary cultures of normal prostatic epithelial cells (E-PZ). Quantitative RT-PCR measurement of MKP5 mRNA levels in E-PZ cells, 6 hours (*dashed line*) and 24 hours (*solid line*) after treatment with 1, 10, and 50 nmol/L 1,25D (*A*) and 0.5, 1, 3, 6 and 24 hours following 50 nmol/L 1,25D treatment (*B*). *C,* quantitative RT-PCR analysis of MKP5 mRNA splice variants in E-PZ cells after 6-hour vehicle (*light columns*) or 50 nmol/L 1,25D (*dark columns*) treatment (mRNA levels for isoform 2 treated with vehicle and 1,25D are 0.003 ± 0.0007 and 0.014 ± 0.0004, respectively, but are not visible on this graph). *D,* diagram of MKP5 mRNA splice variants. Quantitative RT-PCR results are shown relative to untreated control and normalized to expression of housekeeping gene *TBP*. Each experiment was run in triplicate and graphs are representative of two or more separate experiments with different patient-derived E-PZ cells. *Bars,* SD.

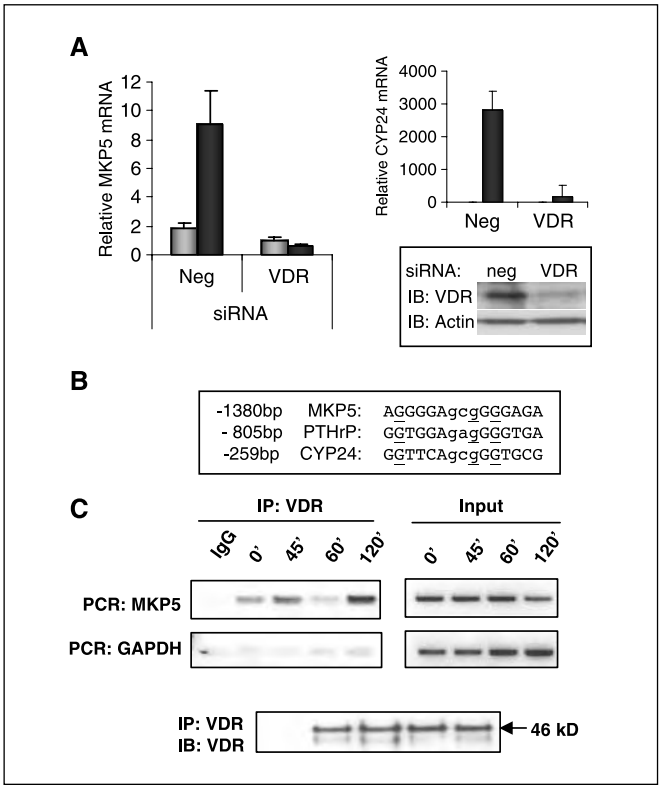

Figure 2. Up-regulation of MKP5 mRNA by 1,25D is VDR dependent and MKP5 promoter contains a putative VDRE that associates with VDR on 1,25D treatment. *A,* quantitative RT-PCR analysis of MKP5 mRNA 6 hours after treatment with vehicle (*light columns*) or 50 nmol/L 1,25D (*dark columns*) in E-PZ cells that were transfected for 24 hours with negative control siRNA or VDR siRNA. CYP24 gene expression was included as positive control for VDR knockdown (untreated mRNA level of CYP24 is equal to one and is not visible on this graph) and immunoblot of nuclear lysate (10 μg) verified VDR knockdown by the siRNA. *B,* diagram of putative VDRE located −1,380 bp of 5′UTR in MKP5 promoter aligned with validated VDREs in parathyroid hormone–related protein and CYP24. *C,* chromatin immunoprecipitation analysis and PCR of putative VDRE in MKP5 promoter and GAPDH promoter following 50 nmol/L 1,25D treatment using rabbit polyclonal VDR antibody for pulldown. Immunoblot of protein precipitate probed with mouse monoclonal VDR antibody shows specific pulldown of VDR. Results are representative of four or more separate experiments with different patient-derived E-PZ cells. Quantitative RT-PCR results are shown relative to untreated control and normalized to expression of housekeeping gene *TBP*. Each experiment was run in triplicate and graphs were representative of two or more separate experiments. *Bars,* SD.

inhibit osmotic stress–stimulated p38 phosphorylation in keratinocytes (26). We observed a similar inhibition of p38 phosphorylation by 1,25D in E-PZ cells (Fig. 3*A*). E-PZ cells were pretreated with 1,25D for 14 hours to allow for sufficient up-regulation of MKP5 protein. MKP5 protein levels could not be directly monitored in this study due to lack of an appropriate antibody. After pretreatment with 1,25D, osmotic stress–stimulated phosphorylated p38 levels were appreciably decreased compared with levels in cells not treated with 1,25D. Transfection with MKP5-specific siRNA attenuated induction of MKP5 mRNA by 1,25D compared with negative control siRNA (Fig. 3*B*) and abolished the suppression of p38 phosphorylation by 1,25D (Fig. 3*A*), implicating MKP5 as the mediator of p38 inactivation by 1,25D.

We examined the effect of 1,25D on MKP5 in various other prostate-derived cells in comparison with the primary cultures of E-PZ cells. The results showed that, like E-PZ cells, pRNS-1-1 cells also induce MKP5 (Fig. 3*C*). In contrast, prostate stromal cells (F-PZ) and established PCa cell lines (PC-3, LNCaP, and DU 145) did not up-regulate MKP5 mRNA following 1,25D treatment (Fig. 3*C*). pRNS-1-1 cells were generated by SV40 transformation and immortalization of E-PZ cells and are not growth inhibited by 1,25D, although they retain VDR and other responses to 1,25D (1). Prostatic stromal cells too express VDR and show certain responses to 1,25D despite lack of induction of MKP-5 in these cells by 1,25D (1). The PCa cell lines PC-3, LNCaP, and DU 145 all express VDR and respond to 1,25D in other ways (1). Immunoblot analysis showed that in DU 145, PC-3, and LNCaP cells, 1,25D pretreatment did not alter NaCl-induced p38 phosphorylation (Fig. 3*D*). These data suggest that MKP5 may specifically mediate 1,25D activity in normal prostate cells and that this activity is lost in advanced PCa.

We suspect that MKP5 up-regulation by 1,25D is not unique to prostatic epithelium. Because inactivation of p38 by 1,25D was reported in keratinocytes, we examined the expression of MKP5 in these cells. Similarly to prostatic epithelial cells, normal human keratinocytes showed up-regulation of MKP5 mRNA on treatment with 1,25D, suggesting that MKP5 may mediate p38 inactivation in keratinocytes as well (Supplementary Fig. S1*A*). Similarly to the PCa cell lines, up-regulation of MKP5 by 1,25D was attenuated in the human squamous cell carcinoma cell lines A431 and SCC-25 (Supplementary Fig. S1*B*).

MKP5 mediates decreased IL-6 production in E-PZ cells by 1,25D. Published studies have shown that 1,25D inhibits UV-induced IL-6 production in keratinocytes; however, no mechanism has been proposed (27). IL-6 overexpression has been strongly associated with PCa progression and, therefore, inhibition of IL-6 may play an important role in PCa prevention. Because IL-6 induction is downstream of p38 activation and often dependent on p38 activation (13, 28), we tested the role of MKP5 in regulating IL-6 expression in E-PZ cells. An *in vitro* p38 kinase activity assay, using ATF-2 as the substrate, showed that 1,25D pretreatment decreased basal and UV-stimulated p38 activity in E-PZ cells (Fig. 4*A*). The 1,000 J/m^2 dose of UVB irradiation used in these experiments did not induce apoptosis or necrosis in E-PZ cells (data not shown). Consistent with p38 inactivation, secreted levels of IL-6 protein following UV treatment were suppressed by 1,25D pretreatment (Fig. 4*B*). SB202190, a specific p38 inhibitor, similarly decreased UV-stimulated IL-6 production (Fig. 4*B*). A decrease in IL-6 mRNA expression was observed in 1,25D pretreated samples and this decrease was blocked by transient transfection with MKP5 siRNA (Fig. 4*C*). The primary mechanism for increased IL-6 production following p38 activation is through IL-6 mRNA stabilization rather than increased mRNA transcription (29). To determine if this is also true for 1,25D regulation of IL-6 mRNA, we examined the effect of 1,25D on IL-6 promoter activity in the absence or presence of UV irradiation. We found that neither UV irradiation nor 1,25D treatment significantly altered IL-6 promoter activity as determined by luciferase assay in E-PZ cells (Fig. 4*D1*), suggesting that 1,25D is not altering mRNA transcription. When 1 μmol/L of actinomycin D was used to inhibit new mRNA transcription, we observed that UV irradiation caused IL-6 mRNA stabilization and 1,25D pretreatment decreased the UV-induced IL-6 mRNA stabilization (Fig. 4*D2*). Under basal conditions, IL-6 mRNA half-life was <45 minutes in E-PZ cells. In UV-irradiated cells, IL-6 mRNA half-life increased to >90 minutes whereas UV irradiation did not significantly alter IL-6 mRNA half-life in 1,25D pretreated cells (Fig. 4*D2*).

1,25D inhibits tumor necrosis factor α–stimulated p38 activation and IL-6 production. The ability of 1,25D to inhibit

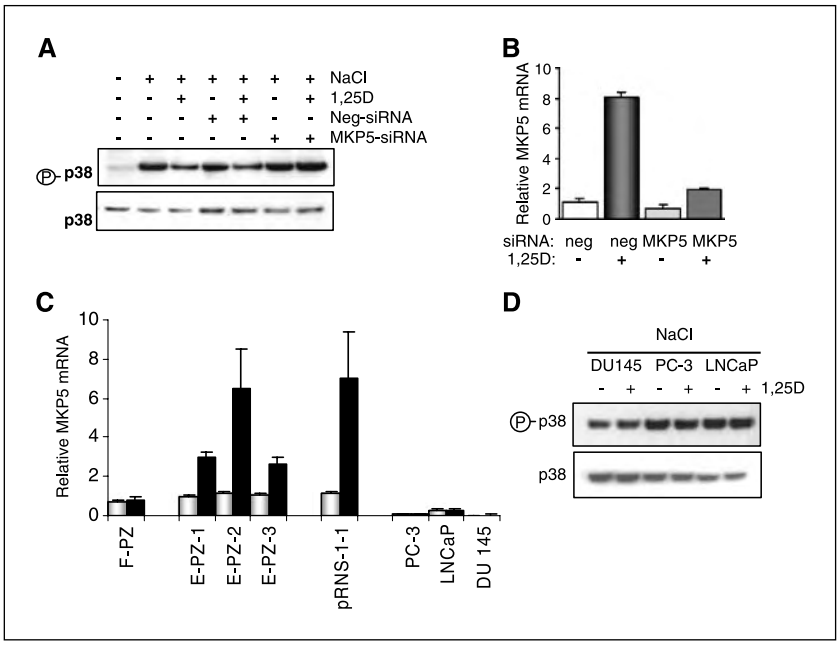

Figure 3. MKP5-mediated p38 inactivation by 1,25D occurs in E-PZ cells and not in PCa cell lines. *A,* immunoblot analysis of p38 phosphorylation in 20 μg of E-PZ cell lysate 20 minutes after treatment with 0.5 mol/L NaCl. Before NaCl treatment, E-PZ cells were transfected with negative control or MKP5 siRNA for 4 hours, then treated with vehicle or 50 nmol/L 1,25D for 14 hours. *B,* quantitative RT-PCR analysis of MKP5 mRNA expression in E-PZ cells transfected with negative control siRNA (*open columns*) or MKP5 siRNA (*striped columns*) 4 hours before vehicle (*light columns*) or 1,25D (*shaded columns*) treatment for 12 hours. Representative of at least three separate experiments with different patient-derived E-PZ cells. Results are displayed relative to negative siRNA control and normalized to expression of the housekeeping gene *TBP. Bars,* SD of triplicate samples. *C,* quantitative RT-PCR analysis of MKP5 mRNA 6 hours after treatment with vehicle (*light columns*) or 50 nmol/L 1,25D (*dark columns*) in primary cultures of prostate stroma (F-PZ) in three different cultures of normal primary prostatic epithelial cells (derived from normal peripheral zone designated E-PZ) and in prostate cell lines pRNS-1-1, LNCaP, PC-3, and DU 145. Quantitative RT-PCR results are displayed relative to control and normalized to expression of the housekeeping gene *TBP. Bars,* SD. *D,* immunoblot analysis of p38 phosphorylation 20 minutes after treatment with 0.5 mol/L NaCl in DU 145, PC-3, and LNCaP cells pretreated for 14 hours with vehicle or 50 nmol/L 1,25D.

p38 phosphorylation was further investigated using a more physiologic stress, tumor necrosis factor α (TNF-α). TNF-α is a proinflammatory cytokine released by inflammatory cells that can trigger cell proliferation, necrosis, apoptosis, and induction of other cytokines (12). Interestingly, elevated serum levels of TNF-α are associated with aggressive pathology and decreased survival of PCa patients (16). In E-PZ cells, TNF-α does not induce apoptosis but does significantly slow cell growth (30). TNF-α binds cell-surface receptors which signal through multiple pathways, including p38 kinase, to increase production of IL-6 and other cytokines (12). Immunoblot analysis showed that TNF-α-stimulated p38 phosphorylation was attenuated by 1,25D pretreatment, similar to the

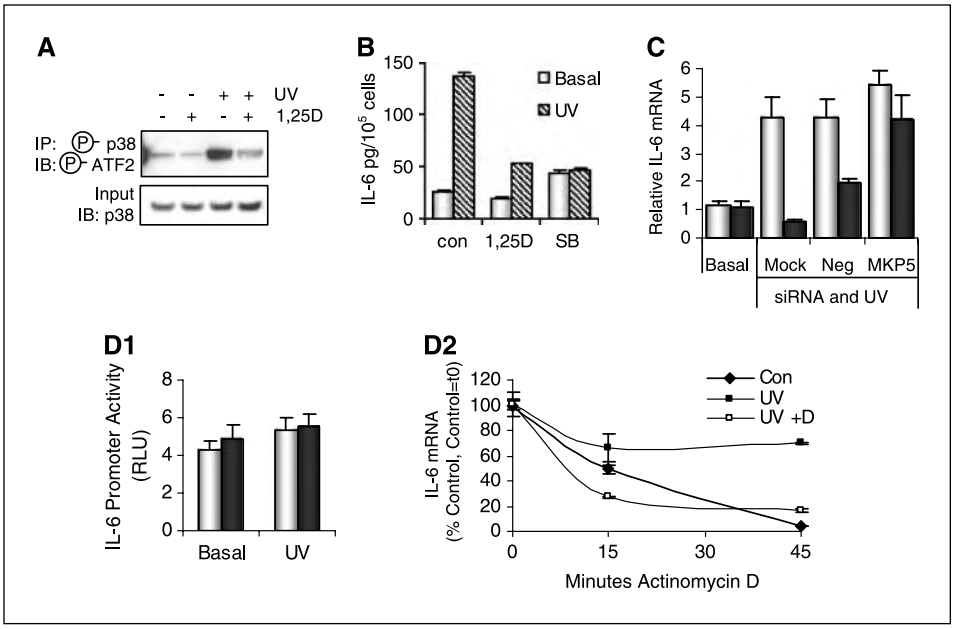

Figure 4. MKP5 mediates decreased IL-6 production in E-PZ cells by 1,25D. *A, in vitro* p38 kinase activity assay, using ATF-2 as a substrate, in E-PZ cells 20 minutes after 1,000 J/m^2 UVB irradiation in E-PZ cells pretreated 14 hours with vehicle or 50 nmol/L 1,25D. *B,* ELISA measurement of secreted IL-6 in cell culture media 24 hours after UVB irradiation (*hatched columns*) in E-PZ cells pretreated with vehicle, 50 nmol/L 1,25D for 14 hours, or 1 μmol/L SB202190 for 1 hour. *C,* quantitative RT-PCR measurement of IL-6 mRNA in E-PZ cells 24 hours after UV irradiation. Cells were either transiently transfected with negative siRNA or MKP5 siRNA for 4 hours, then pretreated for 14 hours with either vehicle (*light columns*) or 50 nmol/L 1,25D (*dark columns*) before UV. *D1,* luciferase activity of pGL3-IL-6 24 hours after UV irradiation in E-PZ cells pretreated for 14 hours with vehicle (*light columns*) or 50 nmol/L 1,25D (*dark columns*). *D2,* quantitative RT-PCR analysis of IL-6 mRNA stability in E-PZ cells following UV irradiation. Cells were treated with 1 μmol/L actinomycin D for 0, 15, and 45 minutes. Actinomycin was dosed 30 minutes after UV and cells were pretreated 14 hours before UV with vehicle (■) or 50 nmol/L 1,25D (□). IL-6 mRNA levels under basal conditions after 15 to 45 minutes of treatment with 1 μmol/L actinomycin D were shown as control (♦).

effect of 1,25D on UV-stimulated p38 phosphorylation in E-PZ cells (Fig. 5*A*). Changes in IL-6 mRNA and secreted protein levels were followed over a time course after TNF-α stimulation and showed that 1,25D pretreatment attenuated the initial production of IL-6 and completely inhibited the accumulation of IL-6 in the media (Fig. 5*B* and *C*).

1,25D up-regulates MKP5 mRNA and inhibits TNF-α-stimulated IL-6 production in matched pairs of normal and tumor cells from individual PCa patients. Because we observed a difference in regulation of MKP5 by 1,25D between E-PZ cells and PCa cell lines, we analyzed the effect of 1,25D on MKP5 and IL-6 in matched pairs of normal (E-PZ) and tumor (E-CA) cells from two PCa patients with localized Gleason grade 4/3 cancers (individuals *A* and *B*). Quantitative RT-PCR analysis showed that MKP5 mRNA was up-regulated by 1,25D in E-CA as well as E-PZ cells from both individuals (Fig. 6*A*). In addition, IL-6 mRNA and protein levels, following TNF-α stimulation, were decreased by 1,25D pretreatment in all of the matched pairs of normal and cancer cultures (Fig. 6*B* and *C*). Although patient-to-patient variability was evident in the extent of TNF-α-stimulated IL-6 production, cancer cells from primary adenocarcinomas retain the ability to up-regulate MKP5 in response to 1,25D, in contrast to the established metastases-derived cell lines (DU 145, LNCaP, and PC-3).

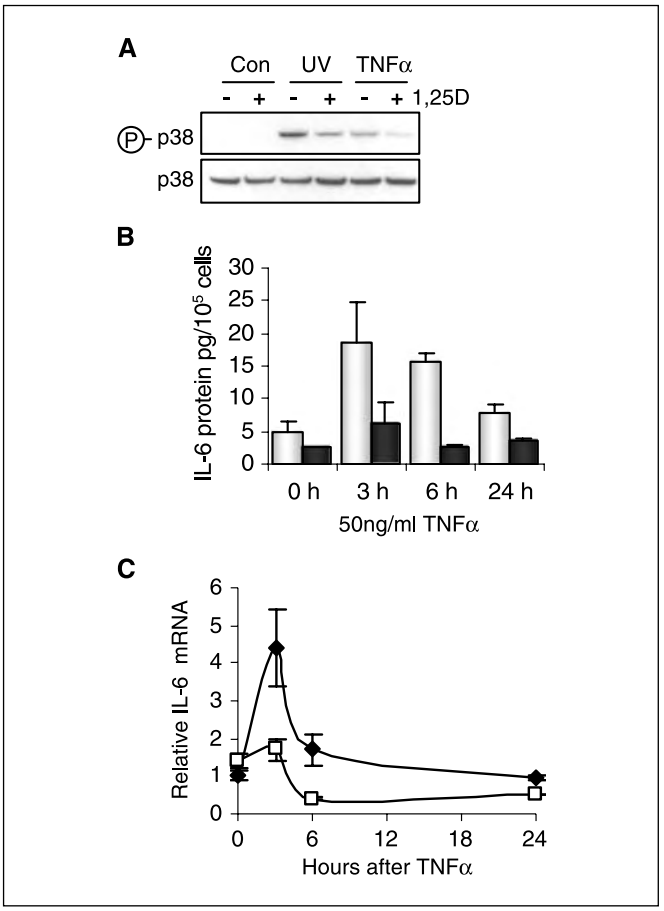

Figure 5. 1,25D inhibits TNF-α-stimulated p38 phosphorylation and IL-6 production. *A,* immunoblot analysis of p38 phosphorylation 20 minutes after treatment with 1,000 J/m^2 UVB or 50 ng/mL TNF-α in E-PZ cells pretreated 14 hours with vehicle or 50 nmol/L 1,25D. *B,* ELISA measurement of secreted IL-6 in cell culture media 3, 6, and 24 hours after 50 ng/mL TNF-α in E-PZ cells pretreated 14 hours with vehicle (*light columns*) or 50 nmol/L 1,25D (*dark columns*). *C,* quantitative RT-PCR analysis of IL-6 mRNA 3, 6, and 24 hours after 50 ng/mL TNF-α in E-PZ cells pretreated for 24 hours with vehicle (♦) or 50 nmol/L 1,25D (□). *IL-6* gene expression relative to untreated control and normalized to expression of the housekeeping gene *TBP. Bars,* SD of triplicate samples.

Discussion

The purpose of these studies was to explore the potential significance of MKP5 in mediating PCa prevention by vitamin D. We previously identified MKP5 as a target of 1,25D in normal human prostatic epithelial cells by microarray analysis (2). The results of our studies suggest that the ability of vitamin D to inhibit p38 signaling, via MKP5 up-regulation, may be a significant antitumor activity of vitamin D (Fig. 7).

MKP5 is likely a direct target of 1,25D, regulated by a positive VDRE in the promoter region of the gene. Treatment of E-PZ cells with 1,25D produced a time- and dose-dependent increase in MKP5 mRNA that was dependent on VDR expression. Furthermore, VDR was found to associate with the VDRE in the MKP5 promoter on 1,25D treatment. These data support direct transcriptional activation of the *MKP5* gene by 1,25D. Consistent with increased levels of MKP5, 1,25D inhibited p38 phosphorylation. MKP5 siRNA blocked p38 inactivation by 1,25D, which further showed that MKP5 mediates p38 inactivation by 1,25D.

The ability of 1,25D to inactivate p38 led us to examine the regulation of IL-6, which is downstream of p38 activation (28), by 1,25D. Suppression of UV-stimulated IL-6 production by 1,25D was previously shown in keratinocytes (27) and we suspected that similar activity could be mediated by MKP5 in normal prostatic epithelial cells. Using MKP5 siRNA, we showed that 1,25D inhibited UV-stimulated p38 activity and IL-6 production in a MKP5-dependent manner in E-PZ cells. UV irradiation did not increase IL-6 promoter activity but did increase mRNA half-life, indicating posttranscriptional regulation of IL-6 mRNA expression. 1,25D pretreatment was able to attenuate the UV-stimulated increase in IL-6 mRNA half-life. Induction of IL-6 by a more physiologically relevant stress, TNF-α, was similarly inhibited by 1,25D.

IL-6 has been shown to be negatively regulated by androgens and the androgen receptor in murine bone marrow–derived fibroblasts (31). It is unlikely that androgen receptor contributes to IL-6 regulation observed in E-PZ cells because E-PZ cells are typical of prostatic basal epithelial cells and do not express androgen receptor (32). There is evidence of cross-talk and regulation of androgen receptor by vitamin D (1). In cells where androgen receptor and VDR are both expressed, such as the luminal cells of the prostate, it is possible that cooperation of the two pathways could facilitate a further decrease in IL-6 expression.

IL-6, as well as other interleukins and/or their receptors, are overexpressed in PCa tissue and/or serum of PCa patients (15, 33). Elevated serum levels of IL-6 and TNF-α are associated with aggressive pathology and decreased survival of PCa patients (16). Increased IL-6 staining is observed in malignant prostate tissue compared with adjacent normal tissue and IL-6 also contributes to the development of hormone-refractory cancer by androgen-independent activation of the androgen receptor (17). *In vitro*, the PCa cell lines DU 145, PC-3, and LNCaP all express the IL-6 receptor and are responsive to exogenous IL-6; however, DU 145 and PC-3 also greatly overexpress endogenous IL-6 whereas the LNCaP cell line does not express any IL-6 (15). The mechanism(s) leading to constitutive overexpression of IL-6 in PCa cells and

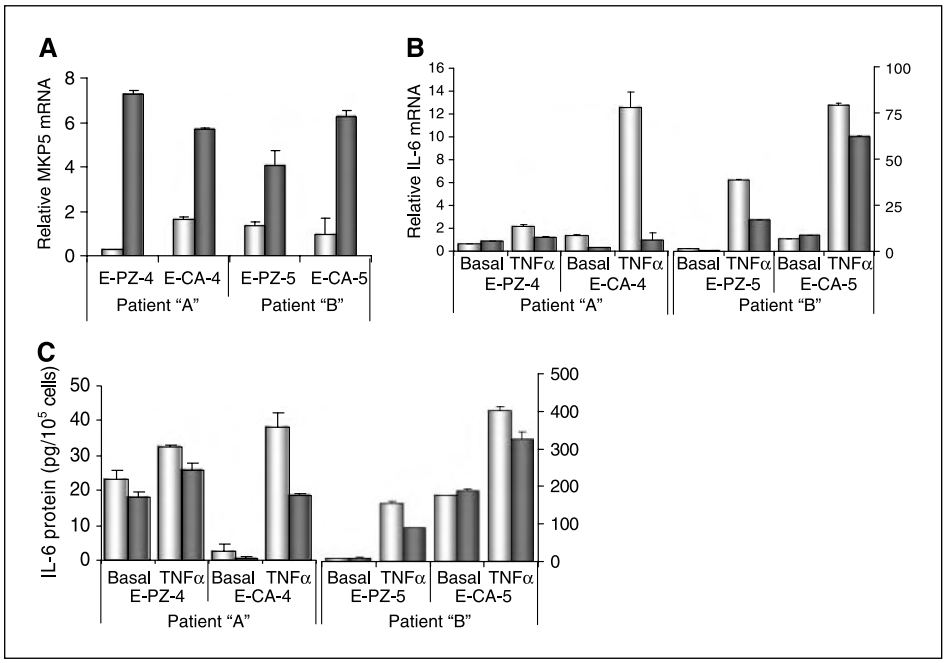

Figure 6. 1,25D up-regulates MKP5 mRNA and inhibits TNF-α-stimulated IL-6 production in matched pairs of normal and tumor cells from individual PCa patients. *A,* quantitative RT-PCR measurement of MKP5 mRNA levels in patient *A* E-PZ and E-CA cells and patient *B* E-PZ and E-CA cells 15 hours after treatment with vehicle (*open columns*) or 50 nmol/L 1,25D (*shaded columns*). *B,* quantitative RT-PCR analysis of IL-6 mRNA 3 hours after 50 ng/mL TNF-α in cells pretreated 15 hours with vehicle (*open columns*) or 50 nmol/L 1,25D (*shaded columns*). *MKP5* and *IL-6* gene expressions are shown relative to untreated control and normalized to expression of the housekeeping gene *TBP*. *Bars,* SD of triplicate samples. *C,* ELISA measurement of secreted IL-6 in cell culture media 3 hours after 50 ng/mL TNF-α in E-PZ and E-CA cells pretreated for 14 hours with vehicle (*light columns*) or 50 nmol/L 1,25D (*dark columns*).

tissues has not been fully characterized but seems to be transcriptional rather than posttranscriptional (34).

Although proinflammatory factors are overexpressed in PCa, it is unclear whether increased levels of these factors are required for development of the cancer originally or are a consequence of the cancer. On one hand, inflammation may trigger the initial expression of these factors in normal prostate tissue and when PCa arises, the PCa cells maintain these features for a survival advantage. On the other hand, because there is significant inflammatory infiltrate in PCa lesions, the possibility of the inflammatory genes becoming expressed later in PCa development cannot be excluded. If the former situation occurs, then our results suggest that the ability of 1,25D to suppress the synthesis of IL-6, and perhaps other inflammatory factors, may be a key component in blocking carcinogenic events associated with inflammation.

Another important finding from our study was that 1,25D up-regulated MKP5 in primary cultures derived from normal prostatic epithelium or primary adenocarcinomas of the prostate and in SV40 Tag–immortalized prostatic epithelial pRNS-1-1 cells, but not in the prostatic stromal cells or in PCa cell lines. pRNS-1-1 cells are not sensitive to growth inhibition by 1,25D yet retain functional VDR (1). Stromal cells (F-PZ) derived from normal prostatic tissue and PCa cell lines did not induce MKP5 when treated with 1,25D although these cells express VDR and are growth-inhibited by 1,25D (1). Furthermore, the squamous cell carcinoma cell lines A431 and SCC-25 displayed attenuated MKP5 up-regulation following 1,25D treatment compared with normal keratinocytes although they too retain VDR and growth inhibition by 1,25D (35, 36). We observed up-regulation of MKP5 by 1,25D in the matched pairs of E-PZ and E-CA cells from individual patients. These E-CA cells were derived from localized PCa whereas PC-3, DU 145, and LNCaP were all derived from PCa metastases. These data suggest that localized PCa may still be responsive to the anti-inflammatory properties of vitamin D. Together these observations show that (*a*) induction of MKP5 by

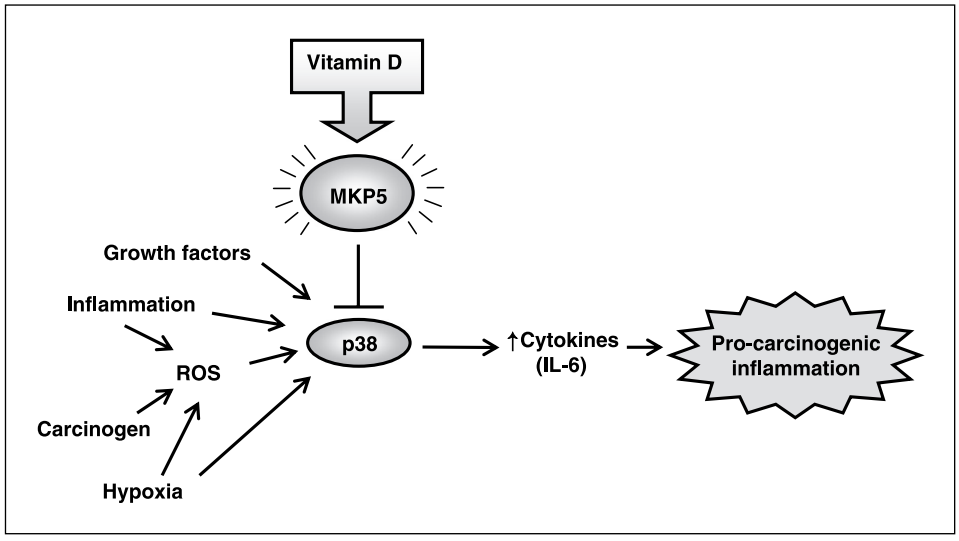

Figure 7. Proposed mechanism for anti-inflammatory activity and PCa prevention by vitamin D.

1,25D is specific to normal and localized malignant prostatic *epithelial* cells and does not occur in normal prostatic *stromal* cells; (*b*) induction of MKP5 is *independent* of growth inhibition by 1,25D; and (*c*) lack of 1,25D-induced MKP5 in PCa cell lines is not a result of immortalization per se because immortalized pRNS-1-1 cells up-regulate MKP5 in response to 1,25D.

The quantitative RT-PCR data show that the basal levels of MKP5 are lower in the PCa cell lines compared with normal prostatic epithelial cells. Because the established metastasis-derived PCa cell lines have low levels of MKP5 and are unable to induce MKP5 in response to 1,25D, it is tempting to speculate that loss of MKP5 may occur during PCa progression as the result of selective pressure to eliminate tumor suppressor activity of MKP5 and/or 1,25D. A number of MKP family members have been suggested to be tumor suppressors. In PCa MKP1 has been shown to be down-regulated (37). Candidate MKP tumor suppressors in other malignancies include MKP7, which is frequently deleted in lymphoblastic leukemia (38), MKP3, hypermethylated or deleted in pancreatic cancer (39, 40), and MKP2, which is deleted in breast carcinoma (41).

The link between inhibition of p38 by 1,25D via MKP5 and PCa prevention becomes more apparent when the many different ways the p38 pathway may become activated are considered. In addition to inflammatory cytokines, osmotic stress, UV irradiation (which we used in these studies), reactive oxygen species and hypoxia also activate p38 (42). Reactive oxygen species can amplify p38 activation because they are generated during hypoxia and as a by-product of inflammation (refs. 6, 8; Fig. 7). Hypoxia has been implicated in PCa metastasis and progression to androgen independence (6).

In addition to a potential role in PCa prevention, p38 inhibition by 1,25D via MKP5 may be farther reaching and mitigate activities of vitamin D in other tissues. Recent cDNA microarray analyses have shown MKP5 up-regulation by vitamin D in skin (43), colon (44), and ovarian cells (45). Furthermore, the overall immunomodulatory activity of vitamin D on the VDR-expressing cells of the innate and adaptive immune system (46) is highly similar to the immunomodulatory role of MKP5 that was shown by Zhang et al. (47) using MKP5 knockout mice. The mechanism by which vitamin D reduced IL-6 mRNA stability, through MKP5-mediated p38 inactivation, may also be responsible for down-regulation of other mRNAs. Activation of the p38 pathway causes a robust and rapid increase in inflammatory response proteins by mRNA stabilization and increased translation through AU-rich elements in the 3′ untranslated region (UTR; ref. 48). Posttranscriptional regulation of inflammatory genes is the basis for the anti-inflammatory activity of p38 inhibitors (48). Decreased mRNA stabilization by vitamin D has been shown to mediate down-regulation of granulocyte macrophage colony-stimulating factor (49) and this mechanism may decrease the stability of other AU-rich 3′-UTR–containing proinflammatory mRNAs by vitamin D.

It is becoming apparent that inflammation, both chronic and acute, contributes to PCa development. The epidemiologic evidence combined with the molecular pathogenesis of PCa supports this hypothesis (7). If inflammation is a significant risk factor for PCa, then PCa prevention will best be achieved with agents, such as vitamin D, which inhibit inflammation and/or decrease the cellular stress response that accompanies inflammation. Our study shows that MKP5 is a mediator of anti-inflammatory effects of 1,25D and suggests that vitamin D may play a significant role in PCa prevention by facilitating p38 inhibition and reduced IL-6 production in prostatic epithelial cells.

Acknowledgments

Received 10/20/2005; revised 1/25/2006; accepted 2/9/2006.

Grant support: Department of Defense Congressionally Directed Medical Research Programs postdoctoral grant PC040616 (L. Nonn), American Foundation for Urological Disease postdoctoral research scholar award, and NIH grant DK42482 (L. Peng and D. Feldman).

The costs of publication of this article were defrayed in part by the payment of page charges. This article must therefore be hereby marked *advertisement* in accordance with 18 U.S.C. Section 1734 solely to indicate this fact.

We thank Drs. Aruna Krishnan and Bryan Husbeck for insightful conversations about research and manuscript preparation; Dr. James M. Ford and the Ford lab members for advice on UV radiation and use of their UV irradiator; and Dr. Oliver Eikelberg for generously providing the pGL3-IL-6 luciferase construct.

References

1. Krishnan AV, Peehl DM, Feldman D. Vitamin D and prostate cancer. In: Glorieux FH, editor. Vitamin D. San Diego: Elsevier Academic Press; 2005. p. 1679–707.
2. Peehl DM, Shinghal R, Nonn L, et al. Molecular activity of 1,25-dihydroxyvitamin D(3) in primary cultures of human prostatic epithelial cells revealed by cDNA microarray analysis. J Steroid Biochem Mol Biol 2004; 92:131–41.
3. Tanoue T, Moriguchi T, Nishida E. Molecular cloning and characterization of a novel dual specificity phosphatase, MKP-5. J Biol Chem 1999;274:19949–56.
4. Theodosiou A, Smith A, Gillieron C, Arkinstall S, Ashworth A. MKP5, a new member of the MAP kinase phosphatase family, which selectively dephosphorylates stress-activated kinases. Oncogene 1999;18:6981–8.
5. Roux PP, Blenis J. ERK and p38 MAPK-activated protein kinases: a family of protein kinases with diverse biological functions. Microbiol Mol Biol Rev 2004;68: 320–44.
6. Hochachka PW, Rupert JL, Goldenberg L, Gleave M, Kozlowski P. Going malignant: the hypoxia-cancer connection in the prostate. Bioessays 2002;24:749–57.
7. Nelson WG, De Marzo AM, DeWeese TL, Isaacs WB. The role of inflammation in the pathogenesis of prostate cancer. J Urol 2004;172:S6–11; discussion S-2.
8. Coussens LM, Werb Z. Inflammation and cancer. Nature 2002;420:860–7.
9. Palapattu GS, Sutcliffe S, Bastian PJ, et al. Prostate carcinogenesis and inflammation: emerging insights. Carcinogenesis 2005;26:1170–81.
10. Platz EA, Rohrmann S, Pearson JD, et al. Nonsteroidal anti-inflammatory drugs and risk of prostate cancer in the Baltimore Longitudinal Study of Aging. Cancer Epidemiol Biomarkers Prev 2005;14:390–6.
11. Fernandez L, Galan Y, Jimenez R, et al. Sexual behaviour, history of sexually transmitted diseases, and the risk of prostate cancer: a case-control study in Cuba. Int J Epidemiol 2005;34:193–7.
12. Brinkman BM, Telliez JB, Schievella AR, Lin LL, Goldfeld AE. Engagement of tumor necrosis factor (TNF) receptor 1 leads to ATF-2- and p38 mitogen-activated protein kinase-dependent TNF-α gene expression. J Biol Chem 1999;274:30882–6.
13. Park JI, Lee MG, Cho K, et al. Transforming growth factor-β1 activates interleukin-6 expression in prostate cancer cells through the synergistic collaboration of the Smad2, p38-NF-κB, JNK, and Ras signaling pathways. Oncogene 2003;22:4314–32.
14. Giri D, Ozen M, Ittmann M. Interleukin-6 is an autocrine growth factor in human prostate cancer. Am J Pathol 2001;159:2159–65.
15. Corcoran NM, Costello AJ. Interleukin-6: minor player or starring role in the development of hormone-refractory prostate cancer? BJU Int 2003;91: 545–53.
16. Michalaki V, Syrigos K, Charles P, Waxman J. Serum levels of IL-6 and TNF-α correlate with clinicopathological features and patient survival in patients with prostate cancer. Br J Cancer 2004;91:1227.
17. Culig Z, Steiner H, Bartsch G, Hobisch A. Interleukin-6 regulation of prostate cancer cell growth. J Cell Biochem 2005;95:497–505.
18. McNeal JE, Redwine EA, Freiha FS, Stamey TA. Zonal distribution of prostatic adenocarcinoma. Correlation with histologic pattern and direction of spread. Am J Surg Pathol 1988;12:897–906.
19. Peehl DM. Growth or prostatic epithelial and stromal cells *in vitro*. In: Russell PJ, Kingsley EA, editors. Prostate cancer methods and protocols. Totowa (NJ): Human Press; 2003. p. 41–57.
20. Rhim JS, Webber MM, Bello D, et al. Stepwise immortalization and transformation of adult human prostate epithelial cells by a combination of HPV-18 and v-Ki-ras. Proc Natl Acad Sci U S A 1994;91: 11874–8.
21. Livak KJ, Schmittgen TD. Analysis of relative gene expression data using real-time quantitative PCR and the 2(−ΔΔC(T)) Method. Methods 2001;25:402–8.
22. Radonic A, Thulke S, Mackay IM, Landt O, Siegert W, Nitsche A. Guideline to reference gene selection for quantitative real-time PCR. Biochem Biophys Res Commun 2004;313:856–62.
23. Peehl DM, Seto E, Hsu JY, Feldman D. Preclinical

activity of ketoconazole in combination with calcitriol or the vitamin D analogue EB 1089 in prostate cancer cells. J Urol 2002;168:1583–8.
24. Masuda K, Shima H, Kikuchi K, Watanabe Y, Matsuda Y. Expression and comparative chromosomal mapping of MKP-5 genes DUSP10/Dusp10. Cytogenet Cell Genet 2000;90:71–4.
25. Kim S, Shevde NK, Pike JW. 1,25-Dihydroxyvitamin D3 stimulates cyclic vitamin D receptor/retinoid X receptor DNA-binding, co-activator recruitment, and histone acetylation in intact osteoblasts. J Bone Miner Res 2005;20:305–17.
26. Ravid A, Rubinstein E, Gamady A, Rotem C, Liberman UA, Koren R. Vitamin D inhibits the activation of stress-activated protein kinases by physiological and environmental stresses in keratinocytes. J Endocrinol 2002;173:525–32.
27. De Haes P, Garmyn M, Degreef H, Vantieghem K, Bouillon R, Segaert S. 1,25-Dihydroxyvitamin D3 inhibits ultraviolet B-induced apoptosis, Jun kinase activation, and interleukin-6 production in primary human keratinocytes. J Cell Biochem 2003;89:663–73.
28. Craig R, Larkin A, Mingo AM, et al. p38 MAPK and NF-κB collaborate to induce interleukin-6 gene expression and release. Evidence for a cytoprotective autocrine signaling pathway in a cardiac myocyte model system. J Biol Chem 2000;275:23814–24.
29. Winzen R, Kracht M, Ritter B, et al. The p38 MAP kinase pathway signals for cytokine-induced mRNA stabilization via MAP kinase-activated protein kinase 2 and an AU-rich region-targeted mechanism. EMBO J 1999;18:4969–80.
30. Chopra DP, Menard RE, Januszewski J, Mattingly RR. TNF-α-mediated apoptosis in normal human prostate epithelial cells and tumor cell lines. Cancer Lett 2004;203:145–54.
31. Bellido T, Jilka RL, Boyce BF, et al. Regulation of interleukin-6, osteoclastogenesis, and bone mass by androgens. The role of the androgen receptor. J Clin Invest 1995;95:2886–95.
32. Peehl DM. Primary cell cultures as models of prostate cancer development. Endocr Relat Cancer 2005;12:19–47.
33. Ricote M, Royuela M, Garcia-Tunon I, Bethencourt FR, Paniagua R, Fraile B. Pro-apoptotic tumor necrosis factor-α transduction pathway in normal prostate, benign prostatic hyperplasia and prostatic carcinoma. J Urol 2003;170:787–90.
34. Zerbini LF, Wang Y, Cho JY, Libermann TA. Constitutive activation of nuclear factor κB p50/p65 and Fra-1 and JunD is essential for deregulated interleukin 6 expression in prostate cancer. Cancer Res 2003;63:2206–15.
35. Cordero JB, Cozzolino M, Lu Y, et al. 1,25-Dihydroxyvitamin D down-regulates cell membrane growth- and nuclear growth-promoting signals by the epidermal growth factor receptor. J Biol Chem 2002;277:38965–71.
36. Enepekides DJ, Black MJ, White JH. The independent and combined effects of RAR-, RXR-, and VDR-selective ligands on the growth of squamous cell carcinoma *in vitro*. J Otolaryngol 1999;28:83–9.
37. Rauhala HE, Porkka KP, Tolonen TT, Martikainen PM, Tammela TL, Visakorpi T. Dual-specificity phosphatase 1 and serum/glucocorticoid-regulated kinase are down-regulated in prostate cancer. Int J Cancer 2005;117:738–45.
38. Montpetit A, Larose J, Boily G, Langlois S, Trudel N, Sinnett D. Mutational and expression analysis of the chromosome 12p candidate tumor suppressor genes in pre-B acute lymphoblastic leukemia. Leukemia 2004;18:1499–504.
39. Furukawa T, Fujisaki R, Yoshida Y, et al. Distinct progression pathways involving the dysfunction of DUSP6/MKP-3 in pancreatic intraepithelial neoplasia and intraductal papillary-mucinous neoplasms of the pancreas. Mod Pathol 2005;18:1034–42.
40. Xu S, Furukawa T, Kanai N, Sunamura M, Horii A. Abrogation of DUSP6 by hypermethylation in human pancreatic cancer. J Hum Genet 2005;50:159–67.
41. Armes JE, Hammet F, de Silva M, et al. Candidate tumor-suppressor genes on chromosome arm 8p in early-onset and high-grade breast cancers. Oncogene 2004;23:5697–702.
42. Liu XH, Kirschenbaum A, Lu M, et al. Prostaglandin E2 induces hypoxia-inducible factor-1α stabilization and nuclear localization in a human prostate cancer cell line. J Biol Chem 2002;277:50081–6.
43. Lu J, Goldstein KM, Chen P, Huang S, Gelbert LM, Nagpal S. Transcriptional profiling of keratinocytes reveals a vitamin D-regulated epidermal differentiation network. J Invest Dermatol 2005;124:778–85.
44. Palmer HG, Sanchez-Carbayo M, Ordonez-Moran P, Larriba MJ, Cordon-Cardo C, Munoz A. Genetic signatures of differentiation induced by 1α,25-dihydroxyvitamin D3 in human colon cancer cells. Cancer Res 2003;63:7799–806.
45. Zhang X, Li P, Bao J, et al. Suppression of death receptor-mediated apoptosis by 1,25-dihydroxyvitamin D3 revealed by microarray analysis. J Biol Chem 2005;280:35458–68.
46. Nagpal S, Na S, Rathnachalam R. Non-calcemic actions of vitamin D receptor ligands. Endocr Rev 2005;26:662–87.
47. Zhang Y, Blattman JN, Kennedy NJ, et al. Regulation of innate and adaptive immune responses by MAP kinase phosphatase 5. Nature 2004;430:793–7.
48. Saklatvala J. The p38 MAP kinase pathway as a therapeutic target in inflammatory disease. Curr Opin Pharmacol 2004;4:372–7.
49. Tobler A, Miller CW, Norman AW, Koeffler HP. 1,25-Dihydroxyvitamin D3 modulates the expression of a lymphokine (granulocyte-macrophage colony-stimulating factor) posttranscriptionally. J Clin Invest 1988;81:1819–23.

Alpha-Methylacyl-CoA Racemase (AMACR) Expression in Normal Prostatic Glands and High-Grade Prostatic Intraepithelial Neoplasia (HGPIN): Association With Diagnosis of Prostate Cancer

Vijayalakshmi Ananthanarayanan,[1] Ryan J. Deaton,[1] Ximing J. Yang,[2,3] Michael R. Pins,[2,3] and Peter H. Gann[1,3]*

[1]*Department of Preventive Medicine, Feinberg School of Medicine, Northwestern University, Chicago, Illinois*
[2]*Department of Pathology, Feinberg School of Medicine, Northwestern University, Chicago, Illinois*
[3]*The Robert H. Lurie Comprehensive Cancer Center, Feinberg School of Medicine, Northwestern University, Chicago, Illinois*

BACKGROUND. Alpha-methylacyl-CoA racemase (AMACR) is strongly expressed in prostate cancer with variable expression in high-grade prostatic intraepithelial neoplasia (HGPIN) and low expression in normal prostate. We examined whether AMACR expression in HGPIN and normal tissue was associated with subsequent diagnosis of cancer or proximity to a cancer focus.

METHODS. Needle core biopsies from 45 patients with isolated HGPIN, 12 radical prostatectomy (RP) specimens with prostatic carcinoma and 6 cystoprostatectomies without prostatic carcinoma were immunostained for AMACR. Among patients with HGPIN, 23 (cases) showed cancer on a later biopsy and 22 (controls) had no cancer with at least 3 consecutive negative biopsies.

RESULTS. In the biopsy set, the mean AMACR expression per gland in the normal compartment of the cases (0.29) was significantly higher than the controls (0.21) ($P = 0.0006$). In the RP set, normal glands near a cancer focus had higher mean AMACR expression than those that were distant ($P = 0.0006$). There was no difference within the HGPIN compartment between cases and controls in the biopsies, or between near and distant glands in the RP set. Mean AMACR staining of normal glands in the cystoprostatectomy specimens was significantly lower than in normal glands in close proximity to a cancer focus.

CONCLUSIONS. Higher expression of AMACR in normal glands near a focus of cancer, as well as in the subjects eventually showing cancer, suggests a possible field effect in prostatic carcinogenesis. AMACR expression in normal glands therefore might be a useful predictor for repeat biopsy outcomes or as an intermediate endpoint in chemoprevention studies. *Prostate 63: 341–346, 2005.*

KEY WORDS: **prostatic intraepithelial neoplasia; immunohistochemistry; prostatic neoplasms; alpha-methylacyl-CoA racemase**

INTRODUCTION

More than one million prostate biopsies are performed annually in the United States, resulting in the detection of almost 200,000 new cancer cases each year [1]. The high negative biopsy rate results in a sizable population of men with a PSA or digital rectal exam abnormality and at least one negative biopsy. Currently, there are no acceptable methods to stratify these

Grant sponsor: National Institutes of Health and the National Cancer Institute; Grant numbers: P50 CA 90386, R01 CA 90759.

*Correspondence to: Dr. Peter H. Gann, MD, ScD, 680 N. Lake Shore Drive, Suite 1102, Chicago, IL 60611.
E-mail: pgann@northwestern.edu

Received 8 July 2004; Accepted 15 September 2004
DOI 10.1002/pros.20196
Published online 15 December 2004 in Wiley InterScience (www.interscience.wiley.com).

patients by risk, and the only logical approach is a sequential follow up with or without a repeat biopsy [2]. If high-risk normal or pre-neoplastic tissue could be characterized at a molecular or cellular level, then these characteristics could be used to predict outcomes of repeat biopsies, and could reduce the morbidity and substantial health care cost associated with serial biopsies. In addition, these same tissue characteristics could be used as intermediate endpoints in Phase 2 chemoprevention trials.

Biomarkers that are differentially expressed in normal, high-grade prostatic intraepithelial neoplasia (HGPIN), and cancer are of particular interest; one recent candidate that has evolved out of subtraction cDNA microarrays is alpha-methylacyl-CoA racemase (AMACR) [3]. AMACR is a peroxisomal and mitochondrial enzyme involved in conversion of branched chain fatty acids and C27-bile acid intermediates to their stereoisomers, which are then diverted towards β oxidation. It has been demonstrated to be consistently over-expressed in a number of cancers and their precursor lesions, particularly in the prostate and colon [4,5]. AMACR is currently used in conjunction with basal cell markers like p63 or 34βE12 for resolving diagnostically challenging biopsies [6–9]. Although AMACR expression has been widely reported in prostate cancer, not much is known about the significance of inter-individual variation in AMACR in non-cancerous tissues. In this study, we sought to determine if increased AMACR expression in non-cancerous areas on negative biopsy samples is associated with the discovery of cancer on a subsequent biopsy. We also aimed to evaluate if AMACR expression in normal and HGPIN glands near a focus of cancer was different compared to expression in comparable glands that were distant. Lastly, we analyzed AMACR expression in the normal compartment of prostates removed from subjects without prostate cancer (cystoprostatectomies), to compare it to normal tissue from glands known to contain a clinically significant cancer.

MATERIALS AND METHODS

Subjects and Specimens

This study consisted of three sets of paraffin embedded prostatic tissue specimens retrieved from the Northwestern Memorial Hospital repository: a set of 45 prostate biopsies, 12 radical prostatectomies and 6 cystoprostatectomies. All sample sets were collected after Institutional Review Board approval. To test if AMACR expression was associated with subsequent diagnosis of cancer, Bouin's-fixed prostate biopsies from 45 patients with HGPIN but no cancer (i.e., isolated HGPIN) archived from the years 1993 to 1999 and 2002 to 2003 were used. Cases (n = 23) were patients with HGPIN who later had a biopsy positive for cancer. Controls (n = 22) were patients with HGPIN who had no subsequent diagnosis of prostate cancer and at least three negative biopsies. In both groups, the earliest biopsy diagnosed with HGPIN was used for the study. Both right and left sided biopsies from a subject were included in the study irrespective of the side that showed HGPIN. Hematoxylin and eosin (H/E) stained slides were reviewed to exclude samples where HGPIN could not be confirmed or where prostate cancer might have been present. Glands were considered histologically normal if there was an intact basal cell layer on the H/E section and if there was no evidence of cytological atypia such as crowding, nuclear enlargement, and nucleolar prominence in the luminal cells.

The second set included 12 radical prostatectomy (RP) specimens from 12 prostate cancer patients with Gleason scores 5–9. Eleven subjects had 1 representative block containing all 3 compartments (i.e., normal, HGPIN, and cancer) whereas 1 subject had a block with only cancer and HGPIN compartments. This set was used to see if there was any difference in the AMACR expression between normal glands adjacent to cancer and normal glands distant to cancer.

The third set was comprised of prostates from six cystoprostatectomy specimens removed from patients with bladder cancer. These prostates were examined grossly for suspicious areas, which if present, were submitted for histopathologic examination. Otherwise, a minimum of four random sections were taken. All sections were studied in detail by a pathologist (MRP) to rule out the presence of cancer.

Immunohistochemistry

We noted no difference in the AMACR staining intensity between the Bouin's and formalin fixed control samples and hence followed the same staining protocol for specimens fixed in either fixative. Two adjacent sections were cut from each paraffin block for all specimens. The first section was stained for H/E and the second was immunostained for AMACR. The second section from all the sets was deparaffinized and rehydrated as per routine protocols. Antigen retrieval was carried out in an electric steamer using Target Retrieval Solution (citrate buffer, pH-6, Dako, Carpinteria, CA) for 25 min. Briefly immunostaining was carried out using an autostainer (Dakocytomation, Carpinteria, CA) with a primary rabbit monoclonal antibody for AMACR (Zeta Corp./P504S) in the dilution of 1:100 for ½ hr at room temperature. The sections were then incubated with a ready-to-use anti-rabbit secondary antibody from Dako (EnVision Plus®) and color reaction was developed using

TABLE I. Selected Characteristics of Patients With (Cases) and Without (Controls) a Subsequent Diagnosis of Prostate Cancer Following a Biopsy Showing High-Grade Intraepithelial Prostatic Neoplasia (HGPIN)

	Cases	Controls
Number of subjects	23	22
Age, (mean years ± SD)	64.5 ± 6.8	65.2 ± 6.9
Days between HGPIN biopsy and most recent biopsy (mean ± SD)	291.7 ± 384.5	504.6 ± 494.3
Total number of biopsies experienced by subject, (mean ± SD)	2.7 ± 0.75	3.7 ± 0.78

diaminobenzidine (DAB) as the chromagen. The slides were then counterstained with hematoxylin. Suitable positive and negative controls were run in tandem.

Scoring

For the biopsy set, the immunostained slides were mounted with photo-etched cover slips (Bellco Glass, Inc.). These cover slips have 520 alphanumeric squares (grids) etched on them, each measuring 0.6 × 0.6 mm. At the outset, the grid locations for the HGPIN and normal glands were recorded for each slide in an Excel® spreadsheet. All HGPIN glands and normal glands from 10 randomly selected grids were scored per slide. For the RP set, the tumor was initially mapped out on the H/E slide using colored marking pens. Different colors were used to mark out normal and HGPIN areas that were 1, 5, and 10 mm away from tumor. Glands that were in close proximity and within 1 mm distance of the tumor were considered to be ''near'' and glands that were at least 5 mm distance away were considered to be ''distant.'' These maps were subsequently traced out on the corresponding immunostained slide. Three near and three distant glands for both normal and HGPIN compartments were randomly selected and scored. When available, a gland that was 10 mm from cancer was chosen over a gland that was just 5 mm distant. All scoring was done by a single pathologist (VA) who was not aware of the case/control status of the biopsy samples being examined. Each individual gland was scored on an ordinal scale of 0–3, where 0 was no staining, 1 was weak focal staining, 2 was continuous moderate staining, and 3 was diffuse strong staining. Small acinar proliferation, basal cell hyperplasia, atrophic glands, other benign histological mimics of malignancy, and areas of inflammation were excluded from evaluation and scoring.

To validate the manual scoring methods, digital photomicrographs were taken at 400× magnification from the normal compartment of the biopsy samples from areas that had been manually scored as 0, 1, 2, or 3 using a Zeiss Axiocam®. Five separate images were taken for each scoring level. These images were captured as Tagged Image File Format (tiff) files and were then analyzed using MetaMorph® image analysis software (Version 4.6, Universal Imaging Corporation, Philadelphia). First, different color thresholds were established for blue and brown areas using the Hue Saturation and Luminosity (HSL) mode. The same color thresholds were then used for all the images, and a mean gray scale and optical density (OD) index was calculated for each image.

Statistical Analysis

The biopsy, RP, and cystoprostatectomy sample sets were analyzed in two ways: first, mean AMACR scores were calculated per person for each compartment (i.e., normal and HGPIN); second, mean AMACR scores were calculated for glands in a compartment with all subjects combined (mean per gland per compartment). Cases and controls, as well as near and distant areas, were compared by computing means with 95% confidence intervals and *t*-statistics. All statistical analyses were performed using SAS® version 8.02 (Cary Institute, NC).

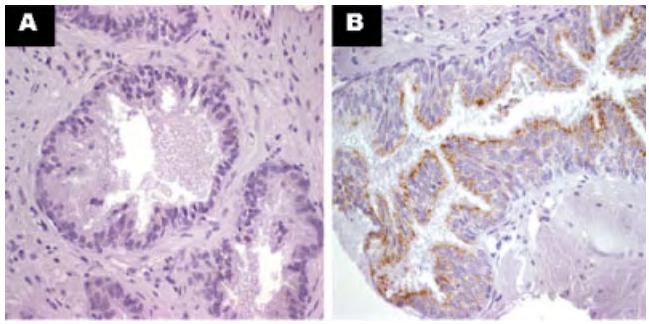

Fig. 1. Normal prostatic gland (**A**) showing no alpha-methylacyl-CoA racemase (AMACR) staining, and an high-grade prostatic intraepithelial neoplasia (HGPIN) gland (**B**) with 3+ intensity staining, 400×. [Color figure can be viewed in the online issue, which is available at www.interscience.wiley.com.]

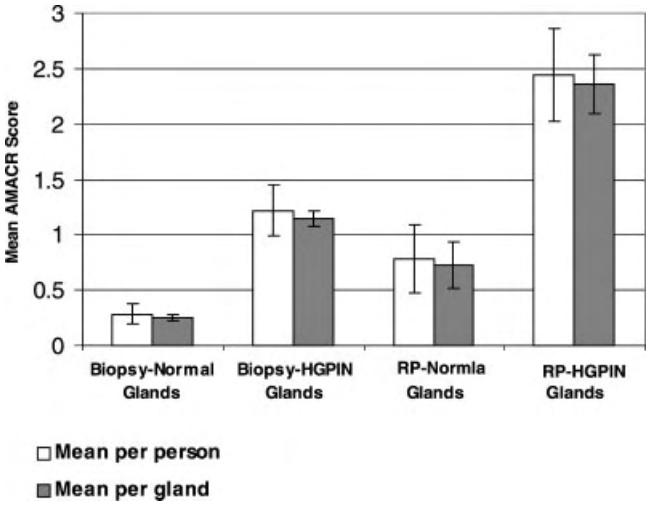

Fig. 2. Mean AMACR score and 95% confidence intervals in the normal and HGPIN compartments for the biopsy and radical prostatectomy (RP) specimens.

RESULTS

AMACR Expression for Cases and Controls in the Biopsy Set

AMACR gave a granular, punctate staining confined to the cytoplasm of epithelial cells with no spill over into the nucleus. There was strong (3+) staining in the positive control slide from a known case of prostate cancer as noted previously [10]. Selected characteristics of patients from the biopsy set are given in Table I. In our biopsy specimens staining in normal glands was negative to weak whereas HGPIN glands stained weak to moderate (Fig. 1). No staining was noted in the stroma or the inflammatory cells. Figure 2 shows that the mean AMACR scores per person and per gland for the HGPIN compartment was significantly higher than the normal compartment. Within the normal compartment, the mean AMACR score per gland for the cases was significantly higher (38% increase) than the controls, as seen in Table II. When data were analyzed as average intensity per person, the difference in mean AMACR intensity in the normal compartment between cases and controls was greater (62% increase in cases); however, the statistical significance was borderline due to smaller numbers. A difference in mean AMACR intensity in the HGPIN compartment between cases and controls was not observed either on a per subject or a per gland basis. The mean and standard deviation of the OD and gray level scores obtained by MetaMorph® compared to the manual scores of 0, 1, 2, and 3 intensity are shown in Table III.

AMACR Expression in RP and Cystoprostatectomy Specimens

As reported previously by others, we found no association between AMACR staining intensity in the cancer compartment in the RP specimens and Gleason scores [11]. Similar to the biopsies, the HGPIN glands showed an overall higher mean AMACR expression per person and per gland when compared to the normal compartment (Fig. 2). For the normal compartment, the mean AMACR score for the near glands per person and per gland was significantly higher than that of the distant glands (Fig. 3, Table IV). There was no difference however, between the near and distant glands for the HGPIN compartment. Mean AMACR staining per person and per gland in the normal compartment of the cystoprostatectomy specimens was significantly lower than that of the normal glands near cancer in the RP set, but was not statistically distinguishable from the distant glands (Table IV).

DISCUSSION

In this study, we demonstrated a significantly higher AMACR expression in normal glands in biopsies from subjects who eventually were discovered to have prostate cancer compared to normal glands from subjects who were not found to have prostate cancer. Furthermore, we observed that AMACR expression in normal glands that were in close proximity to a focus of cancer was significantly higher than the expression in

TABLE II. Alpha-Methylacyl-CoA Racemase (AMACR) Scores in the Normal and HGPIN Tissue Compartments in Biopsy Samples, According to Case-Control Status

		Score per gland			Score per person		
Compartment	Status	n	Mean	95% CI	n	Mean	95% CI
Normal	Cases	804	0.29[a]	0.26–0.33	23	0.34	0.19–0.50
	Controls	812	0.21	0.17–0.24	21[b]	0.21	0.11–0.30
HGPIN	Cases	509	1.17	1.08–1.26	23	1.25	0.96–1.55
	Controls	481	1.12	1.03–1.21	22	1.19	0.81–1.56

[a]The mean AMACR score per gland in the normal compartment of the cases was significantly higher than the controls ($P = 0.0006$).
[b]One subject had no glands meeting the criteria for normal in the biopsy.

TABLE III. Mean AMACR Optical Density (OD) and Gray Level Indices by Metamorph® Image Analysis in Comparison to Manual Scores in Normal Prostate

Manual scores	Mean OD index ± SD	Mean gray level index ± SD
0	0.10 ± 0.18	134.00 ± 236.19
1	0.56 ± 0.48	508.70 ± 395.65
2	3.60 ± 2.87	2661.47 ± 1886.41
3	5.73 ± 3.86	3895.18 ± 2215.74

the normal glands that were distant. No such difference in AMACR immunopositivity was, however, observed for the HGPIN compartment. AMACR expression in the HGPIN compartment was quite variable, with a significantly higher intensity of staining than the normal glands, as previously reported [10].

Taken together, these data suggest that up-regulation of this enzyme in the normal glands may precede morphologic evidence of neoplastic transformation. Previous studies have observed AMACR expression in the normal compartment of the prostate. In their study, Leav et al. [12] found AMACR expression in benign hyperplastic glands juxtaposed to carcinoma as well as in carcinomas arising within BPH nodules. In another recent study, Rubin et al. [13] studied AMACR expression using a sensitive immunofluorescence method and found expression of AMACR in low-grade PIN and histologically benign prostate tissue, suggesting the possibility of an early molecular alteration preceding a morphologic alteration. In contrast, Jiang et al. found that 88% of their benign prostates did not show AMACR expression. This group also did not observe increased staining in benign glands adjacent to a cancer focus [11]. The difference between this study and ours could be attributed to use of different antibody sources, staining and scoring methods.

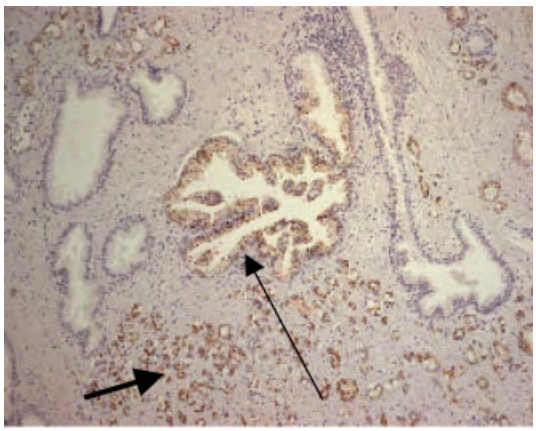

Fig. 3. AMACR staining in a RP specimen: There is increased AMACR expression in the normal gland (normal arrow) adjoining a focus of cancer (bold arrow). [Color figure can be viewed in the online issue, which is available at www.interscience.wiley.com.]

The process of carcinogenesis often involves stepwise progression of molecular events. Events of this nature are represented by the presence of field effects in the adjacent normal tissues [14]. In our study, the presence of AMACR positivity in the normal glands adjoining foci of cancer as well as in the subjects who eventually developed cancer suggests the possibility of a field effect. Indeed, multiple foci of HGPIN have been shown to arise simultaneously within the prostate, lending credibility to the ''field effect'' hypothesis in prostatic carcinogenesis [15]. Bostwick et al. studied the rates of allelic imbalance at 6 different loci in matched areas of HGPIN and cancer, 21 of the 22 informative cases with allelic imbalance in at least 1 focus of HGPIN and 1 focus of carcinoma showed the same pattern of allelic imbalance in the HGPIN foci and the matched cancer foci. Other biomarkers that have shown higher expression in normal prostatic glands adjoining cancerous foci include pS2, an estrogen inducible protein [16] and EPCA, a nuclear matrix protein [17]. We believe that detection and monitoring of altered expression of such biomarkers in the ''field'' areas can have prognostic implications and utility as intermediate markers in prevention trials.

Although the results presented here are promising, limitations exist in the study that merit consideration. First, the small size of our study limits power and precludes stratification for confounders like age, number of biopsies, and PSA. However, we looked at the mean AMACR staining in both the compartments of the control group after dichotomizing by age (median age <67 and ≥ 67) and found no difference (data not shown). Limited study size also does not allow for estimation of odds ratios following selection of an appropriate cutoff. Secondly, the retrospective classification of the cases and controls limits perfect determination of cancer free status. However, misclassification of cases as controls would have biased our results towards the null. In the future, we intend to implement a multivariate model comprised of various biomarkers and clinical parameters to study outcomes following negative biopsies in a larger study set. Manual semi-quantitative methods of scoring—though reasonably reproducible—have a limited capacity to make fine distinctions. In this respect, digital image analysis could help in providing a more precise calibration to discriminate between weak and moderate staining.

CONCLUSION

In the search for tissue biomarkers that reliably discriminate normal and cancerous tissues, AMACR is

TABLE IV. AMACR Scores in the Normal and HGPIN Compartments in the Radical Prostatectomy (RP) and Cystoprostatectomy Cases by Their Distance Status

		Score per gland			Score per person		
Compartment	Specimen subtypes	n	Mean	95% CI	n	Mean	95% CI
Normal	Cystoprostatectomy	60	0.52	0.37–0.66	6	0.52	0.19–0.55
	Distant glands	27	0.37	0.18–0.57	9	0.37	0.13–0.61
	Near glands	32	1.03[a]	0.72–1.34	11	1.01[b]	0.59–1.44
HGPIN	Distant glands	16	2.06	1.46–2.66	7	2.02	1.21–2.84
	Near glands	31	2.52	2.25–2.78	12	2.35	1.90–2.79

[a]P value = 0.0006 for difference in AMACR score per gland between near and distant normal glands.
[b]P value = 0.012 for difference in AMACR score per person between near and distant normal glands.

a promising candidate. Our study suggests that increased AMACR expression might be a characteristic of high-risk normal tissue. It does seem plausible that the AMACR gene product, through its role in fatty acid metabolism, may be an important event in the stepwise development of prostate cancer. A similar mechanism might be involved in colon cancer, where increased AMACR expression has also been found and meat-rich diets have been implicated as etiologic factors [5]. In conclusion, we believe that AMACR potentially can be used as an intermediate endpoint in chemoprevention trials or as a risk stratification tool among patients with negative prostatic biopsies.

ACKNOWLEDGMENTS

The authors thank Erin Anderson, Robert E. Meyer, and Yvonne Chow for their expert assistance on this project.

REFERENCES

1. Porter CR, Crawford ED. Combining artificial neural networks and transrectal ultrasound in the diagnosis of prostate cancer. Oncology 2003;17(10):1395–1399, 1403–1406.
2. Djavan B, Remzi M, Schulman CC, Marberger M, Zlotta AR. Repeat prostate biopsy: Who, how, and when? A review. Eur Urol 2002;42(2):93–103.
3. Xu J, Stolk JA, Zhang X, Silva SJ, Houghton RL, Matsumura M, Vedvick TS, Leslie KB, Badaro R, Reed SG. Identification of differentially expressed genes in human prostate cancer using subtraction and microarray. Cancer Res 2000;60(6):1677–1682.
4. Zhou M, Chinnaiyan AM, Kleer CG, Lucas PC, Rubin MA. Alpha-methylacyl-CoA racemase: A novel tumor marker overexpressed in several human cancers and their precursor lesions. Am J Surg Pathol 2002;26(7):926–931.
5. Jiang Z, Fanger GR, Banner BF, Woda BA, Algate P, Dresser K, Xu J, Reed SG, Rock KL, Chu PG. A dietary enzyme: Alpha-methylacyl-CoA racemase/P504S is overexpressed in colon carcinoma. Cancer Detect Prev 2003;27(6):422–426.
6. Evans AJ. Alpha-methylacyl CoA racemase (P504S): Overview and potential uses in diagnostic pathology as applied to prostate needle biopsies. J Clin Pathol 2003;56(12):892–897.
7. Jiang Z, Wu CL, Woda BA, Dresser K, Xu J, Fanger GR, Yang XJ. P504S/alpha-methylacyl-CoA racemase: A useful marker for diagnosis of small foci of prostatic carcinoma on needle biopsy. Am J Surg Pathol 2002;26(9):1169–1174.
8. Kunju LP, Rubin MA, Chinnaiyan AM, Shah RB. Diagnostic usefulness of monoclonal antibody P504S in the workup of atypical prostatic glandular proliferations. Am J Clin Pathol 2003;120(5):737–745.
9. Yang XJ, Laven B, Tretiakova M, Blute RD Jr., Woda BA, Steinberg GD, Jiang Z. Detection of alpha-methylacyl-coenzyme A racemase in postradiation prostatic adenocarcinoma. Urology 2003;62(2):282–286.
10. Luo J, Zha S, Gage WR, Dunn TA, Hicks JL, Bennett CJ, Ewing CM, Platz EA, Ferdinandusse S, Wanders RJ, Trent JM, Isaacs WB, De Marzo AM. Alpha-methylacyl-CoA racemase: A new molecular marker for prostate cancer. Cancer Res 2002;62(8):2220–2226.
11. Jiang Z, Woda BA, Rock KL, Xu Y, Savas L, Khan A, Pihan G, Cai F, Babcook JS, Rathanaswami P, Reed SG, Xu J, Fanger GR. P504S: A new molecular marker for the detection of prostate carcinoma. Am J Surg Pathol 2001;25(11):1397–1404.
12. Leav I, McNeal JE, Ho SM, Jiang Z. Alpha-methylacyl-CoA racemase (P504S) expression in evolving carcinomas within benign prostatic hyperplasia and in cancers of the transition zone. Hum Pathol 2003;34(3):228–233.
13. Rubin MA, Zerkowski MP, Camp RL, Kuefer R, Hofer MD, Chinnaiyan AM, Rimm DL. Quantitative determination of expression of the prostate cancer protein alpha-methylacyl-CoA racemase using automated quantitative analysis (AQUA): A novel paradigm for automated and continuous biomarker measurements. Am J Pathol 2004;164(3):831–840.
14. Braakhuis BJ, Tabor MP, Kummer JA, Leemans CR, Brakenhoff RH. A genetic explanation of Slaughter's concept of field cancerization: Evidence and clinical implications. Cancer Res 2003;63(8):1727–1730.
15. Bostwick DG, Shan A, Qian J, Darson M, Maihle NJ, Jenkins RB, Cheng L. Independent origin of multiple foci of prostatic intraepithelial neoplasia: Comparison with matched foci of prostate carcinoma. Cancer 1998;83(9):1995–2002.
16. Bonkhoff H, Stein U, Welter C, Remberger K. Differential expression of the pS2 protein in the human prostate and prostate cancer: Association with premalignant changes and neuroendocrine differentiation. Hum Pathol 1995;26(8):824–828.
17. Dhir R, Vietmeier B, Arlotti J, Acquafondata M, Landsittel D, Masterson R, Getzenberg RH. Early identification of individuals with prostate cancer in negative biopsies. J Urol 2004;171(4):1419–1423.

[CANCER RESEARCH 62, 2220–2226, April 15, 2002]

Advances in Brief

α-Methylacyl-CoA Racemase: A New Molecular Marker for Prostate Cancer[1]

Jun Luo, Shan Zha, Wesley R. Gage, Thomas A. Dunn, Jessica L. Hicks, Christina J. Bennett, Charles M. Ewing, Elizabeth A. Platz, Sacha Ferdinandusse, Ronald J. Wanders, Jeffrey M. Trent, William B. Isaacs,[2] and Angelo M. De Marzo

Brady Urological Institute [J. L., S. Z., T. A. D., C. M. E., W. B. I., A. M. D.] and Department of Pathology [W. R. G., J. L. H., C. J. B., A. M. D.], Johns Hopkins University, School of Medicine, Baltimore, Maryland 21287; Department of Epidemiology, Johns Hopkins University, Bloomberg School of Public Health, Baltimore, Maryland 21205 [E. A. P.]; National Human Genome Research Institute, NIH, Bethesda Maryland 20892 [J. M. T.]; and Departments of Pediatrics, Emma Children's Hospital, Clinical Chemistry, Academic Medical Centre, University of Amsterdam, 1105 AZ Amsterdam, the Netherlands [S. F., R. J. W.]

Abstract

Identification of genes that are dysregulated in association with prostate carcinogenesis can provide disease markers and clues relevant to disease etiology. Of particular interest as candidate markers of disease are those genes that are frequently overexpressed. In this study, we describe a gene, *α-methylacyl-CoA racemase* (AMACR), whose expression is consistently up-regulated in prostate cancer. Analysis of mRNA levels of AMACR revealed an average up-regulation of ~9 fold in clinical prostate cancer specimens compared with normal. Western blot and immunohistochemical analysis confirms the up-regulation at the protein level and localizes the enzyme predominantly to the peroxisomal compartment of prostate cancer cells. A detailed immunohistochemical analysis of samples from 168 primary prostate cancer cases using both standard slides and tissue microarrays demonstrates that both prostate carcinomas and the presumed precursor lesion (high-grade prostatic intraepithelial neoplasia) consistently scored significantly higher than matched normal prostate epithelium; 88% of the carcinomas had a staining score higher than the highest score observed for any sample of normal prostate epithelium. Both untreated metastases ($n = 32$ patients) and hormone refractory prostate cancers ($n = 14$ patients) were generally strongly positive for AMACR. To extend the utility of this marker for prostate cancer diagnosis, we combined staining for cytoplasmic AMACR with staining for the nuclear protein, p63, a basal cell marker in the prostate that is absent in prostate cancer. In a simple assay that can be useful for the diagnosis of prostate cancer on both biopsy and surgical specimens, combined staining for p63 and AMACR resulted in a staining pattern that greatly facilitated the identification of malignant prostate cells. The enzyme encoded by the *AMACR* gene plays a critical role in peroxisomal β oxidation of branched chain fatty acid molecules. These observations could have important epidemiological and preventive implications for prostate cancer, as the main sources of branched chain fatty acids are dairy products and beef, the consumption of which has been associated with an increased risk for prostate cancer in multiple studies. On the basis of its consistency and magnitude of cancer cell-specific expression, we propose AMACR as an important new marker of prostate cancer and that its use in combination with p63 staining will form the basis for an improved staining method for the identification of prostate carcinomas. Furthermore, the absence of AMACR staining in the vast majority of normal tissues coupled with its enzymatic activity makes AMACR the ideal candidate for development of molecular probes for the noninvasive identification of prostate cancer by imaging modalities.

Introduction

Prostate cancer initiation and progression are processes involving multiple molecular alterations (1). Genomic alterations, combined with changes in the tissue microenvironment, lead inevitably to altered levels of expression of many individual genes in tumor cells. Identification of these genes represents a critical step toward a thorough understanding of prostate carcinogenesis and an improved management of prostate cancer patients. Of particular biological and clinical interest are those genes that are consistently overexpressed in the vast majority of prostate cancers. Such genes and their products, besides providing possibly valuable insight into the etiology of prostate cancer, may have important utility as diagnostic markers in this disease. However, few genes of this nature have been reported to date.

High-throughput gene expression profiling using cDNA microarray allows for systematic interrogation of transcriptionally altered genes. By comparing the mRNA expression profile of cancerous lesions with noncancerous lesions, multiple candidates of molecular markers for prostate cancer have emerged (2–6). One such candidate, the gene for AMACR,[3] was identified as being overexpressed in prostate carcinoma cells when compared with benign or normal prostate epithelial cells (2, 3). AMACR is a well-characterized enzyme (7) that plays a key role in peroxisomal β-oxidation of dietary branched-chain fatty acids and C27-bile acid intermediates. It catalyzes the conversion of (R)-α-methyl-branched-chain fatty acyl-CoA esters to their (S)-stereoisomers. Only the (S)-stereoisomers can serve as substrates for branched-chain acyl-CoA oxidase during their subsequent peroxisomal β-oxidation. Two aspects of this pathway may have particular relevance for prostate carcinogenesis: (*a*) the main sources of branched chain fatty acids in humans (milk, beef, and dairy products; Ref. 8) have been implicated as dietary risk factors for prostate cancer (9); and (*b*) peroxisomal β-oxidation generates hydrogen peroxide (10), a potential source of procarcinogenic oxidative damage (11, 12).

An initial report by Xu *et al.* (2), using a limited number of samples, indicated that AMACR was overexpressed potentially in a subset of prostate cancers at both the mRNA and protein level. Our previous study compared gene expression profiles of 16 prostate cancer and 9 samples of BPH using cDNA microarrays containing 6500 human genes (3). AMACR was expressed highly in the majority of prostate cancer samples, averaging ~6-fold higher levels than the BPH samples. In this study, we expanded these previous studies by including cDNA microarray data from an additional 35 prostate tissue samples, comprising matched normal tumor pairs, and by performing an extensive IHC analysis of both primary and metastatic prostate cancer specimens, including normal and cancerous prostate tissue from 159 patients analyzed on prostate TMAs. Furthermore, we examined the diagnostic utility of combining staining for AMACR with staining for p63, a prostate basal cell marker that is absent in the vast majority of prostate cancers (13, 14). The consistent and extensive up-regulation

Received 11/19/01; accepted 3/4/02.

The costs of publication of this article were defrayed in part by the payment of page charges. This article must therefore be hereby marked *advertisement* in accordance with 18 U.S.C. Section 1734 solely to indicate this fact.

[1] Supported by the Peter Jay Sharp Foundation and PHS Grants CA58236 and CA78588 and a grant from the Charlotte Geyer Foundation.

[2] To whom requests for reprints should be addressed, at Marburg 115, Johns Hopkins Hospital, 600 North Wolfe Street, Baltimore, MD 21287.

[3] The abbreviations used are: AMACR, α-methylacyl-CoA racemase; IHC, immunohistochemical; KRT8, keratin 8; PIN, prostatic intraepithelial neoplasia; TMA, tissue microarray; BPH, benign prostatic hyperplasia; TBP, TATA-binding protein; GSTP1, glutathione *S*-transferase π; HGPIN, high-grade prostatic intraepithelial neoplasia.

of AMACR that we observe at both the mRNA and protein level strongly suggests that AMACR will be an important new marker for prostate cancer.

Materials and Methods

Prostate Tissue Procurement for cDNA Microarray Analysis. Prostate cancer tissue specimens for cDNA microarray analysis were obtained from 23 patients undergoing radical prostatectomy for clinically localized prostate carcinoma at Johns Hopkins Hospital from 1993 to 2000. Specimens were obtained from the operating room immediately after resection. The seminal vesicles were truncated. If palpable tumor was identified, the specimen was inked and harvested as described previously (15). This results in the banking of the largest palpable tumor, as well as areas of apparent normal and BPH when available. The areas containing tumor that were adjacent to the harvested tumor blocks were submitted for formalin fixation and routine processing. Harvested tissues were flash frozen and stored in −80°C. Paired normal cancer samples were prepared as described previously (3) from 12 of the 23 specimens, whereas only cancer samples were obtained from the other 11 specimens, giving 35 samples total for analysis. Cancer samples were microscopically estimated to contain ≥60% (range from 60 to 90%) adenocarcinoma cells in cellular composition, and the normal samples were estimated to contain ≥50% (range from 50 to 75%) epithelial cells. Institutional Review Board-approved informed consent was obtained from all patients in this study.

cDNA Microarray Analysis. RNA extraction, labeling, and hybridization were carried out as described previously (3). A single reference sample composed of a pool of RNA from two BPH specimens was used throughout all hybridizations. Measurement values were extracted for normalized ratios of signal intensities of sample *versus* reference, which represent the relative mRNA abundance for each gene in each sample when compared with the common reference (3).

Real-time Reverse Transcription-PCR. Quantitative PCR was performed on iCycler (Bio-Rad, Richmond, CA) with gene-specific primers (AMACR: 5′-GAATCCGTATGCCCCGCTGAATCT-3′ and 5′-ACCCTTGCCAGTGCGTGTGC-3′; TBP: 5′-CACGAACCACGGCACTGATT-3′ and 5′-TTTTCTTGCTGCCAGTCTGGAC-3′), as described previously (16). A standard curve was generated by serial dilution of plasmids containing the specific amplicons assayed. AMACR mRNA copy number was normalized to TBP.

Western Blot Analysis. Protein (25 μg) was subjected to SDS–polyacrylamide (10%) gel electrophoresis, transferred to nitrocellulose (Amersham Pharmacia Biotech, Piscataway, NJ), probed with AMACR antiserum (7) at a 1:2000 dilution, and detected by enhanced chemiluminescence (Amersham Pharmacia Biotech) as described previously (16).

TMAs: Construction and Analysis. A total of 159 radical prostatectomy specimens were selected randomly out of a total of >400 cases performed between 1/1/2000 and 8/1/2001 at Johns Hopkins Hospital and used to construct TMAs as described previously (16). Areas representing the largest carcinoma present, as well as areas of normal appearing prostate epithelium, were circled on the glass slides. For each sample of tumor and normal, four tissue cores were taken for TMA construction. Although there is no universal method of sampling prostate cancer tissue for IHC studies, using either standard slides or TMAs, the histological features of these areas that we sampled generally reflect the final Gleason score for the case. Stained TMA slides were scanned using the BLISS imaging system as described by Manley *et al.* (17). Each array spot was then formed into a composite image and viewed and scored on a personal computer monitor as described (16). Data were then further summarized, and statistical analysis was performed using Stata 6.0 and SAS for Microsoft Windows.

Prostate Adenocarcinoma Tissue from Standard Slides. For a number of the cases, standard slides were used to assess overall percentage of positive cells in the tumors and normal tissues and also to further evaluate expression in HGPIN and BPH.

Metastatic Prostate Cancers. For metastatic carcinoma, standard slides from specimens (pelvic lymph node, soft tissue, and bone metastases) from patients with nonhormone refractory tumors were obtained from the archives of the Department of Pathology at The Johns Hopkins University. For hormone refractory cancer specimens, tissues were obtained as a single TMA from the University of Michigan, Specialized Programs of Research Excellence core tissue facility.

IHC Staining. Staining for AMACR was carried out using the Envision+ kit (DAKO Corp., Carpinteria, CA). Briefly deparaffinized slides were hydrated and then placed in citrate buffer (pH 6.0) and steamed for 14 min. Endogenous peroxidase activity was quenched by incubation with DAKO peroxidase block for 5 min at room temperature. Slides were then washed and incubated with primary antibody (1:16,000 dilution of antiserum) overnight at 4°C. Secondary antirabbit antibody-coated polymer peroxidase complex was applied for 30 min at room temperature. Substrate/chromogen was applied and incubated for 5–10 min at room temperature. Slides were counterstained with hematoxylin. For double labeling of AMACR and p63, the anti-p63 mouse monoclonal antibody cocktail (1:100 dilution; Lab Vision Corp., Fremont, CA) was added after the anti-racemese antibody incubation and incubated for 45 min at room temperature. The secondary antirabbit and antimouse HRP conjugates were sequentially added, and the reaction was developed as above.

Scoring of IHC Staining. A scoring method was based on the fact that the specimens clearly showed a varying degree of staining intensity and percentage of cells staining. Therefore, a combined intensity and percentage positive scoring method was used (18). Strong intensity staining was scored as 3, moderate as 2, weak as 1, and negative as 0. For each intensity score, the percentage of cells with that score was estimated visually. A combined weighted score consisting of the sum of the percentage of cells staining at each intensity level was calculated for each sample, *e.g.,* a case with 70% strong staining, 10% moderate staining, and 20% weak staining would receive a score as follows: $(70 \times 3 + 10 \times 2 + 20 \times 1) = 250$. The maximum score is 300.

Results

Analysis of Paired Samples of Normal and Cancerous Prostate Tissue mRNA. In the previous study, we used weighted gene and random permutation analysis to identify 210 genes with statistically different levels of mRNA expression between prostate cancer and BPH (3). Among these genes, AMACR maintained consistently low levels of expression in 9 of 9 BPH samples (signal intensities in the lowest quartile of all genes analyzed) but was overexpressed by an average of 5.7-fold in 13 of 16 cancer samples. We have since generated mRNA profiles of an additional 35 prostate samples, including 12 matched normal cancer pairs and 11 nonpaired cancer samples (data set in preparation for publication) by comparing each sample to a common reference (from BPH). To illustrate the expression pattern of AMACR in these samples in relation to other genes whose expression in prostate tissues has been well documented previously, we extracted expression ratios for AMACR (IMAGE clone ID: 133130), along with those for GSTP1 (IMAGE clone ID: 136235) and KRT8 (IMAGE clone ID: 897781). Reduced GSTP1 expression because of "CpG island" hypermethylation is found in >90% of prostate cancers (19), and KRT8 mRNA is expressed constitutively in the epithelial cells of normal and cancerous prostate tissues (20). As shown in Fig. 1, the majority (20 of 23) of the cancer samples demonstrated overexpression of AMACR mRNA compared with the BPH reference. When the cancer samples were compared with their matching normal samples, AMACR was overexpressed in the cancer samples in 9 of 12 pairs. Moderate overexpression compared with the reference (an average of 3-fold) was also observed in 3 of the 12 normal samples. Consistent with previous reports, GSTP1 expression was down-regulated in the majority of cancer samples compared with BPH reference or their matching normal samples. Expression of KRT8, an epithelial marker, showed little variation among all of the samples, indicating that the sample preparation was effective to enrich and balance the epithelial content in the samples analyzed.

A quantitative reverse transcription-PCR assay was used to estimate the relative difference in AMACR mRNA abundance in samples of normal and cancerous prostate tissue. Although extensive variability was observed, the copy number of AMACR mRNA in prostate cancer specimens was on average 8.8-fold higher than the value for normal prostate samples (average = 60.9, SD = 84.3, range 0.6–260.4, n = 8, for cancer samples compared with an average of 6.9,

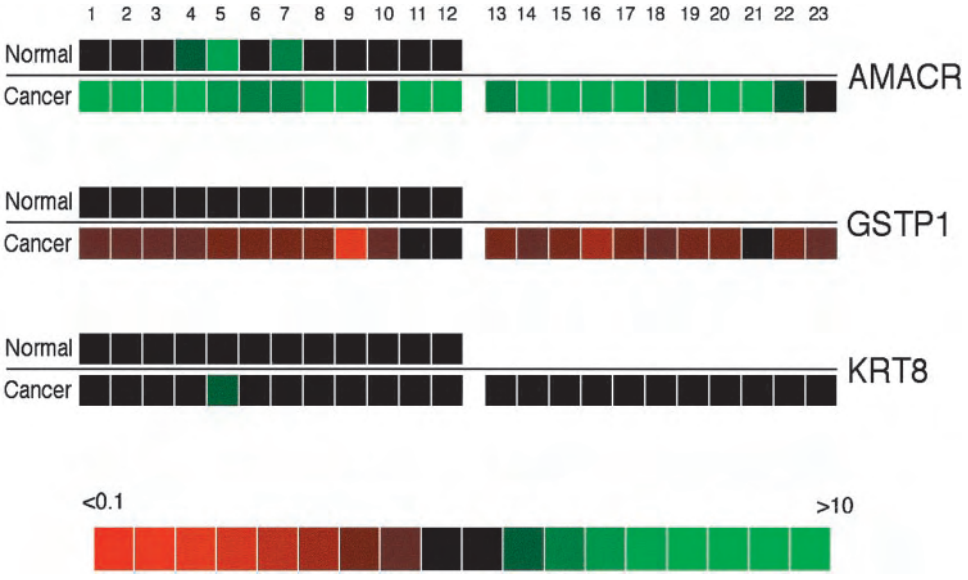

Fig. 1 Gene expression ratios for AMACR, GSTP1, and KRT8. Each *colored square* represents the relative mRNA abundance (ratio of sample: reference) in each sample compared with the common BPH reference. Each of the 12 normal samples (*1–12*) was paired with its matching cancer sample below the *black line* and the other 11 nonpaired cancer samples (*13–23*) positioned at the *right side below* the *line*. The measured expression ratios for each gene were presented graphically as *colored squares*, with the *green squares* representing higher expression in sample compared with the reference (BPH), the *red squares* meaning lower expression in sample than reference (BPH), and *black squares* indicating a ratio of ~1. Color intensities are scaled according to the ratio (sample:reference) as shown at the *bottom*, with the brightest color having a ratio of >10 (*green*) or <0.1 (*red*).

SD = 9.9, range 0.51–32.9, n = 8, for normal) when normalized against copies of TBP. Similarly, the median value for the cancer samples was 7.8-fold higher than for the normal samples.

Western Blot Analysis of AMACR Protein. Expression of AMACR protein was examined using an antiserum demonstrated previously to be specific for this antigen (7). Western blot detection of AMACR in liver, as a positive control (7), and a series of prostate tissue samples is shown in Fig. 2. Although a M_r 47,000 band corresponding to AMACR protein was readily detected in liver and each of the prostate cancer specimens, little or no reactivity was observed in the corresponding normal specimens or any of the BPH samples assayed.

IHC Analysis of Radical Prostatectomy Specimens Using Standard Slides. To obtain the pattern of staining of AMACR in prostate tissues, we examined clinically localized prostate adenocarcinoma specimens using representative standard slides containing normal epithelium, carcinoma, and HGPIN. We used a scoring method that accounts for both the intensity of staining and the percentage of cells staining. In general, normal prostate epithelium was either negative or weakly positive (n = 14 areas from 12 patients, median score = 15, mean score = 19, SD = 22; Fig. 3). Prostate stroma, inflammatory cells, endothelial cells, and nerves were uniformly negative (Fig. 3). Strikingly, adenocarcinomas showed highly intense staining in the majority of tumor cells in most cases (n = 19 carcinoma lesions from 14 patients, median = 290, mean = 277, SD = 30; Fig. 3). The staining was uniformly cytoplasmic and was typically found in small punctate, microbody structures, consistent with the previously reported localization of AMACR predominantly to peroxisomes and mitochondria (7). Staining in HGPIN was also generally positive, although the staining was more variable and often less intense than adjacent carcinoma (Fig. 3, *C* and *D*; n = 10 areas from 6 patients, median 170, mean 179, SD = 63). Staining in atrophic areas was generally negative or positive in a small percentage of cells (n = 5 areas from 3 patients, median = 30, mean = 30, SD = 22). Staining in BPH was generally negative or focally, weakly positive (n = 6 areas from 4 patients, median = 20, mean = 20, SD = 8.9).

IHC Analysis of Radical Prostatectomy Specimens Using TMAs. To survey many tumor and normal specimens, four high-density TMAs, designed to contain samples of clinically localized prostate cancer and matched normal appearing epithelium from 159 patients, were stained. The median age of patients in these TMAs was 58 (range 40–73), and the median prostate-specific antigen was 6.4 (mean 7.5, SD 4.6, range 1.2–38). Array spots (1578) were imaged. The majority of array spots (79%) contained tissue that was readily readable. Of the usable array spot images, 209 were control normal (nonprostatic) tissues. Of the array spots scored for AMACR staining, 417 spots contained adenocarcinoma (334 Gleason pattern 3, 62 Gleason pattern 4, 15 Gleason pattern 5, 4 Gleason pattern 2, 1 ductal adenocarcinoma, 1 pseudo-hyperplastic carcinoma) from 142 patients, 442 spots contained normal prostate epithelium from 144 patients of the patients, and 27 spots contained HGPIN from 23 patients. Other spots consisted of prostate stroma only, atrophy, or were difficult to interpret.

For normal prostate and adenocarcinoma, between 2.5 and 3 TMA spots (duplicate spots) were scored from each patient. For statistical analyses, the mean of the individual spot scores were computed so that for each tissue type from each patient, there was a single IHC score for comparison. Using these mean scores, the AMACR IHC scores for both carcinoma and HGPIN were highly statistically significantly different from normal (Fig. 4, carcinoma *versus* normal, $P < 0.0001$;

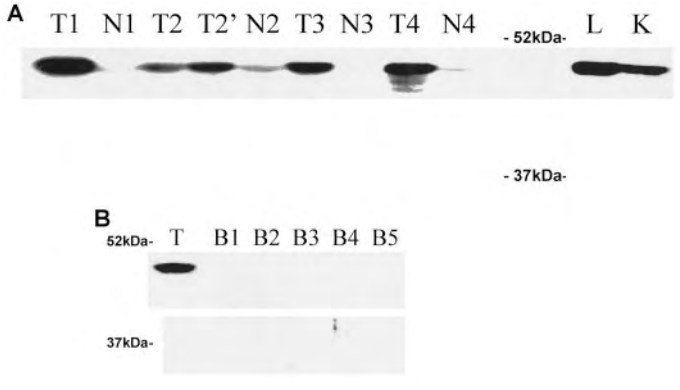

Fig. 2. Western blot analysis of AMACR protein. Total tissue protein (25 μg) was analyzed using anti-AMACR antiserum. In *A*, pairs of tumor and corresponding normal tissue from 4 patients are designated by *T1*, *T2*, *T3*, *T4*, and *N1*, *N2*, *N3*, *N4*, respectively. For the second patient, there were two apparently independent tumors sampled (*T2* and *T2′*). *L*, liver and *K*, kidney. In *B*, five different samples of BPH tissue (*B1–B5*) were analyzed together with a single sample of prostate cancer (*T*). The position of prestained molecular weight markers (ovalbumin at M_r 52,000 and carbonic anhydrase at M_r 37,000) is marked.

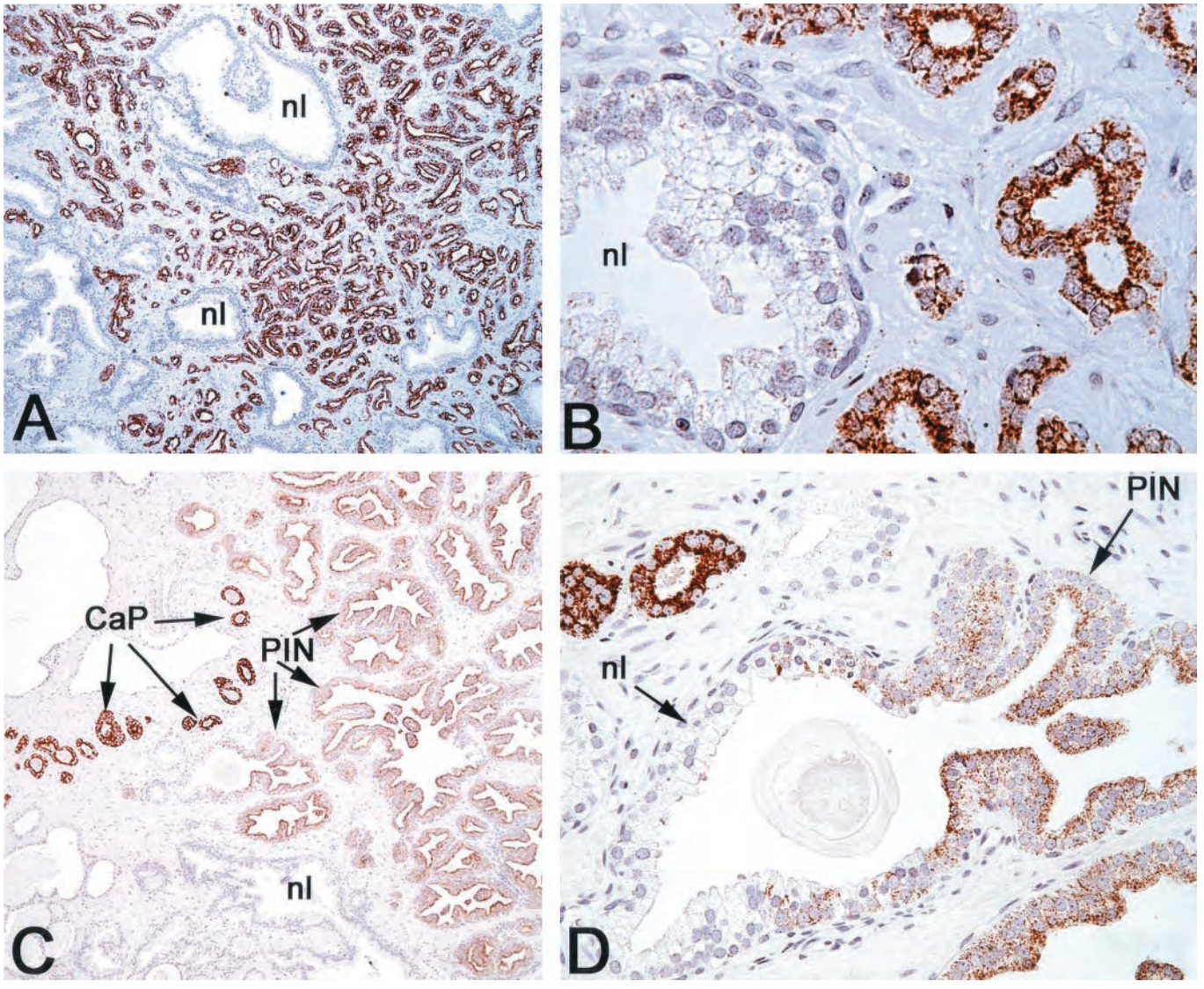

Fig. 3. IHC localization of AMACR in prostate tissue using standard slides. *A*, low-power image of Gleason pattern 3 carcinoma infiltrating between benign normal appearing glands (*nl*) showing homogeneous strong staining (×40). *B*, higher power view of representative region from *A* showing punctate cytoplasmic staining (×400). *C*, another case showing high-intensity staining in carcinoma (*CaP*), intermediate intensity staining in HGPIN (*PIN*), and no staining in normal (*nl*; ×100). *D*, higher power view of *C* showing strong staining in carcinoma glands (*top left*) and staining in acinus in that is involved partially with HGPIN with staining only in atypical HGPIN cells (*PIN*). Note negative staining in the normal appearing acinus just to the *right* of the carcinoma (×200).

HGPIN *versus* normal, $P < 0.001$, Wilcoxon's rank-sum test). The score for HGPIN was significantly less than the score for carcinoma ($P = 0.0002$, Wilcoxon's rank-sum test). If a cutoff of ≥100 is used for positive staining, then 95.6% of carcinomas were positive, whereas 3.5% (5 of 144) of normal epithelium was positive. Using a score of ≥150 for strong positive staining, then 88% of the carcinomas would be considered strong, *versus* none of the normal epithelium. The carcinomas (52%) had a median score of 300 (the maximum).

The distribution of AMACR mean IHC scores for carcinoma (mean for all of the spots for each patient) stratified by Gleason score and pathological stage is shown in Table 1. There was no relation between AMACR IHC score and Gleason grade, pathological stage, patient age, or preoperative serum prostate-specific antigen (Kruskal-Wallis, all *P*s > 0.05). As expected, Gleason score at radical prostatectomy was associated strongly with higher stage disease (Spearman's rank correlation coefficient = 0.42, $n = 142$, $P < 0.0001$; Table 1).

IHC Analysis of Prostate Cancer Metastases. Staining in metastatic prostate cancers from nonhormone refractory disease ($n = 32$ sites from 32 patients: 8 bone, 21 pelvic lymph node, 2 soft tissue, and 1 lung) showed staining in the majority of cases (data not shown). The median score in nontreated metastatic cases was 240 (mean 204, SD 97). By the criteria stated above for positivity, 81% (26 of 32) were positive, and 62.5% were strongly positive (20 of 32). In hormone refractory metastatic prostate ($n = 25$ sites from 14 patients), the median score was 215 (mean = 206, SD = 84). Thus, 93% (13 of 14) of hormone refractory metastatic cancers were positive, and 71.4% were strongly positive.

AMACR Protein Expression in Other Normal Tissues. To examine the overall tissue distribution of AMACR protein expression, staining was performed using a TMA containing a wide variety of human tissues. Staining was strongly positive in virtually all hepatocytes, proximal kidney tubules, and glomerular epithelial cells of the kidney (data not shown). Moderate staining was found in the acinar cells and some ductal cells of major salivary glands. Weak staining was found in distal tubules and collecting ducts of the kidney. Other tissues showed weak and heterogeneous expression, including the following: (*a*) neurons in the central nervous system; (*b*) absorptive

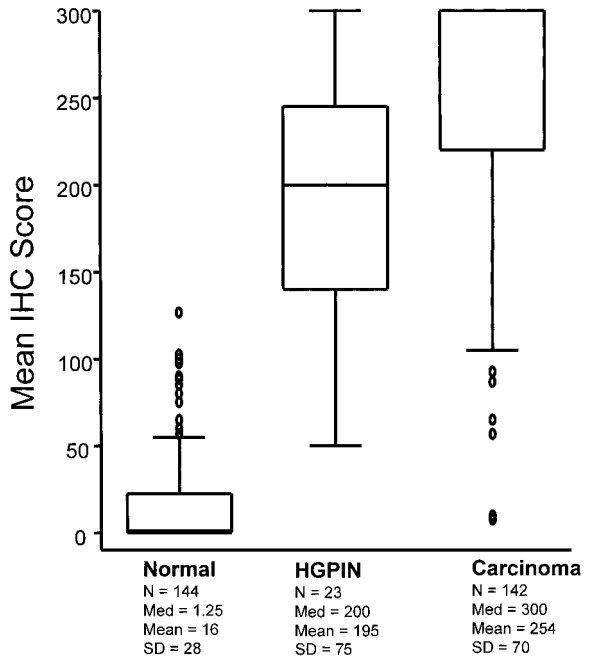

Fig. 4. Relative expression of AMACR by IHC score in normal, HGPIN, and carcinoma by scoring of TMA spots. *Box* shows 25th-75th percentiles, as well as median (*center line*). *Whiskers* show 5th and 95th percentiles, and *ovals* represent outliers.

and paneth cells of the small bowel; (*c*) absorptive cells of the large bowel; and (*d*) Sertoli cells of the testis. Staining was not detectable in the urinary bladder, ovary, endometrium, fallopian tube, uterine cervix, breast, lung, skin, tonsil, lymph nodes, thymus, spleen, laryngeal epithelium, minor salivary glands, pancreas, gall bladder, thyroid, stomach, esophagus, skeletal muscle, or smooth muscle.

Combination of AMACR Staining with p63 Facilitates Detection of Prostate Cancer Cells. The intense staining in tumors with weak staining in normal suggested that AMACR IHC staining might be useful as an adjunct to the diagnosis of prostate cancer on needle biopsy or other clinical specimens. To be useful as a potential diagnostic marker for prostate cancer, carcinoma lesions need to be separated reliably from lesions of HGPIN and other potential mimicars of prostate cancer, such as adenosis and atrophy, as well as from normal prostate tissue. On small needle biopsy samples, this distinction can sometimes be problematic (21). One very useful tool has been IHC staining for basal cell-specific cytokeratins, typically using the 34BE12 monoclonal antibody (22). Because basal cells, which are absent in the vast majority of prostatic adenocarcinomas, are present in normal glands, benign mimicars, such as atrophy and adenosis, and in HGPIN, staining for basal cell cytokeratins is often used in prostate cancer needle biopsies (22). More recently, the p63 protein has been found to be localized to the nuclei of basal cells in prostate epithelium with a basal cell-specific staining pattern nearly identical to 34BE12 (13, 14). Because the staining for p63 is strictly nuclear and is negative in the vast majority of carcinomas, and the staining for AMCAR is cytoplasmic and only strong in carcinoma or HGPIN, we combined the staining for these two markers as a cocktail. There was strong staining of the nuclei of basal cells in benign glands, whereas carcinoma showed no nuclear staining but strong cytoplasmic staining, with no decrease as compared with AMCAR staining alone ($n = 20$, Fig. 5, *A* and *B*). HGPIN showed variable punctate, cytoplasmic AMCAR staining, but strong and homogeneous nuclear staining in basal cells, thus allowing one to reliably distinguish HGPIN from carcinoma (Fig. 5, *C* and *D*). At times, HGPIN appeared to contain buds of epithelium, pinching off into the underlying stroma (23). An example of this phenomenon is shown in Fig. 5*D* (*arrow*), where a single acinus is projecting from an acinus containing HGPIN. The projecting acinus shows very sparse p63 basal cell staining, consistent with early invasion. The surrounding carcinoma cells show complete loss of p63 staining, yet they contain AMACR cytoplasmic staining.

Discussion

In this study, we demonstrate that AMACR is overexpressed in the majority of prostate cancers and cancer cells within these tumors. Using many cases with diverse pathologic characteristics, we find that overexpression at the protein level is very tightly linked to prostate cancer and occurs in virtually all grades and stages and in both hormone refractory and untreated cases. Over 95% of prostate cancers analyzed stained positively for AMACR, whereas <4% of histologically normal prostate epithelium was positive. Using a more stringent scoring scheme, these values are 88 and 0% for cancers and normal cells that are positive, respectively. Because there appears to be such a tight link between overexpression and the histological prostate cancer phenotype, these finding have implications for the pathogenesis, diagnosis, imaging, and treatment of prostate cancer.

In terms of early diagnosis on prostate needle biopsy, whereas basal cell-specific keratin is a useful aid for diagnosis, this marker is lost in prostate cancer. Because there can be artifactual loss of IHC staining, at times, this staining is uninformative and/or misleading. To date, few, if any, validated markers of prostate cancer have been identified that are overexpressed consistently as detected by IHC staining such that they might be of diagnostic use in a large percentage of cases. We now show that AMACR may provide the first example of such a marker. Because AMACR staining can occur intensely in HGPIN, we combined staining using AMACR with staining for p63. Because these markers, when present, are invariably cytoplasmic and nuclear, respectively, there is no need for the use of two color staining. p63 staining has been shown to be comparable with the basal cell-specific keratin 34βE12 monoclonal antibody but has the advantage in this case of a more clearly discernible nuclear location (13, 14). Thus, AMACR is a new positive stain that complements the traditional negative stain to enhance prostate cancer diagnosis. To determine the usefulness of AMACR in diagnostic pathology practice, we have begun to use clinical needle biopsies in prospective studies comparing AMACR, AMACR/p63, and basal cell-specific cytokeratins. Additionally, this marker combination could be of use for nonpathologist researchers studying prostate cancer specimens to enhance diagnostic certainty.

The enzyme encoded by this gene plays a critical role in the metabolism of fatty acid molecules, specifically by peroxisomal β

Table 1 *AMACR IHC score from TMA analysis for 142 patients stratified by Gleason grade and pathological stage at radical prostatectomy*

		Stage			
Grade		T2	T3A	T3B	N1
5–6	n	65	12	2	0
	Median	300	268	258	Na[a]
	Mean	255	218	258	Na
	SD	68	100	60	Na
7	n	24	14	5	1
	Median	293	300	243	300
	Mean	238	263	254	300
	SD	83	60	43	0
8–9	n	5	10	3	1
	Median	300	300	283	300
	Mean	297	274	273	300
	SD	8	58	34	0

[a] Na, not applicable.

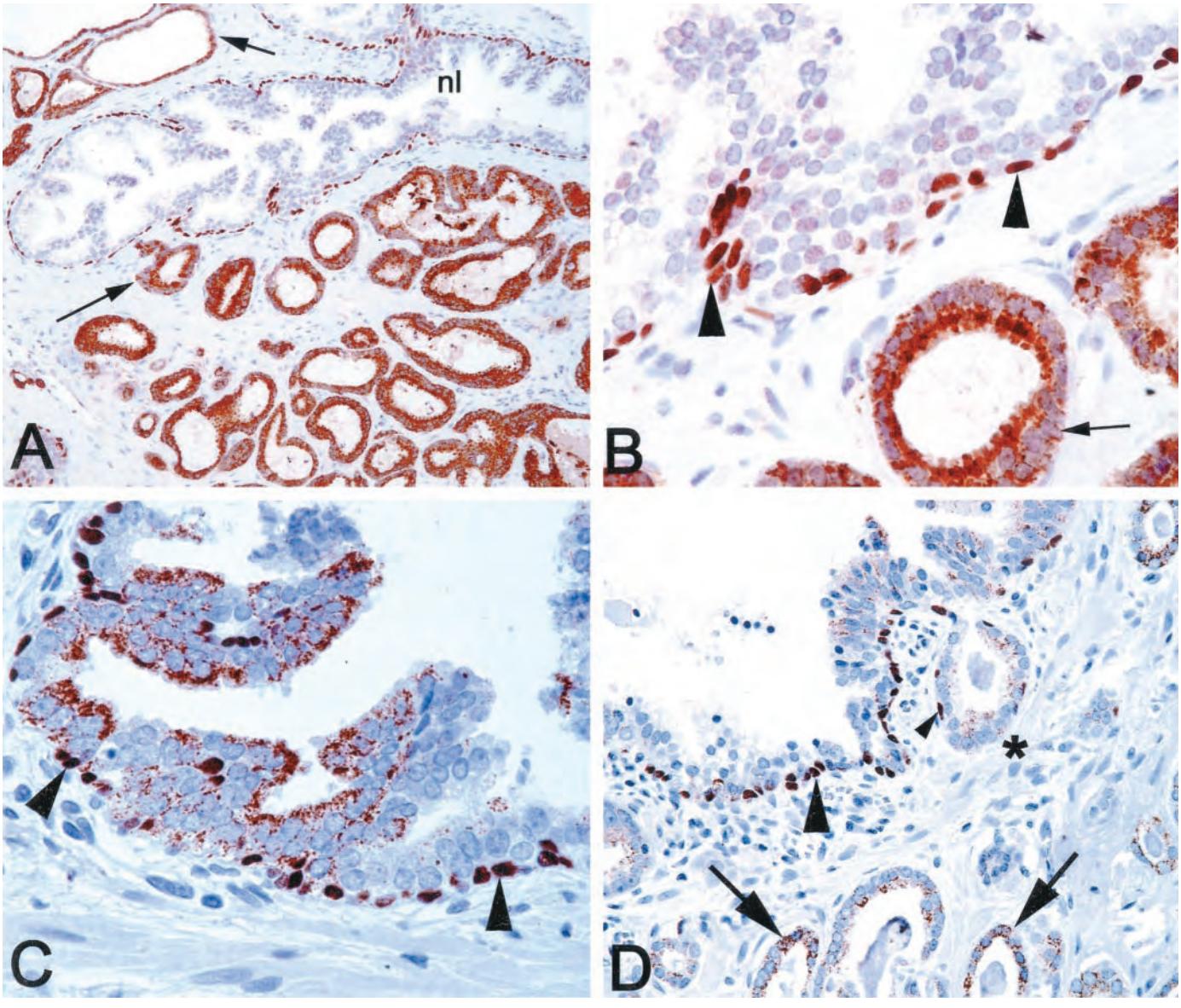

Fig. 5. Simultaneous single color localization of p63 and AMACR. Tissues were stained with a cocktail containing anti-p63 (nuclear) and anti-AMACR (punctate cytoplasmic) antibodies, and staining was localized simultaneously. In *A*, nuclear basal cell staining (p63) is apparent in normal appearing acinus. *Arrows*, infiltrating carcinoma cells (×100). *B*, higher power view of *A*. *Arrowheads*, nuclear basal cells staining (p63); *arrow*, carcinoma (×400). *C*, HGPIN showing moderate to weak punctate cytoplasmic AMACR staining and strong positive staining p63 staining of basal cells (×400). *D*, HGPIN (top gland) with weak cytoplasmic AMACR staining and nuclear basal cells staining (p63). Note small acinus apparently budding off (*) of HGPIN gland showing very sparse basal cell nuclear staining (*arrowhead*). *Below*, there is moderate to weak intensity cytoplasmic staining in infiltrating carcinoma cells that lack p63 nuclear staining.

oxidation (10). Branched chain fatty acids, which originate almost entirely from the diet, contain methyl groups in the R position, whereas the enzymes of the β oxidation pathway can only transform substrates having the S configuration (10). The enzyme AMACR catalyzes this interconversion. One implication of the up-regulation of AMACR is that prostate cancer cells may have a consistently greater capacity to metabolize dietary branched chain fatty acids than would their normal counterparts. Although the contribution of this up-regulation to prostate carcinogenesis, if any, is unclear at present, two interesting aspects of this pathway may be relevant: (*a*) the first step of the pathway in β oxidation of branched chain fatty acids is an oxidation step catalyzed by acyl-CoA oxidases, with the products being oxidized substrate and hydrogen peroxide (10). Experimental overexpression of acyl-CoA oxidase can transform cells (12), and the increase in oxidative stress because of the production of hydrogen peroxide by this pathway has been proposed to play a role in the transformation process (11). Indeed, the potent carcinogenic activity of peroxisome proliferators in animal models is thought to be mediated, at least in part, by up-regulation of the peroxide-producing enzymes of the peroxisome (24); and (*b*) the primary branched chain fatty acid whose metabolism is critically dependent on the action of AMACR is phytanic acid, derived from phytol, a breakdown product of chlorophyll in ruminants. This fatty acid is found primarily in cow's milk, and diary products derived there from, as well as beef but not meat from chickens or some fish (25). An interesting question is whether the increased risk for prostate cancer conferred by consumption of dairy products and/or red meat (9) is related to the up-regulation of this enzyme and its associated pathway in the early stages of prostate carcinogenesis, *e.g.*, in PIN.

Molecular imaging promises the ability to identify individual cells or groups of cells expressing specific proteins or enzymatic activity in real time in living patients (see Louie *et al.*; Ref. 26) The ability to

image AMACR protein or enzymatic activity would likely provide significant value in localization of primary prostate cancer within the prostate. A first application of this would be to help direct the location of needle biopsy sites in the prostate and possibly to assess the extent of cancer within the prostate. In addition, the ability to image AMACR systemically would provide value for detection of metastatic prostate cancer in organs other than the liver and kidney.

The prostate glands of U.S. men are biopsied >1 million times a year, leading to a positive diagnoses of ~180,000 new prostate cancer cases annually. Estimates of equivocal or ambiguous biopsy evaluations that are suspicious for cancer range from 0.3 to 24% (21), resulting in tens of thousands of repeat biopsies. Clearly, markers, which can assist in the accurate evaluation of prostate needle biopsies, are needed urgently. Because of its consistency and robustness, AMACR appears to fit the criteria for such a marker and as such may become routinely used in the pathological diagnosis of prostate cancer. In addition, the biological function of this marker provides exciting new information regarding the etiology of prostate cancer and provides a novel target for prevention and therapeutics. Whether this marker is pathogenic, a potential drug, or *in vivo* imaging target is subject to ongoing studies.

While our manuscript was in preparation, Jiang *et al.* (27) reported overexpression of AMACR by IHC, using a different antibody, in the majority of primary prostate cancers. Although this report did not examine AMACR expression in other tissues, or combine AMACR staining with p63 or evaluate metastatic prostate cancers, the fact that two separate groups simultaneously observe marked overexpression of this protein in primary prostate cancer is a remarkable finding that bolsters the overall importance of AMACR as a new prostate cancer marker.

Acknowledgments

We thank Helen Fedor and Marsella Southerland for their excellent technical assistance in preparing TMAs, Dennis Faith for help with the Microsoft Access database, and Gerrun E. March for diligence in scanning of TMA slides. We thank Dr. Mark Rubin and the University of Michigan Specialized Programs of Research Excellence TMA facility for the hormone refractory prostate cancer TMA. We also acknowledge the generous support of the Peter J. Sharpe Foundation.

References

1. Isaacs, W. B., and Bova, G. S. Prostate cancer. *In:* B. Vogelstein and K. Kinzler (eds.), The Genetic Basis of Human Cancer, pp. 653–660. New York: McGraw-Hill, 1998.
2. Xu, J., Stolk, J. A., Zhang, X., Silva, S. J., Houghton, R. L., Matsumura, M., Vedvick, T. S., Leslie, K. B., Badaro, R., and Reed, S. G. Identification of differentially expressed genes in human prostate cancer using subtraction and microarray. Cancer Res., *60:* 1677–1682, 2000.
3. Luo, J., Duggan, D. J., Chen, Y., Sauvageot, J., Ewing, C. M., Bittner, M. L., Trent, J. M., and Isaacs, W. B. Human prostate cancer and benign prostatic hyperplasia: molecular dissection by gene expression profiling. Cancer Res., *61:* 4683–4688, 2001.
4. Magee, J. A., Araki, T., Patil, S., Ehrig, T., True, L., Humphrey, P. A., Catalona, W. J., Watson, M. A., and Milbrandt, J. Expression profiling reveals hepsin overexpression in prostate cancer. Cancer Res., *61:* 5692–5696, 2001.
5. Bull, J. H., Ellison, G., Patel, A., Muir, G., Walker, M., Underwood, M., Khan, F., and Paskins, L. Identification of potential diagnostic markers of prostate cancer and prostatic intraepithelial neoplasia using cDNA microarray. Br. J. Cancer, *84:* 1512–1519, 2001.
6. Dhanasekaran, S. M., Barrette, T. R., Ghosh, D., Shah, R., Varambally, S., Kurachi, K., Pienta, K. J., Rubin, M. A., and Chinnaiyan, A. M. Delineation of prognostic biomarkers in prostate cancer. Nature, *412:* 822–826, 2001.
7. Ferdinandusse, S., Denis, S., Ijlst, L., Dacremont, G., Waterham, H. R., and Wanders, R. J. Subcellular localization and physiological role of α-methylacyl-CoA racemase. J. Lipid Res., *41:* 1890–1896, 2000.
8. Wanders, R. J. A., Jacobs, C., and Skjeldal, O. H. Refsum disease. *In:* C. R. Scriver, A. L. Beaudet, W. S. Sly, and D. Valle (eds.), The Metabolic and Molecular Bases of Inherited Disease, pp. 3303–3321. London: McGraw Hill, 2001.
9. Chan, J. M., Stampfer, M. J., Ma, J., Gann, P. H., Gaziano, J. M., and Giovannucci, E. L. Dairy products, calcium, and prostate cancer risk in the Physicians' Health Study. Am. J. Clin. Nutr., *74:* 549–554, 2001.
10. Wanders, R. J., Vreken, P., Ferdinandusse, S., Jansen, G. A., Waterham, H. R., van Roermund, C. W., and Van Grunsven, E. G. Peroxisomal fatty acid α- and β-oxidation in humans: enzymology, peroxisomal metabolite transporters and peroxisomal diseases. Biochem. Soc. Trans., *29:* 250–267, 2001.
11. Ockner R. K., Kaikaus R. M., and Bass N. M. Fatty-acid metabolism and the pathogenesis of hepatocellular carcinoma: review and hypothesis. Hepatology, *18:* 669–676, 1993.
12. Tamatani, T., Hattori, K., Naashiro, K., Hayashi, Y., Wu, S., Klumpp, D., Reddy, J. K., and Oyasu, R. Neoplastic conversion of human urothelial cells *in vitro* by overexpression of H2O2-generating peroxisomal fatty acyl CoA oxidase. Int. J. Oncol., *15:* 743–749, 1999.
13. Signoretti, S., Waltregny, D., Dilks, J., Isaac, B., Lin, D., Garraway, L., Yang, A., Montironi, R., McKeon, F., and Loda, M. p63 is a prostate basal cell marker and is required for prostate development. Am. J. Pathol., *157:* 1769–1775, 2000.
14. Parsons, J. K., Gage, W. R., Nelson, W. G., and De Marzo, A. M. Expression of p63 in normal, neoplastic and preneoplastic human prostate tissues. Urology, *58:* 619–624, 2001.
15. Bova, G. S., Fox, W. M., and Epstein, J. I. Methods of radical prostatectomy specimen processing: a novel technique for harvesting fresh prostate cancer tissue and review of processing techniques. Mod. Pathol., *6:* 201–207, 1993.
16. Zha S., Gage W. R., Sauvageot, J., Saria, E. A., Putzi, M. J., Ewing, C. M., Faith, D. A., Nelson, W. G., De Marzo, A. M., and Isaacs, W. B. Cyclooxygenase-2 is up-regulated in proliferative inflammatory atrophy of the prostate, but not in prostate carcinoma. Cancer Res., *61:* 8617–8623, 2001.
17. Manley, S., Mucci, N. R., De Marzo, A. M., and Rubin, M. A. Relational database structure to manage high-density tissue microarray data and images for pathology studies focusing on clinical outcome: the prostate specialized program of research excellence model. Am. J. Pathol., *159:* 837–843, 2001.
18. De Marzo, A. M., Knudsen, B., Chan-Tack, K., and Epstein, J. I. E-cadherin expression as a marker of tumor aggressiveness in routinely processed radical prostatectomy specimens. Urology, *53:* 707–713, 1999.
19. Lee, W. H., Morton, R. A., Epstein, J. I., Brooks, J. D., Campbell, P. A., Bova, G. S., Hsieh, W. S., Isaacs, W. B., and Nelson, W. G. Cytidine methylation of regulatory sequences near the pi-class glutathione *S-transferase* gene accompanies human prostatic carcinogenesis. Proc. Natl. Acad. Sci. U S A, *91:* 11733–11737, 1994.
20. Yang, Y., Hao, J., Liu, X., Dalkin, B., and Nagle, R. B. Differential expression of cytokeratin mRNA and protein in normal prostate, prostatic intraepithelial neoplasia, and invasive carcinoma. Am. J. Pathol., *150:* 693–704, 1997.
21. Epstein, J. I., and Potter, S. R. The pathological interpretation and significance of prostate needle biopsy findings: implications and current controversies. J. Urol., *166:* 402–410, 2001.
22. Wojno, K. J., and Epstein, J. I. The utility of basal cell-specific anti-cytokeratin antibody (34 β E12) in the diagnosis of prostate cancer. A review of 228 cases. Am. J. Surg. Pathol., *19:* 251–260, 1995.
23. McNeal, J. E., Villers, A., Redwine, E. A., Freiha, F. S., and Stamey, T. A. Microcarcinoma in the prostate: its association with duct-acinar dysplasia. Hum. Pathol., *22:* 644–652, 1991.
24. Yeldandi, A. V., Rao, M. S., and Reddy, J. K. Hydrogen peroxide generation in peroxisome proliferator-induced oncogenesis. Mutat. Res., *448:* 159–177, 2000.
25. Flanagan, V. P., Ferretti, A., Schwartz, D. P., and Ruth, J. M. Characterization of two steroidal ketones and two isoprenoid alcohols in dairy products. J. Lipid Res., *16:* 97–101, 1975.
26. Louie, A. Y., Huber, M. M., Ahrens, E. T., Rothbacher, U., Moats, R., Jacobs, R. E., Fraser, S. E., and Meade, T. J. *In vivo* visualization of gene expression using magnetic resonance imaging. Nat. Biotechnol., *18:* 321–325, 2000.
27. Jiang, Z., Woda, B. A., Rock, K. L., Xu, Y., Savas, L., Khan, A., Pihan, G., Cai, F., Babcook, J. S., Rathanaswami, P., Reed, S. G., Xu, J., and Fanger, G. R. P504S: a new molecular marker for the detection of prostate carcinoma. Am. J. Surg. Pathol., *25:* 1397–1404, 2001.